有害な欠陥やき裂がある工業材料の疲労特性の評価と危険荷重の検出について

Doctoral Dissertation of Engineering

Detection of Application of Hazardous Load and Evaluation of Fatigue Properties in Engineering Material Having Inconvenient Defects or Cracks

有害な欠陥やき裂がある工業材料の疲労特性の評価と危険荷重の検出について

March 2021

by

S. M. Moshiar Rahman

Mechanics of Materials
Material, Structural and Energy Engineering
Graduate School of Engineering and Science
University of the Ryukyus

Doctoral Dissertation of Engineering

Detection of Application of Hazardous Load and Evaluation of Fatigue Properties in Engineering Material Having Inconvenient Defects or Cracks

有害な欠陥やき裂がある工業材料の疲労特性の評価と危険荷重の検出について

March 2021

by

S. M. Moshiar Rahman

Mechanics of Materials

Material, Structural and Energy Engineering

Graduate School of Engineering and Science

University of the Ryukyus

Supervisor: Prof. Chobin Makabe

Dissertation Title: Detection of Application of Hazardous Load and Evaluation of Fatigue Properties in Engineering Material Having Inconvenient Defects or Cracks.

Name: S. M. Moshiar Rahman

We, the undersigned, hereby, declare that we have read this thesis and we have attended the thesis defense and evaluation meeting. Therefore, we certify that, to the best of our knowledge this thesis is satisfactory to the scope and quality as a thesis for the degree of Doctor of Engineering in Strength of Materials Engineering under Material, Structural and Energy Engineering, Graduate School of Engineering and Science, University of the Ryukyus.

DISSERTATION REVIEW & EVALUATION COMMITTEE MEMBERS

Signature Chobin Makabe

(Chairman) Professor Chobin MAKABE

Signature Tatsujiro Miyazaki

(Committee) Professor Tatsujiro MIYAZAKI

Signature Masaki Fujikawa

(Committee) Associate Professor Masaki FUJIKAWA

ABSTRACT

Structural components experience different kinds of loads in their life cycle like axial, torsional etc. The existence of some unrecognized cracks results in poor mechanical properties which may bring terminal damage with higher load application. On this aspect, the detection of such kinds of overload and underload and crack initiation and propagation behavior due to the presence of inclusions in the machine structure were investigated. The main contents of the present dissertation are summarized as follows:

A detection technique of the application of unexpected or hazardous over and under load was investigated. S15C carbon steel has been used to conduct this experiment which is called JIS-S15C steel. The specimen was prepared with pre-crack and notch at the center of the specimen. An acceleration behavior of crack growth due to the application of overload and underload during fatigue crack growth test with constant stress amplitude was observed. In some cases, the acceleration of crack growth brings catastrophic failure in machine the structure. Therefore, it is useful for machine maintenance to determine whether an unexpected load was applied or not by doing a daily inspection.

Fatigue limit and crack growth behavior of carbon fiber reinforced epoxy composites and hybrid composites has been studied with a slit specimen. Then the results were compared between epoxy carbon fiber reinforced composites and the hybrid composites. The fatigue limit was defined by the maximum stress amplitude that the specimen endured 10^6 times or more repeated stress when *S*-*N* curve was used. For both cases, the highest fatigue limit was obtained for parallel loading fiber direction. According to those results, it was expected that the fatigue limit of smoothed specimens of carbon composites and hybrid composites can be evaluated from the results of the slit specimens.

The fatigue life and fatigue limit of carbon steels having pre-cracks and inclusions, and prediction of fatigue limit by correction of crack initiation length were investigated. Presence of pre-cracks and inclusions may affect the crack initiation length and crack propagation behavior. Also, crack initiation behavior is related to the distribution of microstructure and inclusions present in the materials. Inclusion size higher than expected may decrease the fatigue strength of the material. This result is shown in the study of 0.25% carbon steel. For the material 0.45% carbon steel, there were some inclusions but fewer than 0.25% carbon steel. As initial crack length varied due to the presence of inclusions, a correction method has been proposed and fatigue life and limit have been predicted based on the correction.

LIST OF PUBLICATIONS

List of academic papers using data in this paper

1. S.M. Moshiar Rahman, Kaito Naka, Chobin Makabe, “A Method for Prediction of Fatigue Limit and Life of Carbon Steel (in Japanese),” Journal of High Pressure Institute of Japan, Vol.59, No.3, 2021 (Accepted).
2. S.M. Moshiar Rahman, Chobin Makabe, Kaito Naka, Akihiro Yamauchi, “Effect of Existence of Inclusions on Fatigue Strength”, Journal of High Pressure Institute of Japan, Vol.58, No.4, pp.11-17, 2020, ISSN 0387-0154 Atsuryoku gijitsu.
3. S.M. Moshiar Rahman, Md. Shafiul Ferdous, "Fatigue and Fracture Mechanism of Aluminum Carbon Fiber Reinforced Hybrid Composites", Key Engineering Materials, ISSN:1662-9795, Vol. 841, pp.288-293, May 2020, doi: 10.4028/www. scientific. net/KEM. 841.288.
4. Md. Shafiul Ferdous, S.M. Moshiar Rahman, Chobin Makabe, “Effect of Fiber Direction and Stress Ratio on Fatigue Property in Epoxy Carbon Composites,” Material Science Forum, ISSN: 1662-9752, Vol. 940, pp.79-83, doi: 10.4028/www.scientific.net/MSF.940.79.
5. S.M. Moshiar Rahman, Md. Shafiul Ferdous, Chobin Makabe, “Method of Detecting Unexpected Load Leading to Crack Growth Acceleration,” Key Engineering Materials, ISSN:1662-9795, Vol.775, pp.517-523, 2018, doi:10.4028/ www.scientific. net/ KEM.775.517.
6. S.M. Moshiar Rahman, Md. Shafiul Ferdous, Kounosuke Tada, Chobin Makabe, “A Method for Detecting an Unexpected Application of a Hazardous Load During Operation”, Advances in Materials Science and Applications, Vol.6, Iss.1, 2017, pp.9-16 (DOI: 10.5963/ AMSA0601002).

ACKNOWLEDGEMENT

I would like to express my special gratitude to my academic advisor Professor Chobin Makabe for his continuous encouragement, guidance and advice during my study in University of the Ryukyus. His supervision, criticism and comments have made it possible to finish my research with a lot of learning experience and to survive here without my family members and friends.

My heartfelt gratitude to Professor Tatsujiro Miyazaki and Associate Professor Masaki Fujikawa for serving on the advisory committee.

Also, I would like to thank all the Professors and administrative members of Mechanical Systems Engineering Department at the University of the Ryukyus for providing me research facilities and technical assistance.

I highly appreciate for kind support and help from all my lab member of University of the Ryukyus for their kind cooperation and support. I would like to extend my grateful thanks to Mr. Kaito Naka and Mr. Kazuo Takara and other staff for their help on specimen preparation and instructive discussions on preparation of specimen.

A special thanks to QUEST Scholarship Foundation for their financial support and Ms. Akie Igei for administrative support for the scholarship in the University of the Ryukyus. I am grateful to the staffs and personnel Ms. Oshiro, Ms. Chikako Takaesu of International Student Center, Mr. Kunimitsu Soma, Mr. Kensei Miyazato, Ms. Yuka MATSUKAWA in Engineering office and Ms. Takaesu in the Mechanical System Engineering office for their great administrative support in the University of the Ryukyus during my study. I would like to thank to the university's Japanese Language study section, especially Assistant Professor Ms. Seiko Tomari for her cordial and helpful support and advice.

I would like to extent my heartfelt gratitude to the Personnel and Staff of the Student Support Section for their great, patient and cordial support for dealing with tuition fees exemption application. During the tenure of my studentship, all the tuition fees have been exempted. That was a great support for my study. I wish to offer my sincere appreciation to Ms. Jiroku and Ms. Serina of the Niche Department for their career advocacy service and support.

During my study, I studied as a privately finance international student. Part-time job was my main income source. I worked in different Companies and Hotels in Okinawa, Japan. I would like

to thank for their wonderful support and co-operation while I was working there.

Finally, my sincere gratitude goes to my family members for their kind support and constant confidence and positive encouragement over the years staying in Japan.

S M Moshiar Rahman

March 2021

TABLE OF CONTENTS

ABSTRACT ……...….. iv

LIST OF PUBLICATION ……... v

ACKNOWLEDGEMENT……...……. vi

TABLE OF CONTENT …….…….. viii

LIST OF TABLES……...……. xii

TABLE OF FIGURES…….. xiii

LIST OF SYMBOLS……...……. xvii

Chapter One: Introduction 1

1.1 Fatigue and Fracture and Methods of Evaluating Them 1

1.2 Detection of Dangerous Situation by Fatigue Crack Growth in Metal 3

1.3 Crack Growth Behavior in the Case of a Composite. 4

1.4 Prediction of Fatigue Life and Strength. 5

1.5 Outline of Present Dissertation 7

1.5.1 A method for detecting an unexpected application of a hazardous load during operation. 7

1.5.2 Method of detecting unexpected load leading by using strain information. 7

1.5.3 Effect of fiber direction and stress ratio on fatigue property in carbon fiber reinforced epoxy composites. 8

1.5.4 Fatigue and fracture mechanism of aluminum-carbon fiber reinforced hybrid composites.....8

1.5.5 Effects of existence of unexpected defects on fatigue strength. 8

1.5.6 A method for prediction of fatigue limit and life of carbon steel. 9

1.6 Conclusion.....9

1.7 Reference.....11

Chapter Two: A Method for Detecting an Unexpected Application of a Hazardous Load During Operation 14

2.1 Introduction 14
2.2 Material and Crack Growth Testing Procedure 15
2.3 Method of Measuring Crack Opening and Closing Stresses 17
2.4 Results and Discussion 18
2.4.1 Crack growth behavior 19
2.4.2 Detecting the application of dangerous load 21
2.4.3 Observation in the vicinity of crack tip 26
2.5 Conclusions 28
2.6 References 29
Chapter Three: Method of Detecting Unexpected Load Leading by Using Strain Information 31
3.1 Introduction 31
3.2 Material and Testing Procedure 32
3.3 Results and Discussion 33
3.4 Conclusion 42
3.5 References 43
Chapter Four: Effect of Fiber Direction and Stress Ratio on Fatigue Property in Carbon Fiber Reinforced Epoxy Composites 44
4.1 Introduction 44
4.2 Materials and Experimental Method 44
4.3 Experimental Results and Discussion 46
4.3.1 Evaluation of fatigue limit 46
4.3.2 Fatigue crack growth and fracture pattern 49
4.3.3 Discussion for tendency of present experiment 50
4.4 Conclusions 52
4.5 References 53

Chapter Five: Fatigue and Fracture Mechanism of Aluminum-Carbon Fiber Reinforced Hybrid Composites 54

5.1 Introduction 54

5.2 Materials and Experimental Method 54

5.3 Experimental Results and Discussion 55

5.3.1 Determination of fatigue limit 55

5.3.2 Obervation of crack growth behavior 58

5.4 Conclusion....62

5.5 References 63

Chapter Six: Effects of Existence of Unexpected Defects on Fatigue Strength 64

6.1 Introduction 64

6.2 Material and Experimental Procedure....65

6.3 Results and Discussions 67

6.3.1 Fatigue limit and crack growth 67

6.3.2 Observation of crack growth and fracture surface 69

6.4 Conclusion....74

6.5 References 75

Chapter Seven: A Method for Prediction of Fatigue Limit and Life in Carbon Steel 77

7.1 Introduction 77

7.2 Materials and Experimental Methods 78

7.3 Experimental Results and Discussion 80

7.3.1 Fatigue limit obtained from S-N curve 80

7.3.2 Crack growth behavior of smooth specimen 81

7.3.3 Evaluation of S-N curve and fatigue limit due to difference in crack initiation length 88

7.4 Conclusion....94

7.5 Reference.....95

Chapter Eight: Conclusion **97**

Chapter Two: A Method for Detecting an Unexpected Application of a Hazardous Load During Operation.....97

Chapter Three: Method of Detecting Unexpected Load Leading by Using Strain Information 98

Chapter Four: Effect of Fiber Direction and Stress Ratio on Fatigue Property in Carbon Fiber Reinforced Epoxy Composites 98

Chapter Five: Fatigue and Fracture Mechanism of Aluminum-Carbon Fiber Reinforced Hybrid Composites.....99

Chapter Six: Effects of Existence of Unexpected Defects on Fatigue Strength.....100

Chapter Seven: A Method for Prediction of Fatigue Limit and Life in Carbon Steel.....100

LIST OF TABLES

Table 2. 1 Chemical composition and mechanical properties of 0.15% carbon steel (σ_S; Yield stress [MPa], σ_B; Ultimate tensile strength [MPa], ψ Reduction of area [%]) 15

Table 5. 1 Experimental result for *C* type specimen at stress ratio, $R = 0$ 58

Table 7. 1 Chemical composition of the material tested..... 78

Table 7. 2 Mechanical properties..... 78

Table 7. 3 Coefficients for prediction of *S-N* curve from crack growth curves (l_0=12μm, l_f =2.0mm)..... 86

Table 7. 4 Coefficients for prediction of *S-N* curve from crack growth curves (l_0=0.05mm, l_f =2.0mm)..... 91

TABLE OF FIGURES

Chapter Two

Figure 2. 1 (a) Geometry of the specimen and (b) Position of strain gages (Unit: mm)..... 16

Figure 2. 2 Fatigue testing machine and procedure..... 17

Figure 2. 3 Schematic representation of the measurement of the crack opening and closing stresses; (a) Original stress – strain loop, (b) σ vs. H in the case of $\varepsilon_e > \varepsilon_p$, (c) σ vs. H in the case of $\varepsilon_e < \varepsilon_p$; Where, ε_e is elastic strain and ε_p plastic strain. 18

Figure 2. 4 Crack length a vs. number of cycles N 20

Figure 2. 5 da/dN vs. K_{max} 20

Figure 2. 6 In the case of σ_{ou} = -113MPa and 113MPa; (a) Before the application of overload (N = 313760, a= 3.10mm), (a_1) σ-H loop, (a_2) Waveforms of σ/σ_{max}, and H_1, (a_3) Waveforms of σ/σ_{max}, and H_2 ; (b) After the application of overload (N = 322000, a= 3.15mm), (b_1) σ-H loop, (b_2) Waveforms of σ/σ_{max}, and H_1, (b_3) Waveforms of σ/σ_{max}, and H_2..... 22

Figure 2. 7 In the case of σ_{ou} = -185MPa and 185MPa; (a) Before the application (N = 269005, a= 3.10mm), (a_1) σ-H loop, (a_2) Waveforms of σ/σ_{max}, and H_1, (a_3) Waveforms of σ/σ_{max}, and H_2 ; (b) After the application (N = 272609, a= 3.20mm), (b_1) σ-H loop, (b_2) Waveforms of σ/σ_{max}, and H_1, (b_3) Waveforms of σ/σ_{max}, and H_2 23

Figure 2. 8 In the case of σ_{ul} = -113MPa; (a) Before the application (N = 20000, a= 3.10mm), (a_1) σ-H loop, (a_2) Waveforms of σ/σ_{max}, and H_1, (a_3) Waveforms of σ/σ_{max}, and H_2 ; (b) After the application (N = 28506, a= 3.13mm (b_1) σ-H loop, (b_2) Waveforms of σ/σ_{max}, and H_1, (b_3) Waveforms of σ/σ_{max}, and H_2..... 24

Figure 2. 9 In the case of σ_{ul} = -185MPa; (a) Before the application (N = 240110, a=3.10mm), (a_1) σ-H loop, (a_2) Waveforms of σ/σ_{max}, and H_1, (a_3) Waveforms of σ/σ_{max}, and H_2 ; (b) After the application (N = 241108, a=3.13mm), (b_1) σ-H loop, (b_2) Waveforms of σ/σ_{max}, and H_1, (b_3) Waveforms of σ/σ_{max}, and H_2..... 25

Figure 2. 10 Comparison of crack opening behavior after applying unexpected load: (a) In the case of σ_{ou} = -113MPa and 113MPa, (a1) Before application of overload and underload (N=313500, a=3.05mm), (a2) Just overloading (N=313760, a=3.10mm), (a3) After application of overload and underload (N= 314760, a= 3.12mm), (b) In the case of σ_{ou} = -185MPa and 185MPa, (b1) Before application of overload and

underload (N=85229, a=2.35mm), (b2) Just overloading N=269000, a=3.10mm), (b3) After application of overload and underload (N= 272609, a= 3.20mm). 27

Chapter Three

Figure 3. 1 Position of pasted strain gages (mm) 33

Figure 3. 2 Schematic representation of overload and underload 33

Figure 3. 3 Crack length a vs number of cycles N 34

Figure 3. 4 da/dN vs K_{max} 35

Figure 3. 5 Stress-strain loops: (a) σ - ε loop, (b) $\sigma - h1$ loop, (c) σ - $h2$ loop. Arrow shows the crack opening point 36

Figure 3. 6 Variation of λ (= $\Delta\varepsilon_1 / \Delta\varepsilon_2$) against the half-crack length. Arrow shows the overloading and/or underloading point. 37

Figure 3. 7 Example of the relationship between stress and strain functions in the case of σ_{ul} = -113MPa. [Before OL & UL N = 313760, a = 3.10 mm and after OL & UL N = 332000, a = 3.15 mm, OL = Overload, UL = Underload]: (a) $\sigma - h1$ (λ =1), (b) $\sigma - h2$ (λ =1), (c) $\sigma - h2$ ($\lambda = \Delta\varepsilon_1 / \Delta\varepsilon_2$). 38

Figure 3. 8 In the case of applying σ_{ul} = -113MPa, when $\lambda = \Delta\varepsilon_1 / \Delta\varepsilon_2$: (a) Before underloading N = 20000, a = 2.9mm, (b) After underloading N = 28506, a = 3.13mm. 40

Figure 3. 9 In the case of applying σ_{ul} = -113MPa, σ_{ol} = 113MPa when $\lambda = \Delta\varepsilon_1 / \Delta\varepsilon_2$, (α) Before application of UL & OL N=313760, a = 3.10mm, (b) After application of UL & OL N = 322000, a = 3.15mm 40

Figure 3. 10 In the case of σ_{ul} = -185MPa, σ_{ol} = 185MPa when $\lambda = \Delta\varepsilon_1 / \Delta\varepsilon_2$, (a) Before application of UL & OL N= 240110, a = 3.10mm; (b) After application of UL & OL N = 241108, a = 3.13mm 41

Figure 3. 11 Comparison of $\sigma - h_2$ when $\lambda = \Delta\varepsilon_1 / \Delta\varepsilon_2$ [UL = Underload & OL = Overload]: (a) σ_{ul} = -113MPa and σ_{ol} = 113MPa, (b) σ_{ul} = -185MPa and σ_{ol} = 185MPa. 41

Chapter Four

Figure 4. 1 Epoxy based carbon composites: (a) Geometry of the specimen, (b) Unidirectional carbon sheets, (c) Combination of different orientations, (d) Side view of the Specimen. 45

Figure 4. 2 Example of Load Increase Test (*LIT)* 47
Figure 4. 3 *S-N* curve at *R*= -1 47
Figure 4. 4 Results of fatigue limit by *LIT*s: (a) *R*= -1, (b) *R*=0 48
Figure 4. 5 Observations of fracture surface of *B* type specimen; (a) *b*=3mm, *t*=4mm, σ_w=102MPa in the case of *R* = -1, (b) *b*=1.4mm, *t*=5.5 mm, σ_w=410MPa in the case of *R* = 0. 51

Chapter Five

Figure 5. 1 Epoxy based carbon composites: (a) Geometry of the specimen (A type, B type and C type) (b) Combination of carbon fiber sheet and aluminum foil (B type specimen), (c) Combination of carbon fiber sheet and aluminum plate (C type specimen)..... 56
Figure 5. 2 *S-N* curve: (a) *R*=-1, (b) *R*=0 57
Figure 5. 3 Fracture surface of A type specimen. (a) Naked eye view, (b) Fracture behavior, (c) Microscopic view 59
Figure 5. 4 Fracture surface of *B* type specimen (Microscopic view). 59
Figure 5. 5 Fracture surface of *C* type specimen at *R* = -1 (shear fracture):, (a) & (b) Microscopic view(c) Naked eye view 60

Chapter Six

Figure 6. 1 Relationship between σ_w, σ_B and carbon% in annealed carbon steels. 65
Figure 6. 2 Microstructure (Longitudinal section) and inclusions; (a) Large inclusion, (b) Plural small inclusions. 66
Figure 6. 3 Geometry of the specimen, partial notch and hole; (a) Specimen, (b) Partial notch, (c) hole. 67
Figure 6. 4 *S-N* curves of smooth specimen, partial notch specimen and holed specimen. 69
Figure 6. 5 Crack growth curves: (a) *l* vs. $N/N_{f,}$ (b) ln *l* vs. N/N_f 70
Figure 6. 6 Observation of crack (σ_α= 205MPa); (a) N=5.0x10^4, N/N_f=0.41, *l*=0mm, (b) N=6.0x10^4, N/N_f=0.49, *l*=0.16mm, (c) N=9.0x10^4 , N/N_f=0.70, *l*=0.82mm..... 70
Figure 6. 7 Observation of crack (σ = 190MPa); (a) N=1.8x10^5 N/N_f=0.47, *l*=0mm, (b) N=2.4x10^5 N/N_f=0.62 *l*=0.105mm, (c) N=2.7x10^5 N/N_f=0.70, *l*=0.21mm 71
Figure 6. 8 Observation of fracture surface by a surface view microscope (σ_a=180MPa); (a) Plural initiation sits, (b) Detail of part A. 72
Figure 6. 9 Schematic representation of crack growth from defects. 73

Figure 6. 10 Observation of fracture surface of holed specimen when specimen broken from another part of hole (σ_α= 180MPa); (a) Top view, (b) View from inclined direction. 73

Chapter Seven

Figure 7. 1 Microstructure (Longitudinal section) 79

Figure 7. 2 Specimen geometry; (a) Dimensions of the specimen (mm), (b) Partial notch, (c) Hole. 79

Figure 7. 3 *S-N* curves 81

Figure 7. 4 Crack propagation curve; (a) Crack length l_0 vs. relative number of cycles N/N_f, (b) ln l_0 vs. N/N_f 82

Figure 7. 5 Example of observation of fracture surface(σ = 260MPa, Arrow shows inclusion) 83

Figure 7. 6 Observation of crack initiation and growth; (a) σ_a = 320MPa, (a_1) l_0 = 0.0mm and N/N_f=0.03, (a_2) l_0 = 0.004mm, N/N_f=0.059, (a_3) l_0 = 0.008mm, N/N_f=0.089, (a_4) l_0 = 0.013 mm, N/N_f=0.177; (b) σ_a = 260MPa, (b_1) l_0 = 0.0mm, N/N_f=0.03, (b_2) l_0 = 0.019mm, N/N_f=0.068, (b_3) l_0 = 0.032mm, N/N_f=0.102, (b_4) l_0 = 0.038mm, N/N_f=0.170. 83

Figure 7. 7 Correction of crack initiation length; (a) Method of correction of the crack growth curve, (b) Corrected crack growth curves 85

Figure 7. 8 Relationship between corrected (dl/dN)/l vs. stress amplitude σ 87

Figure 7. 9 *S-N* curve which predicted from crack growth curves 88

Figure 7. 10 Crack growth curves of holed specimen, l_0=0.15mm, l_f = 3.0mm. 89

Figure 7. 11 *S-N* curve and evaluated fatigue limit from Eq. (2) for holed specimen 90

Figure 7. 12 Evaluation of fatigue life and fatigue limit of a plain specimen with initial crack (l_0=50μm). 92

LIST OF SYMBOLS

Symbol	Description
σ/σ_a	Applied stress amplitude
R	Stress ratio
f	Frequency
Hz	Hertz
σ_{mean}	Mean stress
N_f	Number of cycles to failure
A	Amplitude ratio
ΔK	Stress intensity factor range
K_t	Stress concentration factor
S_{max}/σ_{max}	Maximum cyclic stress
S_{min}/σ_{min}	Minimum cyclic stress
W	Length of half width of specimen
b	Thickness of the Specimen
t	Slit length of the specimen
$2a$	Total crack length
ΔK_{eff}	Effective stress intensity factor range
ε_e	Elastic strain
ε_p	Plastic strain
σ_{ou}	Overload and underload
σ_o	Overload
σ_u	Underload
σ_{uo}	Underload and overload
C	Strain -stress ratio
σ_{cl}	Crack closing stress
σ_{op}	Crack opening stress
λ	Strain ratio

fcc ……..…Face centered cubic

*H*v …… Vickers Hardness

μm ……Crack Length

ℓ_0 ..... Crack initiation length

ℓ_f ……...Final crack length

N'_f ……...Corrected number of cycles to failure

N' ……..... Arbitrary number of repetition cycles

σ_w ……...Fatigue limit

σ_a ……. Stress amplitude

Chapter One
Introduction

1.1 Fatigue and Fracture and Methods of Evaluating Them

Structural components contain geometrical discontinuities. For instance, threaded connections, windows in aircraft, keyways in shafts, teeth of gear wheels, etc. The size and shape of these features are important since they determine the strength of the components. Conventionally, the strength of components or structures containing defects is assessed by evaluating the stress concentration caused by the discontinuity features. However, such a conventional approach would give erroneous answers if the geometrical discontinuity features have a very sharp radius or notch.

Generally, a fracture is caused due to the crack initiation in a material. So, Fracture mechanics has been developed to evaluate the strength of cracked materials. Fracture mechanics describes the behavior of solids or structures with geometrical discontinuity of the structure. Fracture mechanics has now evolved into a mature discipline of science and engineering and has dramatically changed the understanding of the behavior of engineering materials. One of the important impacts of fracture mechanics is the establishment of a new design philosophy: damage tolerance design methodology, which has now become the industry standard in spacecraft, ships, and automobile parts design. In the case of small-scale yielding, the stress intensity factor, K, is used as the evaluation factor of cracked material.

$$K = F\sigma\sqrt{\pi a} \tag{1.1}$$

Where, F is the correction factor depending on the shape of material, a is the crack length.

In the case of machine components, static fractures and fatigue fractures have the possibility to happen. Especially, care is taken to prevent fatigue fractures in the machine design. Structural members subjected to repeated cyclic loading can undergo progressive damage which is shown by the propagation of cracks. This damage is called fatigue and is represented by a loss of resistance to failure with respect to time. Failure occurs even when the applied stress or strain is well below the value corresponding to failure under monotonic loading. Since most engineering structures are subject to fluctuating loads, fatigue is the largest single source of structural failure of metals in service.

To evaluate fatigue life and strength is very important for machine design. Fatigue properties of materials are often described by using the fatigue limit or the *S*-*N* curve. The *S*-*N* curve describes the relationship between applied cyclic stress, σ, and the number of cycles to failure, N_f. In the typical *S*-*N* curve, the number of cycles to failure, $N_{f,}$ is given on logarithmic scale on the horizontal axis of the graph. On the vertical axis (either linear or logarithmic) the stress amplitude, σ in MPa.

For example, in the case of carbon steel, the fatigue limit of the material is defined as the applied stress amplitude for which the material or structure does not fail even after more than 10^7 cycles. The fatigue limit is different for different materials. Carbon steel and its alloys show a clear fatigue limit but nonferrous materials like copper, aluminum and their alloys, and brass do not show a clear fatigue limit.

Fatigue failure can be divided into three stages as follows,

1. Crack initiation
2. Crack propagation, and
3. Final failure.

The first stage of fatigue is the crack initiation stage. With few exceptions, in high-cycle life testing, fatigue cracks initiate from the surface of the specimen. However, if there is any material defect present, cracks tend to nucleate at subsurface flaws of unusual severity. Given in instances where subsurface crack nucleation was observed, the life of the part is governed by the cracks that initiate at the surface.

The second stage of fatigue is the crack growth stage. For an example of a small-scale yielding case, when a constant cyclic stress range, $\Delta\sigma$ (= σ_{max} - σ_{min}), is applied to a cracked or defective structure, stable fatigue crack growth occurs at stress levels which are below the yield stress of the material. In fact, the range of the stress intensity ΔK, where $\Delta K = K_{max} - K_{min}$ in a cycle may also be well below the materials fracture toughness. The reason is that the material near the crack tip is under severe plastic deformation. Since the stress-strain field near a crack tip is uniquely determined by the stress intensity factor, fatigue crack growth rates can be correlated to ΔK. In cases outside (other than) of small-scale yielding, the parameters related to the yielding area in front of the crack and *J*-integral are used for evaluation of crack growth.

Fatigue failure refers to the fracturing of any given material due to the progressive cracking of its brittle surface under applied stresses of an alternating or cyclic nature. Over time, fatigue failure can lead to safety issues and the premature loss of critical infrastructure.

Generally, the components of machine structures have a notch or defect. There is stress concentration around the notch or defect. Stress concentration factor, α, which reflects the severity of a notch or hole or defect in the structure, is defined as the dimensionless ratio of the maximum stress at the root of a notch or hole or defect, to the nominal applied stress. The stress concentration factor can be evaluated using analytical, numerical and experimental techniques; for common notch shapes the values of α can also be obtained from tables and charts which can be referred in Engineering handbooks. The relatively shallow notches and plural defects can cause high stress concentration. The presence of a notch or defect can be critical to the safety of components made of brittle materials.

1.2 Detection of a Dangerous Situation by Fatigue Crack Growth in Metal

In terms of fatigue, critical parts of structures, vehicles, and machines, fatigue crack propagation under service conditions generally involves random or variable amplitude rather than constant amplitude loading conditions. Under fluctuating stress condition, i.e., during the application of overload and underload, the crack growth rate may vary, that is the significant retardation and acceleration in the crack growth rate occur which makes it difficult to quantitatively predict the crack propagation behavior and fatigue life. Therefore, good understanding regarding overload and/or underload, are very important to develop the damage tolerance design and life prediction methodology.

There have been numerous research studies conducted to determine the crack growth rate phenomena, which include the experimental studies [1-8]. Among them, the plasticity induced crack closure concept suggested by Elber has attracted much attention. Elber introduced the effective stress intensity factor range as a fatigue crack tip driving force, emphasizing the significance of the crack closure phenomenon of cracks.

As unstable crack growth may bring catastrophic failure of the machine structure or engineering material due to the application of dangerous load, it is necessary to detect whether an overload or underload was applied or not during machine operation. It’s been established by

researchers that a crack initiates from the stress concentration region of the machine structure in its loading condition, and crack initiation from a notch can be detected by using a strain gage during operation [9-11]. Nondestructive testing offers detection of crack initiation in the structure, which is very effective, but the disadvantage of this method is that, the machine operation needs to be stopped to inspect machine parts. On the other hand, crack initiation and propagation in the machine structure can be observed and detected by using strain a gauge during the machine operation, i.e. there is no suspension or stoppage time required to detect crack initiation and propagation during machine operation.

1.3 Crack Growth Behavior in the Case of a Composite.

The deformation and fracture phenomena of the composites are somewhat different from those of metals. Some composites of light weight show higher strength than steel. However, anisotropy behavior of fracture is observed in a composite material. Therefore, care should be taken when a composite is used for machine equipment.

Facing the uncompromising requirements for fuel economy in the automotive and aircraft industries, composite materials are seen to be used for structural light weight. Carbon fiber reinforced epoxy composite materials are among the engineering materials with the highest stiffness to weight and strength to weight ratio [12-14]. Since structural components may be subjected to complex cyclic loading, fatigue fractures can become one of the crucial causes of failure. Therefore, from the point of view of safety, an accurate assessment of fatigue life and loading conditions for carbon fiber reinforced epoxy composite components is essential.

Composites made from prepregs have a number of drawbacks due to the manufacturing process used. These materials have a higher tendency towards delamination, i.e. formation and growth of interlaminar cracks that propagate through interfacial bonding under both static and fatigue conditions. This characteristic decreases the stiffness and strength and affects the mechanical behavior of the material and can significantly reduce its service life. During the last few decades scientists and researchers have been making efforts on the importance of the phenomenon of interlaminar fractures, it is still a matter of concern that limits the use of laminates in structural components.

It should be noted that the specimens used for tension-tension (T-T) fatigue life tests are usually longer than those for tension-compression (T-C) and compression-compression (C-C) fatigue tests

[29]. There are several methods to determine the fatigue limit and strength of the materials like the *S-N* curve, Load Increase Test (*LIT*) method etc. The fatigue limit is defined by the maximum stress amplitude that the specimen can withstand 10^6 repetition stress cycles for the use of the *S-N* curve. The highest fatigue limit may be obtained when all the fiber directions are parallel to the loading direction and tested in tension-tension (T-T) loading condition. By comparing the fatigue limit of slit or partially notched specimens, the fatigue limit of unnotched or plain specimens can be determined. The experimental results obtained from the above fatigue test can be used for maintenance purposes of the machine structure. But before using these results, more testing and evaluation is required.

1.4 Prediction of Fatigue Life and Strength.

For the maintenance of the machine structure, monitoring crack initiation is important. Also, the prediction of fatigue life and evaluation of fatigue limit are important for keeping the safety of the machine structure. Some machine structures made with pure materials i.e. material having no impurities and no inclusions and subjected to tensile load may fail down by reducing the area of testing section for its work hardening properties [15]. A crack nucleates and propagates by overcoming interatomic strength and grain boundaries of the material. On the other hand, materials containing inclusions and internal defects may fails earlier than anticipated fatigue life due to the application of much lower loads. A crack nucleates at the inclusion and the crack grows from the inclusion. If there are multiple inclusions, multiple cracks initiate. Once the crack initiates, further application of stress causes each crack to increase independently. Upon further growth, a crack interacts with its neighboring crack and eventually they combine to form a unified longer length of crack which leads to the final fracture of the structure.

Scientists and researchers have spent plenty of time to understand the fatigue phenomena, fracture mechanism and their governing equation and established some parameters to determine the fatigue strength. Among these, yield strength σ_Y, ultimate tensile strength σ_B, and hardness *HV* or H_B attract interest; and ultimate tensile strength and hardness are being used from early on to determine the fatigue limit through the following equations:

$$\sigma_w = 0.5\sigma_B \tag{1.2}$$

$$\sigma_w = 1.6HV \tag{1.3}$$

But there are some limitations for the application of the above Eq. (1.2 & 1.3) [18, 26] because these equations are only valid for plain specimens or material having no pre-cracks or defects or inclusions.

Normally the manufacturing process has developed, and now-a-days Additive Manufacturing technology is being used to produce structural material with improved mechanical characteristics. Despite having more advantages now in the production of more complex geometric components, disadvantages like defects, micro-cracks or inclusions are still concern for flawless manufacturing procedure. These cause decrease in the fatigue strength of the materials.

Based on the above discussion, it was necessary to determine the fatigue limit of the structural material with consideration of defects, pre-cracks, inclusions whatever it contained in the structural material. But the size and shape of the defect and inclusion are too complex to unite and therefore the evaluation of the fatigue limit of the material containing defects and inclusions is too difficult. To mitigate this problem, many researchers have investigated the effect of defects and inclusions but Murakami and Endo [18] have given a comprehensive and quantitative evaluation for various sizes of defect and inclusion and proposed the following equation to evaluate the fatigue limit accurately which is being widely used.

$$\sigma_w = \frac{1.43(HV + 120)}{(\sqrt{area})^{1/6}} \tag{1.4}$$

In this equation, Vickers Hardness (*HV*) represents the material properties and √area is described as the geometrical parameter of the defect or inclusion of the material. Unit of area is considered as μm (micrometer). To calculate the area used in Eq. (1.4) defect or inclusion size was measured, then the crack initiation size was measured from the specimen surface which is considered as the defect or inclusion size [27]. Then the area was calculated based on the following semi-circle equation;

$$\text{Area} = \pi (l^2)/8 \tag{1.5}$$

here l is the crack initiation length or defect length.

Generally, defects or inclusions exist in various sizes in materials. Therefore, the crack initiation length also varied. The following is attempted to explain this. To evaluate the crack

growth rate under various conditions of crack initiation length, the fatigue life N_f is corrected by the following parameter λ [28];

$$\lambda = (1+\beta)\, N/N_f \tag{1.6}$$

where, 'β'represents the corrected value which is difference for different size of crack initiation length due to the defect or inclusion contained in the material. N/N_f is the dimensionless relative number of cycles.

By analyzing and measuring the crack initiation size or critical defect size, it is possible to predict the fatigue life and fatigue limit of a structural component having unknown defects or internal cracks.

1.5 Outline of Present Dissertation

Based on the explanation above, the following experimental studies were performed to understand the landscape of fatigue phenomena, fatigue life, fatigue limit, detection method of dangerous load application, crack growth behavior, prediction of fatigue life and limit, etc.

1.5.1 A method for detecting an unexpected application of a hazardous load during operation.

A method for detecting the application of an unexpected dangerous load was investigated. An acceleration behavior of crack growth due to the application of overload and or underload during fatigue crack growth test with constant stress amplitude was observed. In some cases, the acceleration of crack growth brings catastrophic failure in machine structures. Therefore, it is useful for machine maintenance to know whether an unexpected load was applied or not by doing a daily inspection. In the present study by using a center-crack specimen, a simple method of detecting the application of overload or underload was investigated. Such an unexpected load can be detected by the waveform of the function of stress and strain in the vicinity of the crack.

1.5.2 Method of detecting unexpected load leading by using strain information.

The crack growth can accelerate after applying as unexpected overload or underload during the usual operation of a machine structure. An acceleration or deceleration of the crack growth was observed depending on the experimental conditions. In the present study, a method of detecting the application of an unexpected hazardous load, that is a high level of overload or

underload, was investigated. It is expected that the acceleration of crack growth brings catastrophic failure in a machine structure. Therefore, it is useful for machine maintenance to know whether an unexpected load was applied or not by doing daily inspection. In the present study by using center-crack specimens, a simple method of detecting the application of overload or underload was investigated by using strain information.

1.5.3 Effect of fiber direction and stress ratio on fatigue property in carbon fiber reinforced epoxy composites.

The fatigue limit and crack growth behavior of slit specimens of carbon fiber reinforced epoxy composites were investigated. The fatigue limit was defined by the maximum stress amplitude that the specimen endured 10^6 times repeated stress when the *S*-*N* curve was used. The highest fatigue limit was obtained when all the fiber directions were parallel to the load axis. The fatigue limits were evaluated in the cases of composites using laminate layers alternately parallel and perpendicular to the load axis which were then compared with the results of specimens where all the carbon fiber orientations were parallel to the load axis. When the measured value of the fatigue limit was lower, shear damage to the epoxy resin and peeling of fiber from epoxy resin occurred clearly. According to those results, it was expected that the fatigue limit of smooth specimens of carbon composites with long fibers can be evaluated from the results of the slit specimens.

1.5.4 Fatigue and fracture mechanism of aluminum-carbon fiber reinforced hybrid composites.

The fatigue limit and fracture behavior of epoxy carbon fiber reinforced composites and hybrid composites were investigated. Aluminum foil or a thin aluminum plate was incorporated with the carbon fiber to make the hybrid reinforced composites. Several specimens were prepared, and a series of fatigue tests were carried out to investigate the fatigue life and fracture behavior. Then the results were compared between the epoxy carbon fiber reinforced composites and the hybrid composites. It is discussed whether the *S*–*N* curves show similar characteristics for these two types of hybrid composites or not. As for the present result, the stress ratio and the type of hybrid composite affect the fatigue life. The interfacial bonding plays an important role in the strength and fracture behavior of notched specimens of the fabricated composites.

1.5.5 Effects of existence of unexpected defects on fatigue strength.

There is a good correlation between the static strength and fatigue limit in many carbon steels. However, in the case of some commercially sold carbon steel, the fatigue limit cannot be evaluated from the static strength. Care should be taken when those materials are used for machine equipment. In the case of some materials, there is a decrease in fatigue limit from the expected values of Vickers hardness. In this study, one such case was investigated by push-pull. The examinations of the *S-N* curves and crack growth behavior were performed. Then, it was discussed that the decrease in the fatigue limit was related to the existence of defects of unexpectedly large size. The material tested is not expected to be used for machine equipment. However, it is not good if such materials are sold without any warning about the existence of such defects.

1.5.6 A method for prediction of fatigue limit and life of carbon steel.

There is a good correlation between the *S-N* curve and the crack growth law in carbon steel. Also, the fatigue limit of that can be evaluated from the parameters of hardness and crack initiation conditions. The crack initiation behavior is related to the distribution of microstructures and the sizes of inclusions. Therefore, when the fatigue limit and life of carbon steel are predicted, it is better to consider the initial crack length and crack growth behavior. In this study, one such case was investigated by push-pull with constant stress amplitude by using 0.45% carbon steel. The initial crack lengths were varied with the specimens used and testing conditions. The prediction method of the *S-N* curve from a corrected crack growth law in such case was proposed. Also, a method of prediction of fatigue limit and life from the point of safety was discussed in this study.

The last section of the present thesis lists is the conclusions based on this dissertation and provides suggestions for further research directions.

1.6 Conclusion

Fatigue is a failure at relatively low stress levels of structures that are subjected to fluctuating and cyclic stresses. Fatigue testing is conducted to determine fatigue limit so the load that applied must under the fatigue limit to make sure that the specimen is in safe condition. Fatigue limit is the maximum stress amplitude level below which material can endure an essentially infinite number of stress cycles and not fail. Therefore, this testing is important to know the fatigue limit.

The factors that affect fatigue life is mean stress $\sigma_{m,}$ which is when reduced the mean stress will be increased the fatigue life. The surface face also will affect the fatigue life. Consequently, most

cracks leading to fatigue failure originate at surface positions specifically at stress amplification sites. It can be reduced by polishing the surface. Beside eliminating sharp surface discontinuities and imposing surface residual compressive stresses by shot peening also can be increased fatigue life.

The failure may be due the discontinuity, poor design, improper maintenance, or other causes. A failure analysis can determine the cause of the failure. Therefore, redesign can be taken to solve the problems. The fatigue testing is one of fracture analysis to know the fatigue limit to make sure that the engineers design the product in safe condition.

1.7 Reference

[1] W. Elber, "The Significance of Fatigue Crack Closure," ASTM STP 486. ASTM International, West Conshohocken, pp. 230-242, PA 1971.

[2] A. J. McEvily, "Current Aspects of Fatigue," Metal Science, Vol. 11 (1077), pp. 274-284.

[3] A. J. McEvily, Z. Yang, "The Nature of the Two Opening Levels Following an Overload in Fatigue Crack Growth," Metallurgical Transactions, Vol. 21A, pp. 2717-27, 1990.

[4] H. Bao, A.J. McEvily, "The Effect of Overload on the Rate of Crack Propagation under Plane Strain Conditions," Metallurgical and Materials Transactions, 26A, pp.1725-1733, 1995.

[5] D. H. Chen, H. Nisitani, "Analytical and Experimental Study of Crack Closure Behavior based on an S Shaped Unloaded Curve," ASTM STP 982, Mechanics of Fatigue crack Closure, pp. 475-488, 1988.

[6] C. M. Ward-Close, A.F. Blom, O. R. Richie, "Mechanism Associated with Transient Fatigue Crack Growth Under Variable-Amplitude Loading: An Experimental and Numerical Study," Engineering Fracture Mechanics, Vol. 32, pp. 613-618, 1989.

[7] C. Makabe, A. Purnowidodo, A. J. McEvily, "Effects of Surface Deformation and Crack Closure on Fatigue Crack Propagation After Overloading and Underloading," International Journal of Fatigue, Vol. 26, pp. 1341-1348, 2004.

[8] C. Makabe, A. Purnowidodo, T. Miyazaki, A. J. McEvily, "Deceleration and Acceleration of Crack Propagation After an Overload under Negative Baseline Stress Ratio," Journal of Testing and Evaluation, Vol. 33, pp.181-187, 2005.

[9] C. Makabe, H. Kaneshiro, "A Method of Detecting the Fatigue Crack Initiation and Growth in a Holed Specimen Based on Crack Tip Opening and Closing," Engineering Fracture Mechanics, Vol. 41, pp. 395-403, 1992.

[10] C. Makabe, H. Kaneshiro, S. Nishida, C. Urashima, "Detection of 1 mm Fatigue Crack Initiation Using Strain Waveform," Journal of Engineering Materials and Technology, ASME, Vol. 116, pp.483-487, 1994.

[11] C. Makabe, A. Purnowidodo, T. Sueyoshi, T. Utsunomiya, “Detecting Overload From Strain Information During Fatigue Crack Propagation Under Negative Stress Ratio,” Testing and Evaluation, Vol. 32, pp. 56-61, 2004.

[12] Haolong Liu, Avinesh Ojha, Ziang Li, Carlos C. Engler-Pinto Jr., “Xuming Su, Qingping Sun, Hongtae Kang, Weidong Wen, Haitao Cui, “Fatigue Modeling for Carbon/Epoxy Unidirectional Composites Under Various Stress Ratios Considering Size Effects.” International Journal of Fatigue, Vol.120, pp.184-200, 2019.

[13] C. Makabe, M. Fujikawa, M.S. Ferdous, S. A. Setyabudi, Journal of High-Pressure Institute, Vol.51, No. 6, pp. 303, 2013.

[14] C. Makabe, T. Nakayama, M. Fujikawa, K. Arakawa, D. Chen, Advanced Materials Research, Vol. 1110, p. 13, 2015.

[15] Y. Murakami, Metal Fatigue, Elsevier Science Ltd., Oxford pp.1-128, 2002.

[16] S. Nishida; “Failure Analysis in Engineering Applications”, Butterworth-Heinemann Ltd, pp. 1-5, 1991.

[17] M. F. Garwood, H. H. Zurburg and M. A. Erickson; “Correlation of Laboratory Tests and Service Performance”, Interpretation of Tests and Correlation with Service, ASM, Publication, PA, pp. 1-77, 1951.

[18] Y. Murakami and M. Endo; “Effects of Hardness and Crack Geometry on ΔKth on Small Cracks”, J. Soc., Mater. Sci., Japan, Vol. 35, No. 395, pp. 911-917 (1986).

[19] C. Makabe, S. A. Jafari, K. Ishikawa and T. Miyazaki; “A Study on Relationship Among Crack Initiation Size, Fatigue Limit and Hall Petch Relation”, J. Soc., Mater. Sci., Japan, Vol .66, No. 5, pp. 365-371, 2017.

[20] Mechanical system design handbook, “Fatigue Strength of Steels”, URL of Japanese Standard Association Group, http://ebw.engbook.com/pdfs/ecb7c8688913e12a4494 93 9494498e79.pdf#search='%E7%82%AD%E7%B4%A0 %E9%8B%BC%E3%81%AE% E7%96%B2%E5%8A% B4%E5%BC%B7%E5%BA%A6'（2012）

[21] H. Nisitani and K. Takao; “Significant if Initiation, Propagation and Closure of Microcracks in High Cycle Fatigue of Ductile Metals”, Eng. Frac. Mech., Vol. 15. No. 3-4, pp. 445-456, 1981.

[22] H. Nisitani and M. Goto; “Effect of Stress Ratio on the Propagation of Small Crack of Plain Specimen Under High and Low Stress Amplitudes (Fatigue Under Axial Loading of Annealed 0.45% Carbon Steel)”, Tras. Japan Soc. Mech. Eng., Ser. A., Vol. 50, No. 453, pp. 1090-1096, 1984.

[23] Y. Murakami, Md S. Ferdous and C. Makabe; “Low Cycle Fatigue Damage and Critical Length Affecting Loss of Fracture Ductility”, Int. J. Fatigue, Vol. 82, No. 1, pp. 89-97, 2016.

[24] Y. Nakai, K. Tanaka and Y. Kawashima; “Propagation and Non-Propagation of Fatigue Cracks in Notched Plates of Low-Carbon Steel”, J. Soc., Mater. Sci., Japan, Vol. 32, No. 356, pp. 535-541, 1983.

[25] A. J. McEvily, “Metal Failure”, John Wiley & Sons, Inc., (2002)

[26] T.Isibashi, “Strength of Metals for Design Engineers (in Japanese)”, Yokendo Ltd., Tokyo, pp.16, 1965.

[27] Chobin Makabe, Shinya Yamazaki, Tatsujiro Miyazaki, Masaki, Fujikawa, “Fatigue Life and Crack Growth Behavior in Annealed and Normalized 0.83% Carbon Steel,” Surface Review and Letters, Vol.22, No.1, pp. 1550001-10, 2015.

[28] Chobin Makabe, Hideo Kaneshiro, Masaya Itokazu, “Fatigue Crack Propagation and Life of Specimen with Inclusion in A Low Cycle Fatigue Regime,” Proceedings of the Third International Conference on Very High Cycle Fatigue (VHCF-3), pp.232-239, 2004.

[29] Haolong Liu, Avinesh Ojha, Ziang Li, Carlos C.Engler-Pinto Jr., XUMing Su, Qingping, Sun, Hongtae Kang, Weidong Wen, Haitao, Cui, “Fatigue modeling for carbon/epoxy unidirectional composites under various stress ratios considering size effects”, International Journal of fatigue, Vol.120, pp.184-200, 2019.

Chapter Two

A Method for Detecting an Unexpected Application of a Hazardous Load During Operation

2.1 Introduction

The fatigue crack growth rate would vary from an expected situation when stress amplitude fluctuates. It is well known that the crack growth decelerates or accelerates when an overload or an underload is applied during the crack growth test with constant stress amplitude [1-8]. The focus of the present study is the acceleration behavior of fatigue crack growth. If the crack growth rate becomes higher, a machine structure or equipment will be in a dangerous situation.

The crack growth rate after overloading and underloading is related to the formation of residual stress in front of the crack tips. The crack opening stress is affected by the residual stress conditions. It is well known that the crack growth rate can be summarized with effective stress intensity factor range ΔK_{eff} [1-8]. The crack growth can be evaluated by the ΔK_{eff} to know whether the crack growth rate accelerates or decelerates after applying overload or underload. Therefore, to understand the crack growth behavior, crack opening and closing behavior should be evaluated.

The acceleration of crack growth is dangerous, because there is the possibility of catastrophic failure in machine structure due to unstable crack growth. If cracks grow stably, the crack length after definite loading cycling can be predicted under the application of a crack growth law. In that case, the applied load can be evaluated or measured. When an unexpected load is applied during machine operation, it is important to know whether a dangerous overload or underload is applied or not. In the present study, the main objective is to detect the application of an unexpected load which leads to the acceleration of the crack growth. The crack initiation from a notch can be detected by using a strain gage during the operation [9, 10]. That method was applied to detect the application of the overload during fatigue test with constant stress amplitude in the previous study [11]. This work was improved in the present study and was understood that crack opening and closing behavior is strongly related with the acceleration of crack growth. In this paper, is shows the effectiveness for detecting a dangerous load by evaluating the relationship in the variation between local strain and applied stress.

2.2 Material and Crack Growth Testing Procedure

The material used for the experiment was 0.15% carbon steel. This is called JIS-S15C in Japan (JIS = Japanese Industrial Standards). The chemical compositions and mechanical properties of the material are shown in Table 2.1. A center-cracked type of specimen was employed in this experiment. Figure 2.1 shows the specimen geometry and the positions where strain gages were pasted on. Dimensions of the specimens are 20 mm in length and 4 mm in width. A notch of 4 mm in length was cut in the center section of the flat part of specimen by electric discharge machine. Then the specimens were polished by emery paper and metal polisher.

Before the main experiment, about 1 mm of crack was introduced from both sides of the notch root by a pull-push hydraulic fatigue testing machine. The initial crack length of the present specimen is about 6 mm which includes notch length of 4mm.

After annealing at 600˚C for 1 hour in a vacuum furnace, strain gages were pasted on the specimen surface as shown in Figure 2.1 to detect an unexpected load application. The fatigue crack growth tests were carried out using a hydraulic testing machine with a constant loading frequency of 10Hz with negative stress ratio R= -1 in laboratory room conditions. Figure 2.2 shows the overview of the equipment used for testing. Overload or underload was applied when the crack length reached about 6 mm. This crack length is defined as including the notch length. The crack opening and closing stresses were measured by using the strain gages. Crack length was measured by an optical microscope which was connected to an image display system device to make it easy to measure the crack length.

Table 2.1: Chemical composition and mechanical properties of 0.15% carbon steel (σ_S; Yield stress [MPa], σ_B; Ultimate tensile strength [MPa], ψ Reduction of area [%])

Chemical composition [wt., %]									Mechanical properties [MPa, %]		
C	Si	Mn	P	S	Cr	Ni	Cu	Fe	σ_S	σ_B	ψ
0.15	0.30	0.50	0.013	0.013	0.19	0.05	0.14	Bal.	283	449	60

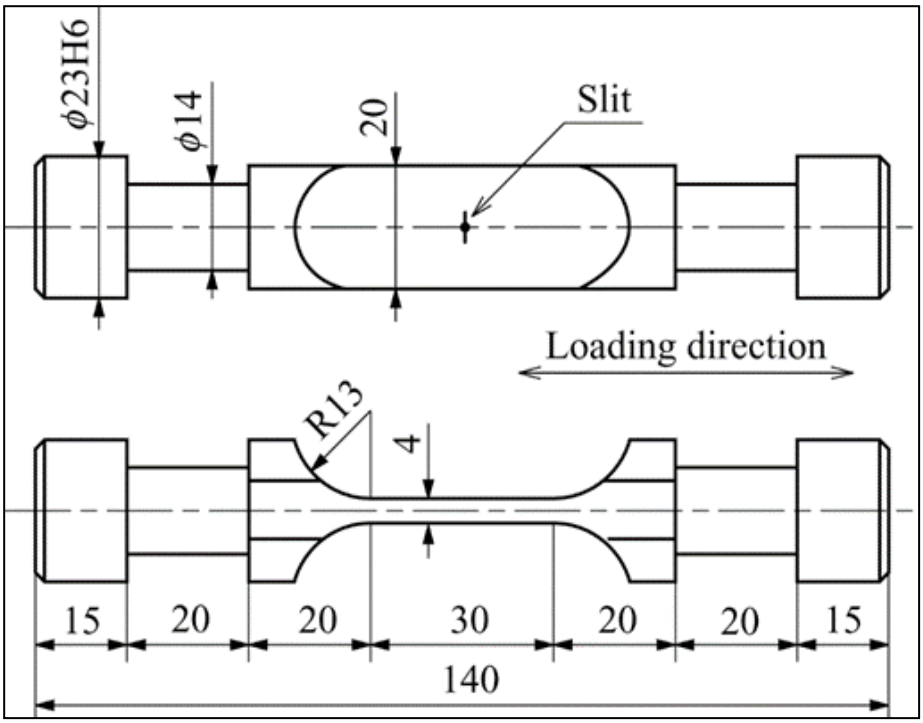

(a)

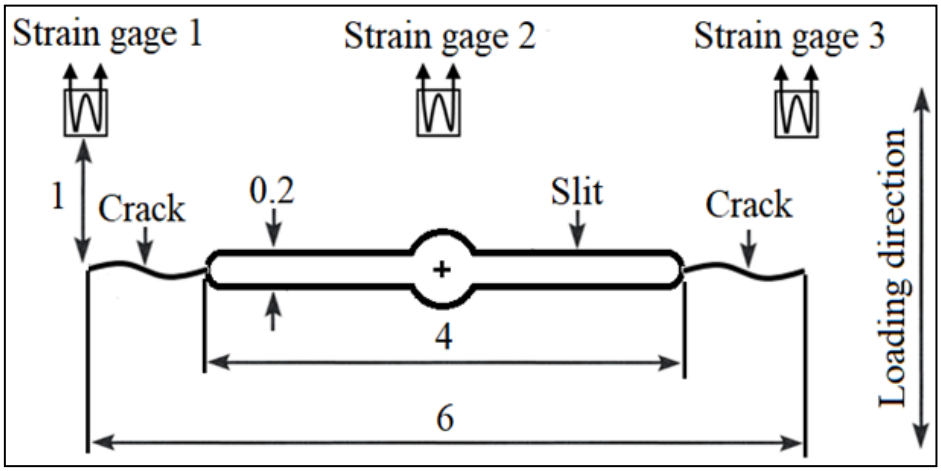

(b)

Figure 2. 1 (a) Geometry of the specimen and (b) Position of strain gages (Unit: mm)

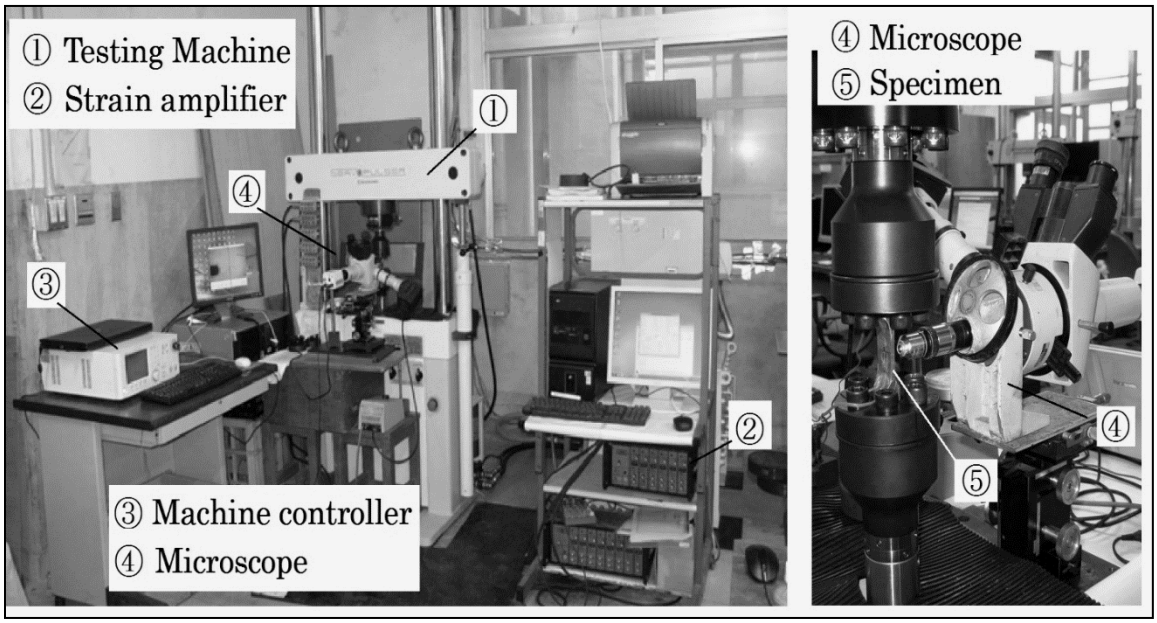

Figure 2. 2 Fatigue testing machine and procedure

2.3 Method of Measuring Crack Opening and Closing Stresses

There are some methods of measuring crack opening and closing stress. We employed the "Unloading elastic compliance method" which was proposed by Kikukawa et al. [12]. Figure 2.3 shows the schematic representation of that method of the present study. Due to the applied stress level and positions of pasted strain gages, the hysteresis loops of stress - strain curve showed different shapes depending on the elastic-plastic behavior. First of all, the gradient C of the stress σ - strain ε relation on unloading stage within a range of $0.9\sigma_{max}$ - $0.6\sigma_{max}$ was measured. Then the following strain function was calculated,

$$H_i = \varepsilon_i - C\sigma_i \tag{2.1}$$

Where, $C = \Delta\varepsilon_i/\Delta\sigma_i$ in the range of $0.9\sigma_{max}$ - $0.6\sigma_{max}$ on unloading stage, and the subscript 'i' shows the measurement position of strain as shown in Figure 2.1.

As shown in Figure 2.3, the points of crack opening and closing stress are measured by turning points or changing points of curvature of $\sigma - H$ loop [5, 12]. In some cases, the minimum value of H coincides with the crack opening stress. Where, σ_{op} represents crack opening stress and σ_{cl} crack closing stress.

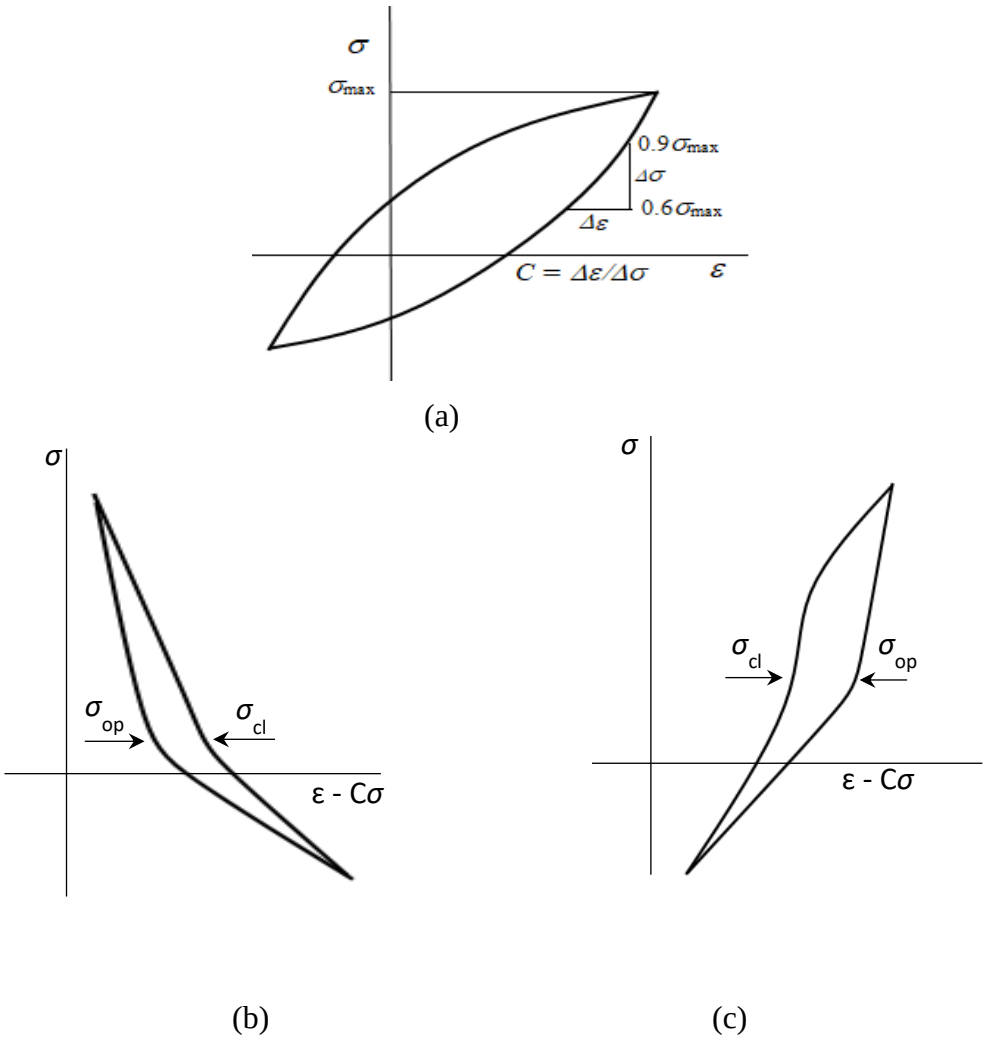

Figure 2. 3 Schematic representation of the measurement of the crack opening and closing stresses; (a) Original stress – strain loop, (b) σ vs. H in the case of $\varepsilon_e > \varepsilon_p$, (c) σ vs. H in the case of $\varepsilon_e < \varepsilon_p$; Where, ε_e is elastic strain and ε_p plastic strain.

2.4 Results and Discussion

There are some cases of machine failure related to metal fatigue [13, 14]. It is well known that the specimen does not fail immediately after the fatigue crack initiation. Thus, even if a fatigue crack is initiated, the machine structure can be available for work on condition that the fatigue crack growth behavior is safe or the fatigue crack stops growing [14, 15]. So, some machines were in operation for a limited term though a crack initiated in the equipment. When the crack length is measured and crack growth behavior is predicted by the crack growth law during operation when an unexpected load is not applied, the machine is controlled under safe conditions. However, once

an unexpected load is applied, the crack growth behavior changes. Sudden stopping of machine operation is affected to the loading conditions. The occurrence of an earthquake is expected to bring damage to machine structure. Such possible cases of unexpected load applications had better be considered.

In the present study, the acceleration of crack growth behavior was confirmed after the application of overloading and underloading during fatigue test with a center-cracked specimen with constant amplitude. Then a method of detecting the application of such an unexpected load was examined.

2.4.1 Crack growth behavior

The crack growth behavior after the application of overload and or underload was examined. After the application of such a load manually, the fatigue test was continued under the same testing conditions as that before the application. The following are conditions of manual load application; the case of overload and underload are σ_{ou} =185 MPa & -185MPa, -185 MPa & 185 MPa, -113 MPa & 113MPa and the cases of single underload are σ_{ul} = -113MPa, -185 MPa. Because it is known that the acceleration behavior tends to occur when the underload is applied in the cases of negative stress ratio [7, 8], the loading conditions of the present investigations was chosen. Now, the order of unloading and overloading was not affected by the tendency of the crack growth. Hereinafter, those loads are called unexpected load or unexpected stress, conveniently. Also, the symbols of unexpected stress are defined as follows, σ_{ul} is underload, σ_{ol} overload and σ_{ou} overload and underload. The crack growth test was performed with constant stress amplitude σ_a = 86 MPa with stress ratio R = -1.

Figure 2.4 shows the relationship between half-crack length a and number of stress cycles N. A series of fatigue tests were carried out to investigate the crack growth behavior. The crack growth behavior with the application of unexpected load was compared with that without unexpected load (which is the baseline of the present study's data). The arrow shows the application point of such unexpected load. In comparison with the baseline, the crack growth rate accelerated when the applied unexpected load was over some critical stress level. In the present study, the acceleration of crack growth was observed when σ_{ou} = ±185MPa. In the case of σ_{ul} = -113MPa, the crack growth rate was almost the same as that of the baseline. In the case of σ_{ou}= ±113MPa, the crack growth decelerated from the base line.

Figure 2.5 shows the relationship between the crack propagation rate *da/dN* and stress intensity *K* at maximum stress. It is clear that the crack growth rate is higher than the baseline when the unexpected load was applied with σ_{ou} = ±185MPa.

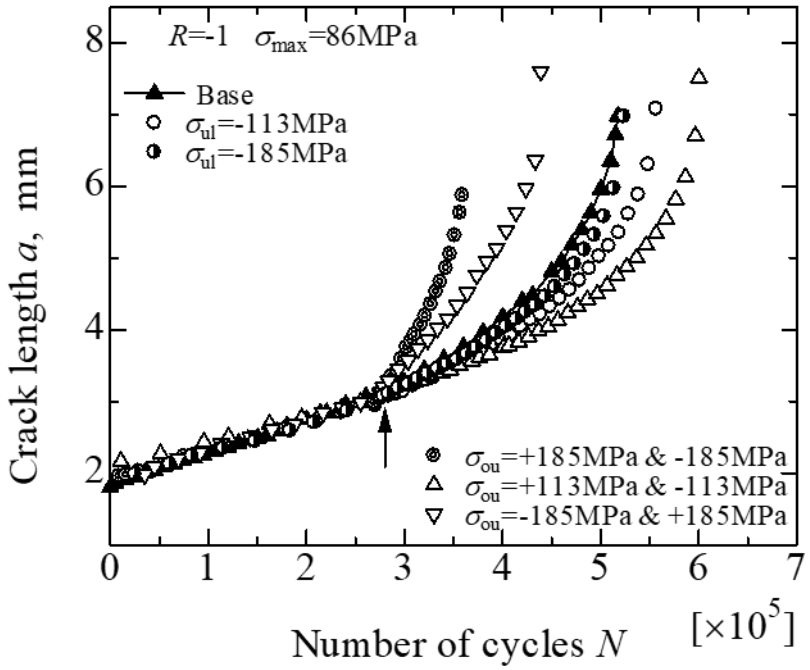

Figure 2. 4 Crack length *a* vs. number of cycles *N*

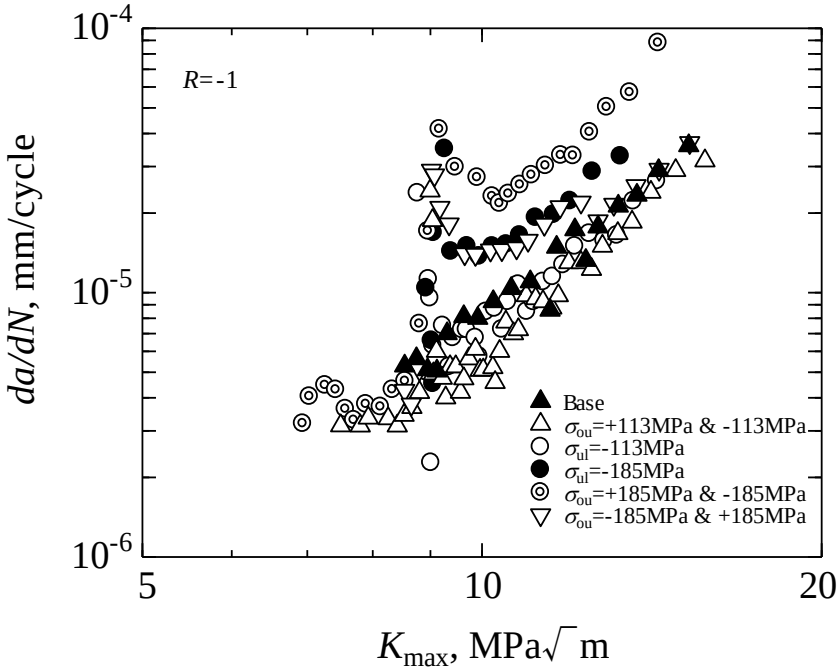

Figure 2. 5 *da/dN* vs. K_{max}

2.4.2 Detecting the application of dangerous load

To detect the application of a dangerous load, the crack opening and closing stresses was measured. Because the crack growth rate is evaluated well by using the effective stress intensity range which is determined by the crack opening or closing stress, even if fluctuating stress is applied [1-8]. When the crack opening and closing stress level became lower than the baseline case after applying an unexpected load, the crack growth rate became higher than the baseline case. On the other hand, the higher-level stresses of the crack opening and closing bring a lower crack growth rate after applying an unexpected load. Such behavior of cracks can be applied to the detection of the application of a dangerous load. So, we measured the crack opening and closing by using the loop and waveform of the stress σ and strain function H shown in Equation (2.1). Figures 2.6 and 2.7 show the loop and waveform of σ and H in the cases of overload and underload application. Figures 2.8 and 2.9 show those in the case of a single underload application. The loop and waveform shapes were compared before and after the unexpected load was applied. Their change is strongly related to the crack opening and closing behavior.

Figure 2.6 shows the case of σ_{uo}= -113MPa and 113MPa. Now, the data was taken at N = 313760 and a= 3.10mm before applying unexpected load, and at N = 322000 and a= 3.15mm after that. In the other cases, the data were detained in almost the same situation as the case of Figure 2.6. As shown in Figure 2.4 and 2.5, the crack growth was not accelerated after applying unexpected load. Also, the crack opening and closing stress were measured as shown in Figure 2.3. It is understanding from the loop of σ - H (Figures. 2.6 (a_1) and (b_1)) that the crack opening and closing stresses keep the value close to 0 MPa before and after the overload. When the crack opening and closing stresses hardly varied before and after applying an unexpected load, the crack growth did not accelerate after applying that. Whether a dangerous unexpected load was applied or not was examined by using the waveform shape of the strain function H after spending some time on the application of unexpected load. It is found that the crack opening and closing stresses were determined by the time where the waveform of strain function H showed the changing. The dotted lines show the times of crack opening and closing. In the case of Figure 2.6, that waveform hardly changed and the local maximum point and turning point of the waveform of H were crack opening and closing points.

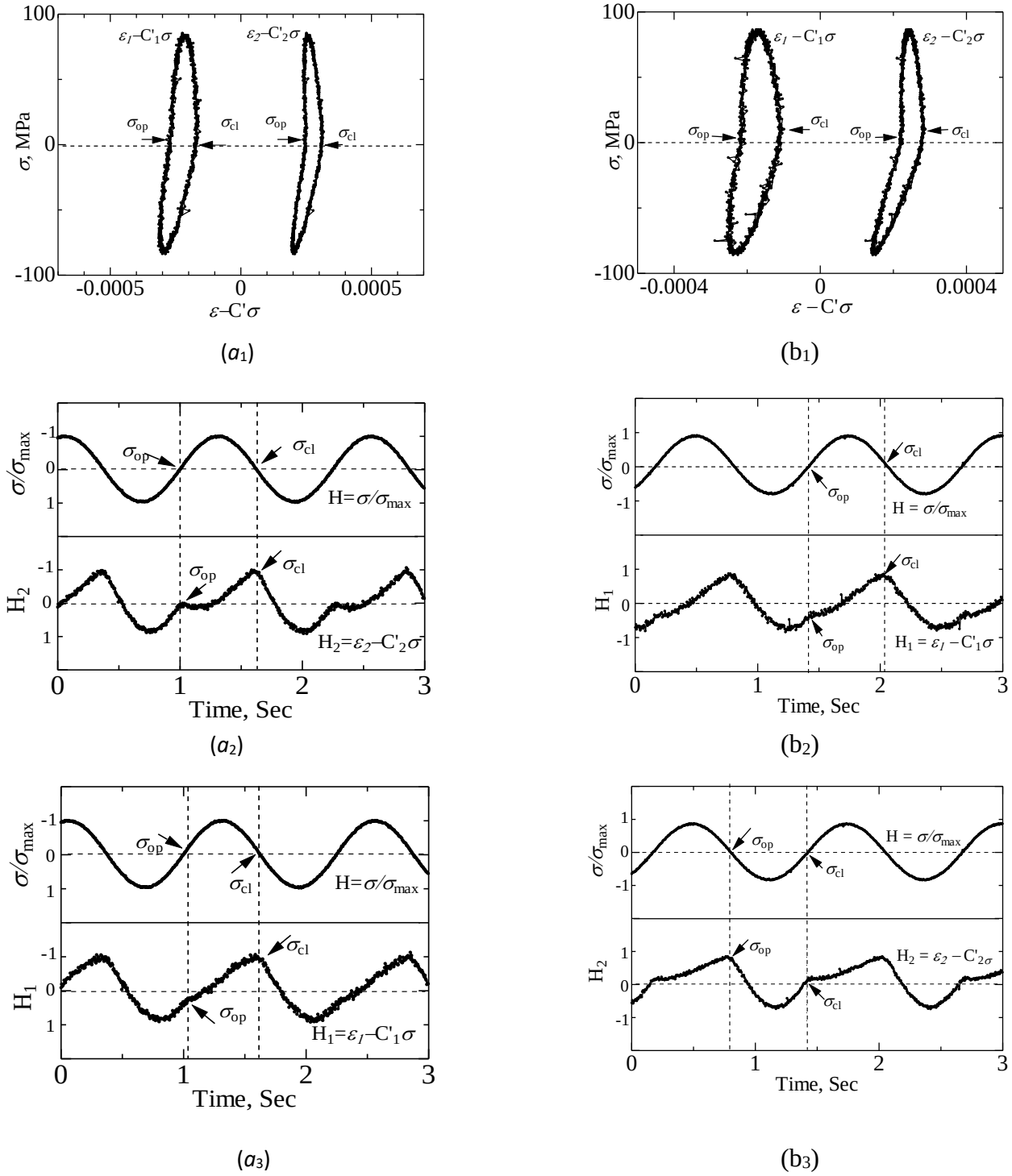

Figure 2. 6 In the case of σ_{ou} = -113MPa and 113MPa; (a) Before the application of overload (N = 313760, a= 3.10mm), (a_1) σ-H loop, (a_2) Waveforms of σ/σ_{max}, and H_1, (a_3) Waveforms of σ/σ_{max}, and H_2 ; (b) After the application of overload (N = 322000, a= 3.15mm), (b_1) σ-H loop, (b_2) Waveforms of σ/σ_{max}, and H_1, (b_3) Waveforms of σ/σ_{max}, and H_2

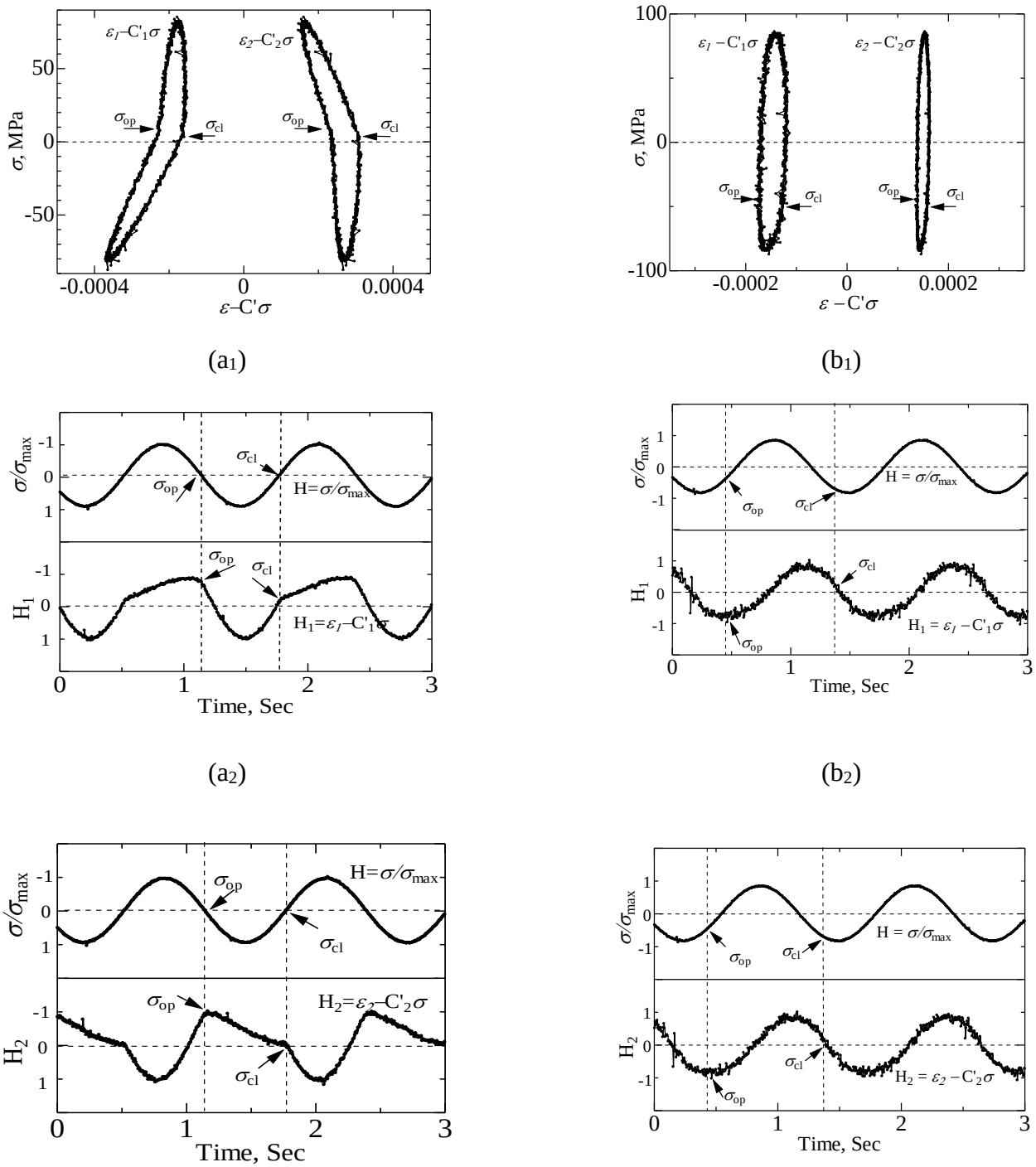

Figure 2. 7 In the case of σ_{ou} = -185MPa and 185MPa; (a) Before the application (N = 269005, a= 3.10mm), (a$_1$) σ-H loop, (a$_2$) Waveforms of σ/σ_{max}, and H_1, (a$_3$) Waveforms of σ/σ_{max}, and H_2 ; (b) After the application (N = 272609, a= 3.20mm), (b$_1$) σ-H loop, (b$_2$) Waveforms of σ/σ_{max}, and H_1, (b$_3$) Waveforms of σ/σ_{max}, and H_2

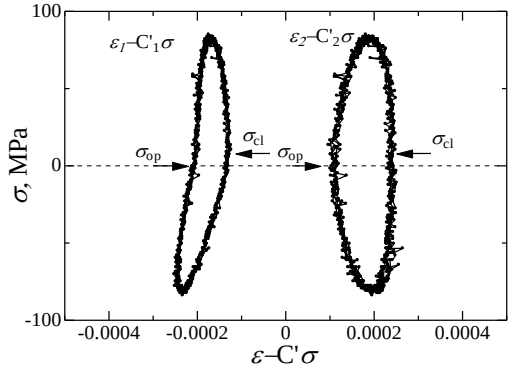

(a1)

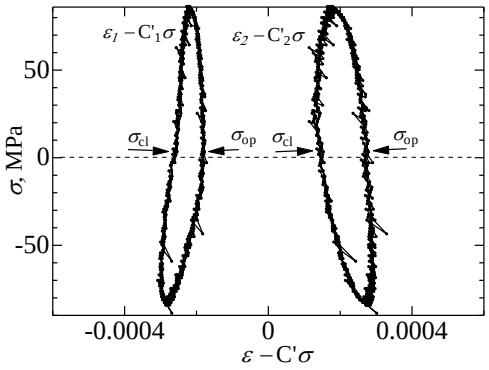

(a2)

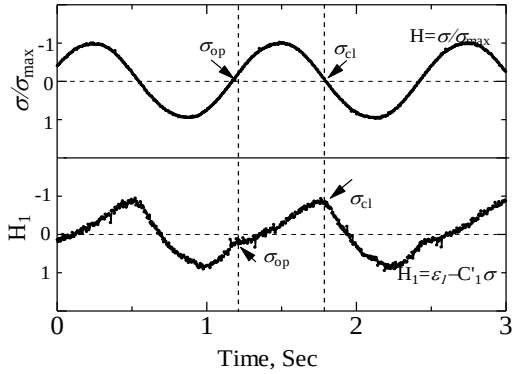

(a2)

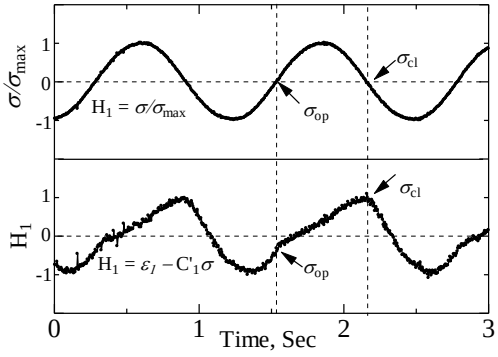

(b2)

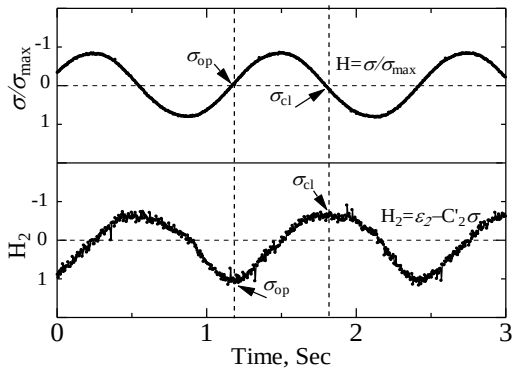

(a3)

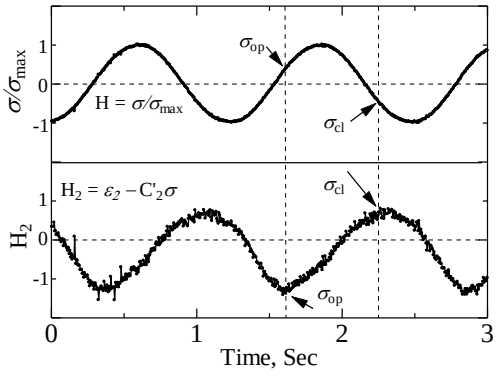

(b3)

Figure 2. 8 In the case of σ_{ul} = -113MPa; (a) Before the application (N = 20000, a= 3.10mm), (a1) σ-H loop, (a2) Waveforms of σ/σ_{max}, and H_1, (a3) Waveforms of σ/σ_{max}, and H_2 ; (b) After the application (N = 28506, a= 3.13mm (b1) σ-H loop, (b2) Waveforms of σ/σ_{max}, and H_1, (b3) Waveforms of σ/σ_{max}, and H_2

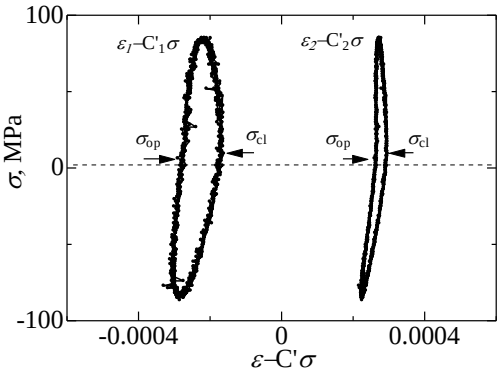

(a1)

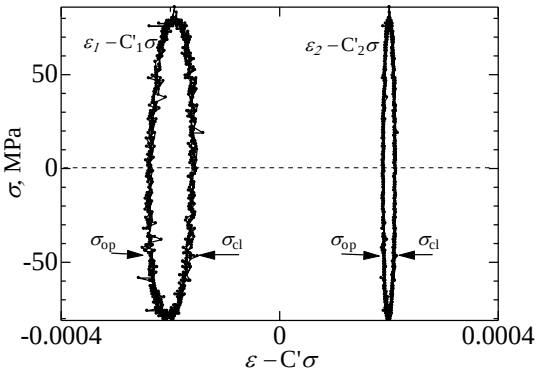

(b2)

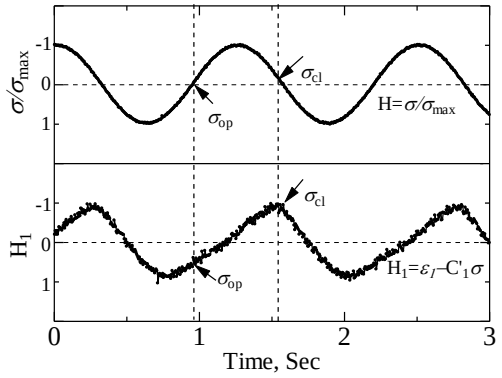

(a2)

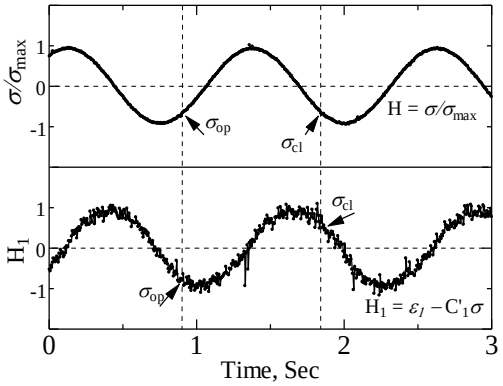

(b2)

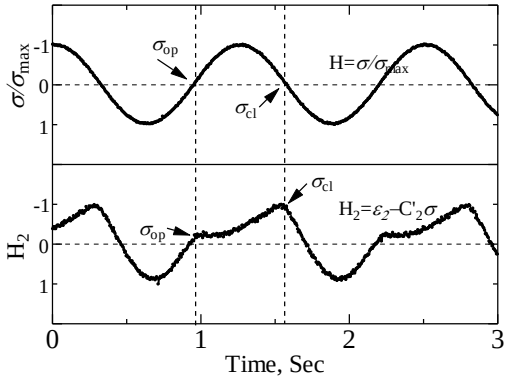

(a3)

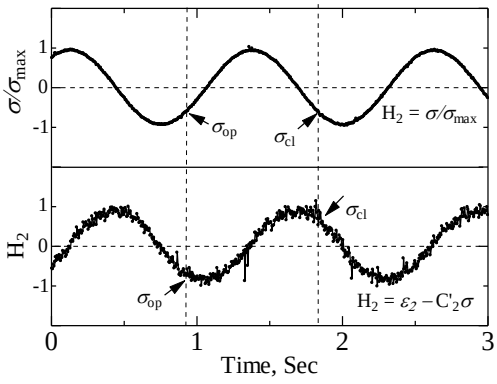

(b3)

Figure 2. 9 In the case of σ_{ul} = -185MPa; (a) Before the application (N = 240110, a=3.10mm), (a_1) σ-H loop, (a_2) Waveforms of σ/σ_{max}, and H_1, (a_3) Waveforms of σ/σ_{max}, and H_2 ; (b) After the application (N = 241108, a=3.13mm), (b_1) σ-H loop, (b_2) Waveforms of σ/σ_{max}, and H_1, (b_3) Waveforms of σ/σ_{max}, and H_2

Figure 2.7 shows the case of σ_{uo}= -185MPa and 185MPa. Since the crack growth accelerated after applying an unexpected load, the detection of changes in the loop and waveform is very important to detect the crack growth acceleration. It is found that the loop and waveform of σ and H after applying an unexpected load were changed from those before applying an unexpected load. Before applying an unexpected load, the loop and waveform were almost the same as the case of Figure 2.6 (a). However, in the case of Figure 2.7, the crack opening and closing stress moved to the negative stress level. Also, it is expected that the crack tip was fully opened just after applying unexpected load. In the case of Figure 2.6 (b), the shapes of the waveform H are clearly different from a sine waveform. However, in the case of Figure 2.7 (b), the turning points in the waveform H are not clear, and the waveform of this is closer to a sine waveform than the case of Figure 2.6 (b). Therefore, the application of a dangerous unexpected load by inspection of the waveform could be detected.

Human health can be checked by the electrocardiogram. We can check the waveform of strain function, like the electrocardiogram, continuously; then whether the dangerous load was applied or not can be detected. Therefore, it is better to continuously check the strain waveform for the purpose of inspecting machine health.

Similar results were obtained in the cases of Figure 2.8 and Figure 2.9. A single underload was applied in those cases. It is known that the acceleration of crack growth tends to happen in the case of applying an underload rather than in the case of applying an overload [10]. The purpose of the present study is to investigate a simple method of detecting the application of a dangerous load. In the present stage of study, it is found that the application of a higher level of overload and underload bring acceleration of crack growth, and those loads can be detected by the waveform of a strain function. In the future, the detailed condition of acceleration of fatigue crack growth will be investigated.

2.4.3 Observation in the vicinity of crack tip

The acceleration and deceleration of crack growth are related to the residual stress conditions in front of the crack tips. The residual stress conditions are related to the applied stress amplitude, stress ratio, and unexpected load levels. Also, crack tip deformation is related to the residual stress conditions [7, 8].

Figure 2.10 shows the observation results of crack tip. In the case of acceleration of the crack growth (σ_{ou} = -185MPa and 185MPa), from the comparison of the situation of the crack tip before (Figure 2.10 (b1)) and after (Figure.2.10 (b2) and (b3)) applying an unexpected load, it is observed that the crack tip was once blunted and sharpened again. As discussed by Makabe et al. [8], when the opened crack was closed again, tensile residual stress was created in front of the crack tip. Now, arrow shows the position of crack tip in Figure 2.10. In the case where the crack tip was not blunted much after applying an unexpected load as shown in Figure 2.10 (a), compressive residual stress was created in front of the crack tip. One of the mechanisms of crack growth acceleration and deceleration after applying an unexpected load is shown in the present paper. In future, the residual stress and strain distributions in the vicinity of the crack will be calculated, then a more effective method of detecting dangerous loads will be discussed.

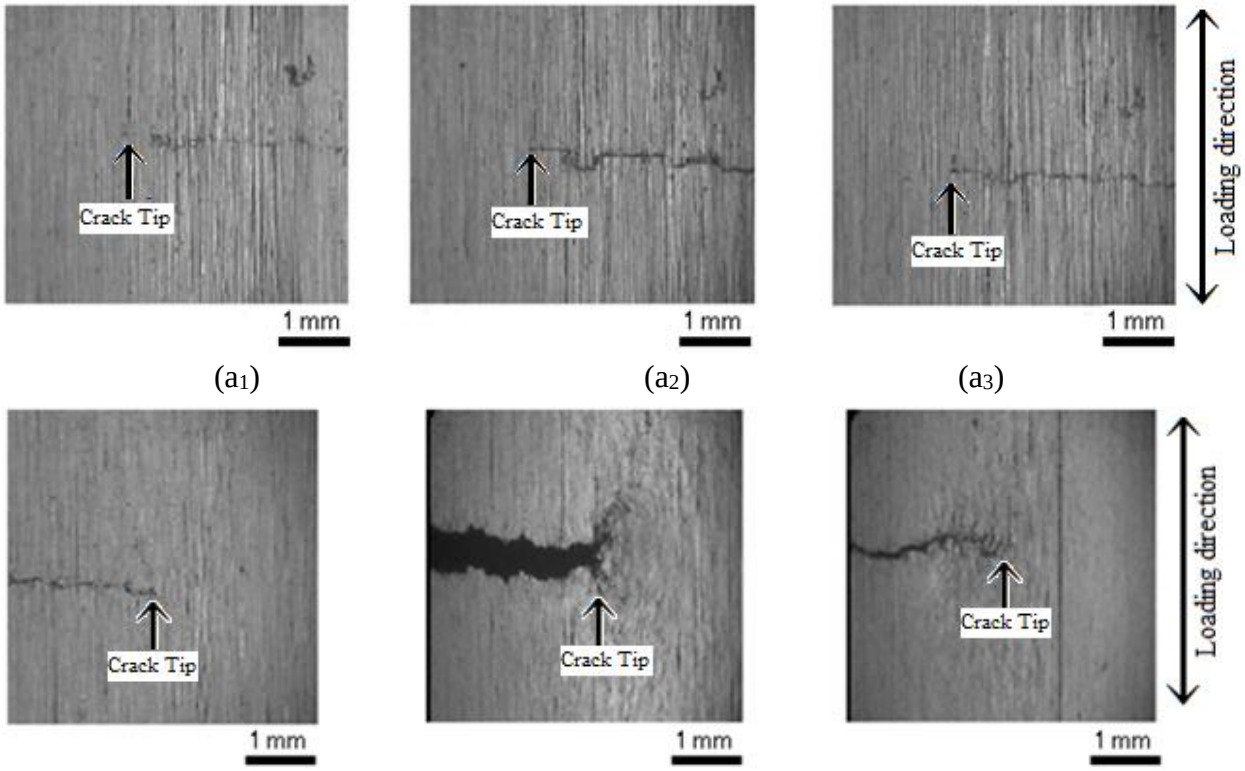

Figure 2. 10 Comparison of crack opening behavior after applying unexpected load: (a) In the case of σ_{ou} = -113MPa and 113MPa, (a1) Before application of overload and underload (N=313500, a=3.05mm), (a2) Just overloading (N=313760, a=3.10mm), (a3) After application of overload and underload (N= 314760, a= 3.12mm), (b) In the case of σ_{ou} = -185MPa and 185MPa, (b1) Before application of overload and underload (N=85229, a=2.35mm), (b2) Just overloading N=269000, a=3.10mm), (b3) After application of overload and underload (N= 272609, a= 3.20mm).

2.5 Conclusions

The method of detecting application of an unexpected load which leads to the acceleration of fatigue crack growth. The main results obtained are as follows:

(1) In the present study, an application of overload and / or underload was performed during fatigue crack growth test with constant stress amplitude. The acceleration of fatigue crack growth occurred when the tensile residual stress created in front of the crack tips and the crack opening and closing stresses reached a lower level.

(2) The shapes of stress – strain loops were changed when the crack growth rate was changed due to applying an unexpected load. This phenomenon was related to the crack closure behavior.

(3) The crack opening and closing stresses could be easily measured by using the relationship between the stress and the strain function which was proposed by Kikukawa et al. [12].

(4) Monitoring for the detection of an application of a dangerous load can continuously be performed by using the waveform of the stress and the strain function. Those waveforms changed when the crack growth rate varied due to the application of dangerous load.

2.6 References

[1] W. Elber, “The Significance of Fatigue Crack Closure,” ASTM STP 486. ASTM International, West Conshohocken, pp. 230-242, PA 1971.

[2] A. J. McEvily, “Current Aspects of Fatigue,” Metal Science, Vol. 11 (1077), pp. 274-284, 1977.

[3] A. J. McEvily, Z. Yang, “The nature of the two opening levels following an overload in fatigue crack growth,” Metallurgical Transactions, Vol. 21A, pp. 2717-27, 1990.

[4] H. Bao, A.J. McEvily, “The Effect of Overload on the Rate of Crack Propagation under Plane Strain Conditions,” Metallurgical and Materials Transactions, 26A, pp.1725-1733, 1995.

[5] D. H. Chen, H. Nisitani, “Analytical and Experimental Study of Crack Closure Behavior based on an S Shaped Unloaded Curve,” ASTM STP 982, Mechanics of Fatigue Crack Closure, pp. 475-488, 1988.

[6] C. M. Ward-Close, A.F. Blom, O. R. Richie, “Mechanism Associated with Transient Fatigue Crack Growth under Variable-amplitude Loading: An Experimental and Numerical Study,” Engineering Fracture Mechanics, Vol. 32, pp. 613-618, 1989.

[7] C. Makabe, A. Purnowidodo, A. J. McEvily, “Effects of surface deformation and crack closure on fatigue crack propagation after overloading and underloading,” International Journal of Fatigue, Vol. 26, pp. 1341-1348, 2004.

[8] C. Makabe, A. Purnowidodo, T. Miyazaki, A. J. McEvily, “Deceleration and Acceleration of Crack Propagation after an Overload under Negative Baseline Stress Ratio,” Journal of Testing and Evaluation, Vol. 33, pp.181-187, 2005.

[9] C. Makabe, H. Kaneshiro, “A Method of Detecting the Fatigue Crack Initiation and Growth in a Holed Specimen Based on Crack Tip Opening and Closing,” Engineering Fracture Mechanics, Vol. 41, pp. 395-403, 1992.

[10] C. Makabe, H. Kaneshiro, S. Nishida, C. Urashima, “Detection of 1 mm Fatigue Crack Initiation Using Strain Waveform,” Journal of Engineering Materials and Technology, ASME, Vol. 116, pp.483-487, 1994.

[11] C. Makabe, A. Purnowidodo, T. Sueyoshi, T. Utsunomiya, “Detecting Overload from Strain Information during Fatigue Crack Propagation under Negative Stress Ratio,” Testing and Evaluation, Vol. 32, pp. 56-61, 2004.

[12] M. Kikukawa, M. Jono, K. Takaka, M. Takatani, “Measurement of Fatigue Crack Propagation and Crack Closure at Low Stress Intensity Level by Unloading Elastic Compliance Method,” Journal of the Society of Materials Science Japan, Vol. 25, pp.899-903, 1976.

[13] S. Nishida, “Failure Analysis in Engineering Applications,” Butterworth Heinemann Ltd., pp.1-5, 1992.

[14] A. J. McEvily, “Metal Failures Mechanisms, Analysis, Prevention,” Wiley Interscience Publication, pp.1-20, 2002.

[15] C. Makabe, K. Naka, Y. Katsushima, “Example of Arresting Crack Growth in Welded Parts,” Industrial Engineering & Management, Vol. 4, http://dx.doi.org/10.4172/2169-0316.1000176, pp.1-4, 2015.

Chapter Three

Method of Detecting Unexpected Load Leading by Using Strain Information

3.1 Introduction

The presence of cracks can lead to failure in members of structures or engineering applications. An application of unexpected sudden high load can bring unstable crack growth according to the applied load conditions. This study investigates the technique to determine the application of such load on the structural member or equipment while it's in operation. In the previous study [1], one of the detection techniques the application of dangerous load was by analysing the strain function based on the unloading elastic compliance method [2]. However, the application of that method is limited in the cases that the loading waveform is measured. The background of this method is that the moving of the crack closure points related to the crack growth rate after the changing loading conditions. Also, another method for detecting the effects of loading conditions on crack growth behaviour in a cracked material was shown in the previous study [3].

Design criteria which considered allowable conditions of operation follow important theories to prevent fractures or damage [2]. However, when an unexpected hazardous load is applied, a method of machine or structure maintenance should be reconsidered against the basic design criteria. Before reconsidering the operating conditions or replacing members of structures or engineering applications, the detection of which unexpected hazardous load was applied or not had better be done. In the case of cracked material, the growth behavior is monitored during operation, and then the residual fatigue life should be analyzed for safe operation. When an unexpected hazardous load is applied, the residual fatigue life should be analyzed again.

In the case of cracked materials, the crack closure behavior affects the crack growth rate. So, the application of an unexpected hazardous load can be detected by the measurement of the crack closure point. The unloading compliance method [2] is very effective to measure the crack closure point. However, when the loading data is unknown, we should detect the variation of crack closure point by local strain. In the present study, the method of detecting whether a hazardous load was applied or not was examined by using the waveform of local strains. Just application of overload

could be detected by the method of reference [3], too. However, the occurrence of the acceleration or deceleration of crack growth can be distinguished with strain waveform by the present method.

3.2 Material and Testing Procedure

The material used for the experiment was 0.15% carbon steel. This is called JIS-S15C in Japan (JIS = Japanese Industrial Standards). The chemical composition (wt, %) was 0.15% C, 0.30% Si, 0.50% Mn, 0.013% P, 0.013% S, 0.19% Cr, 0.05% Ni, 0.14% Cu and balance of Fe. The Mechanical properties of the material were 283 MPa of yield stress, 449 MPa of ultimate tensile strength and 60% of reduction of area.

A center-cracked type specimen was used in this experiment. Dimensions of the specimens are 20 mm in length and 4 mm in width. A notch of 4 mm in length was cut in the center section of the flat part of specimen by electric discharge machine. Then the specimens were polished by emery paper and metal polisher. Before starting the experiment, 1.0mm length of cracks were introduced from both sides of the notch root. The initial crack length was about 6 mm which included a notch length of 4mm. After annealing at 600˚C for 1 hour in a vacuum furnace, strain gages were pasted on the specimen surface as shown in Figure 3.1 to measure the crack opening and closing stress to detect an unexpected hazardous load application.

The fatigue crack growth tests were carried out by using an electric hydraulic testing machine with a constant loading of 10Hz frequency under constant stress amplitude σ = 86 MPa and negative stress ratio R= -1 in laboratory room conditions. Where R is defined by the ratio of minimum cyclic stress σ_{min} to maximum cyclic stress σ_{max}. Overload (which stress is represented by σ_{ol}) or underload (represented by σ_{ul}) was applied when the crack length reached about 6 mm. Crack length was measured by an optical microscope which was connected to an image display system to make it easy to measure the crack length.

Figure 3.2 shows the schematic representation of overload and underload application. In this figure, σ_{min} represents minimum cyclic stress, σ_{max} maximum cyclic stress, σ_{ol} stress at overloading and σ_{ul} stress at underloading.

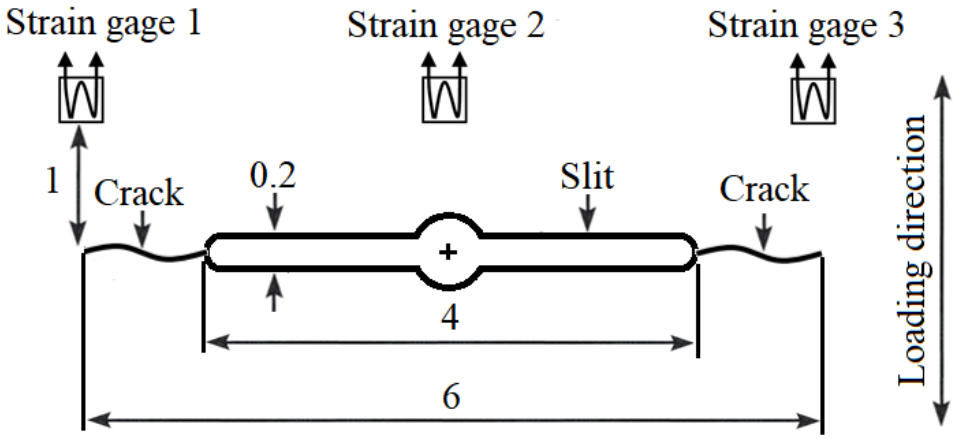

Figure 3. 1 Position of pasted strain gages (mm)

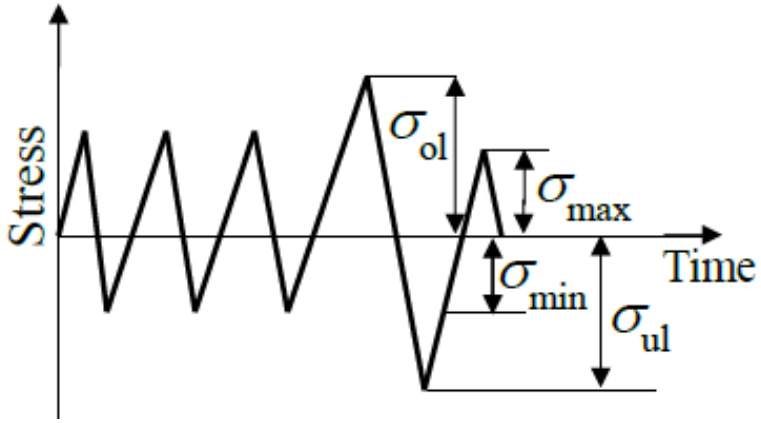

Figure 3. 2 Schematic representation of overload and underload

3.3 Results and Discussion

A series of fatigue tests were conducted to investigate the crack growth behavior with the application of overload and underload, and results were compared with those of the baseline which was experimental case without overload or underload. So, the overload and underload were regarded as an unexpected hazardous load in the present study. The stress level at overloading was set as σ_{ol} = 185MPa and 113 MPa and underload as σ_{ul} = - 185 MPa and -113 MPa. Stress amplitude before and after the applying overload and underload was 86 MPa and stress ratio at that was R = -1.

Figure 3.3 shows the relationship between half-crack length *a* and number of stress cycle *N*. It is known that the crack growth rate accelerated when overload was applied with critical conditions [3]. In this study the acceleration and deceleration were obsereved depending on the conditions of overload or underload, in comparison with baseline data. The acceleration of the crack growth is an unexpected situation. In this study, the acceleration of crack growth behavior was observed when the overload and underload were ±185MPa. When those values are ±113 MPa, the retardation of crack growth was observed. For the case of σ_{ul} = -113MPa crack growth rate was almost the same as for the baseline.

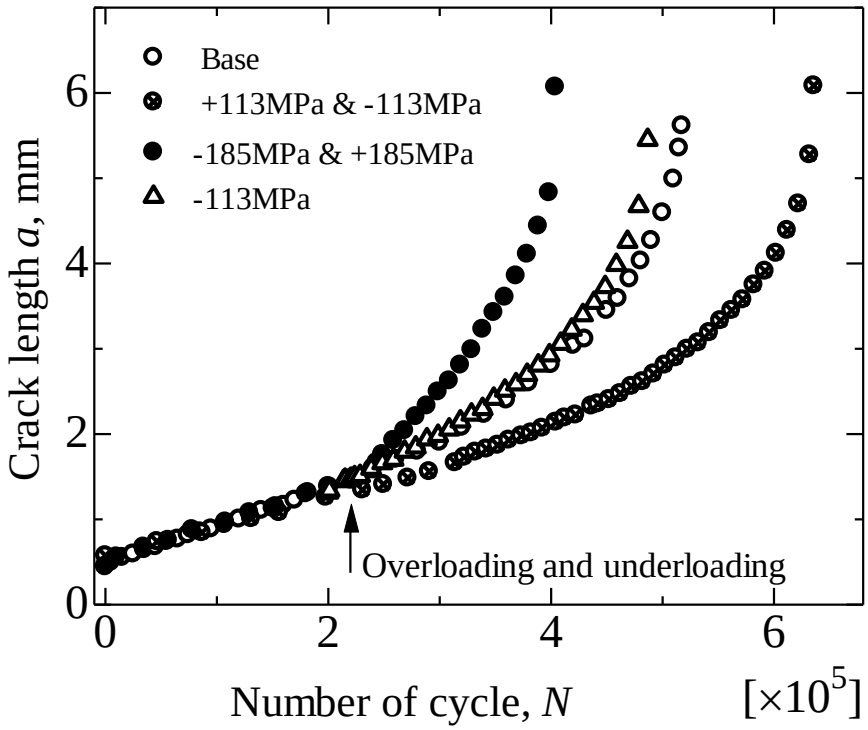

Figure 3. 3 Crack length *a* vs number of cycles *N*

Figure 3.4 shows the crack growth rate *da/dN* as a function of the maximum of the stress intensity factor K_{max}. It is clear that the acceleration of crack growth occured in the cases where the values of overload and underload were ±185 MPa. When those were ±113 MPa, the crack growth was retarded but this behavior is unclear in Figure3.4.

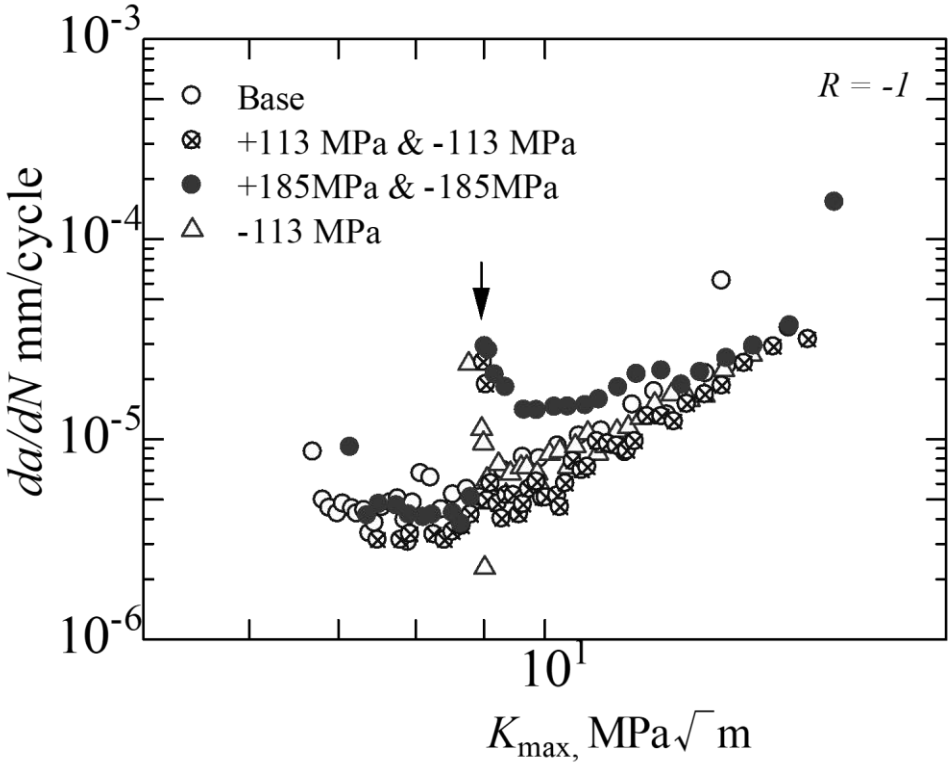

Figure 3. 4 *da/dN* vs K_{max}

Figure 3.5 shows the schematic representation of the stress – strain loop and the relationship between the stress and strain function. The strain functions are defined as follows;

$$h1 = \varepsilon_1 + \lambda\varepsilon_2 , \; h2 = \varepsilon_1 - \lambda\varepsilon_2 \tag{3.1}$$

where, λ = 1 or $\Delta\varepsilon_1 / \Delta\varepsilon_2 : \Delta\varepsilon_1$ and $\Delta\varepsilon_2$ are cyclic strain ranges of ε_1 and ε_2, respectively. The crack closure point can be measured by theoretical background of the elastic compliance method [2]. Therefore, this method has been applied by many researchers. In this study, we detect the crack closure behavior by using the relationship between stress and strain function *h2*. This method is a practical method but not theoretical one. However, for the purpose of detecting a hazardous load when stress data is unknown, the strain functions were determined in this study. The crack opening point is the knee point shown with arrow in the figure (Figure 3.5 (c)).

Figure 3.6 shows the relationship between the function λ and half-crack length *a*, where $\lambda = \Delta\varepsilon_1 / \Delta\varepsilon_2$. The variation of λ is compared in three cases, that is, crack growth of base line,

acceleration of crack growth and deceleration of crack growth. In the case of base line and deceleration of crack growth after applying overload and underload at a = 3 mm, the value of λ is hardly changed. On the other hand, in the case of acceleration of crack growth, λ is clearly varied. That value is increased with the growth of crack. So, we can predict the acceleration of crack growth after overloading and underloading. By using this relation, it is possible to know whether an unexpected hazardous load which led to the crack growth acceleration was applied or not during operation.

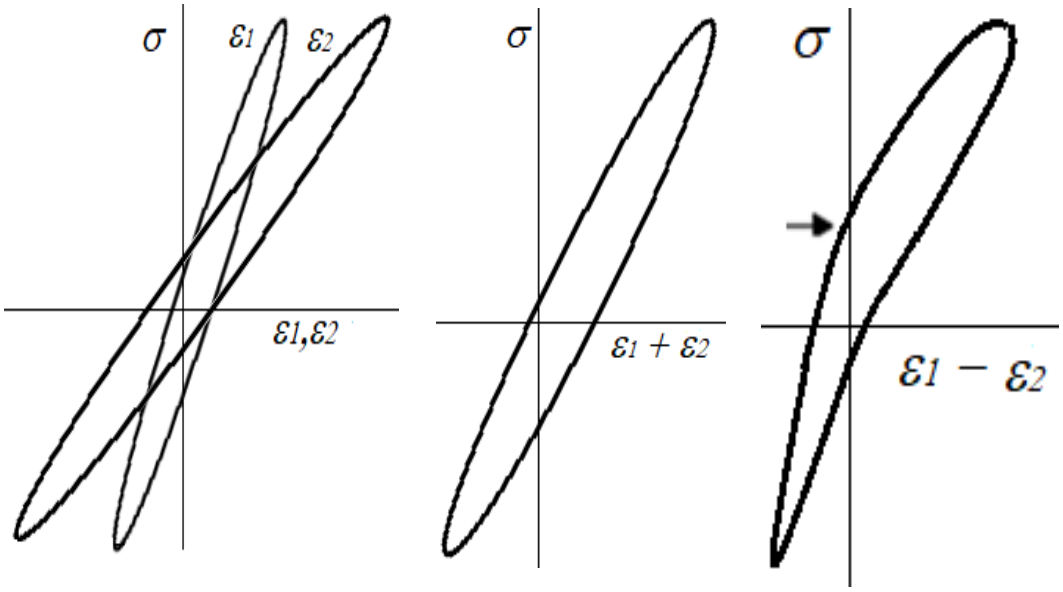

(a) (b) (c)

Figure 3. 5 Stress-strain loops: (a) σ - ε loop, (b) $\sigma - h1$ loop, (c) σ - $h2$ loop. Arrow shows the crack opening point

Figure 3.7 shows the examples of loops of stress and strain functions in the cases of applying overload or underload. According to Equation (3.1), the coefficient λ is determined. In the cases of Figure 3.7 (a), the shape of $\sigma - h1$ loop after application of overload and underload were not so much changed from those before the application. The same tendency was obtained in the case of $\lambda = \Delta\varepsilon_1 / \Delta\varepsilon_2$. Therefore the quality of variation in strain function *h1* is regarded as almost the same as that of stress variation. In the cases of Figure 3.7 (b) and (c), the $\sigma - h2$ loop after applying overload and underload were compared with that before applying overload and underload. When $\lambda = 1$ in Figure 3.7 (b), there is small change in the shape of $\sigma - h2$ loop by applying overload and underload. When $\lambda = \Delta\varepsilon_1 / \Delta\varepsilon_2$ in Figure 3.7 (c), the clear change of the shape of $\sigma - h2$ loop by applying overload and underload were observed. The turning points of $\sigma - h2$ loop, which were observed in Figure 3.7 (b) and (c), are the crack opening and closing point. In the figures, the point of crack opening stress σ_{op} is shown by arrow. The point of crack closing stress σ_{cl} is almost the same point as σ_{op}. From these results, it is understood that the crack opening point and closing point are emphasized when $\lambda = \Delta\varepsilon_1 / \Delta\varepsilon_2$.

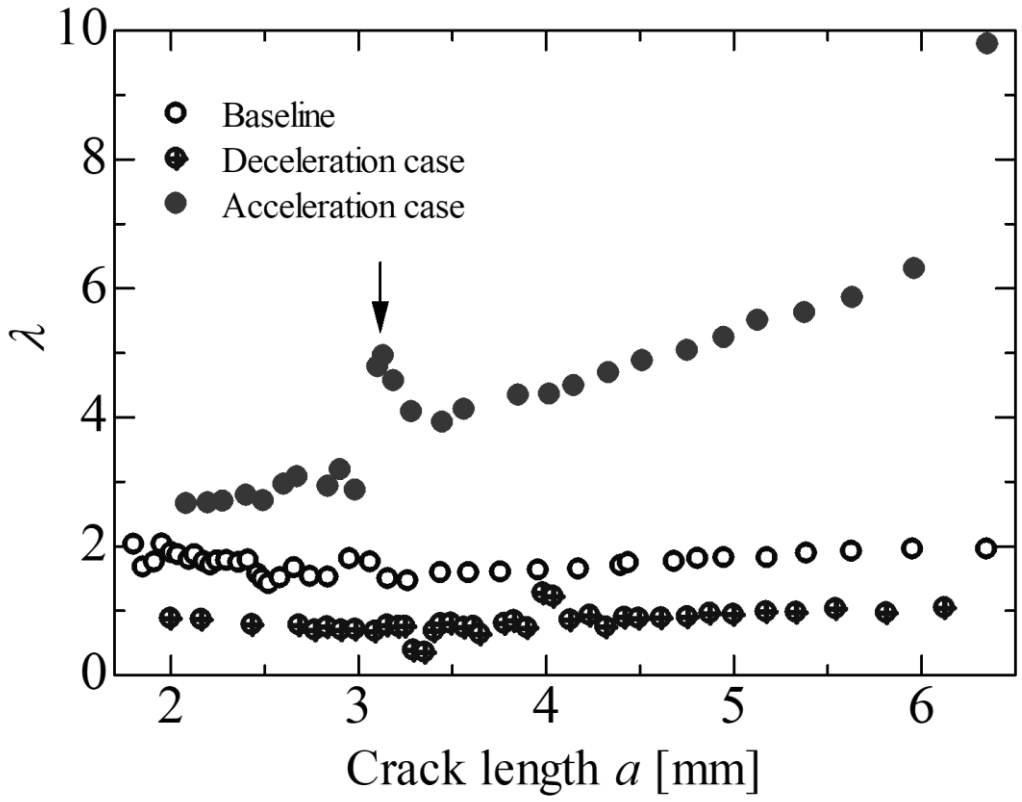

Figure 3. 6 Variation of λ (= $\Delta\varepsilon_1 / \Delta\varepsilon_2$) against the half-crack length. Arrow shows the overloading and/or underloading point.

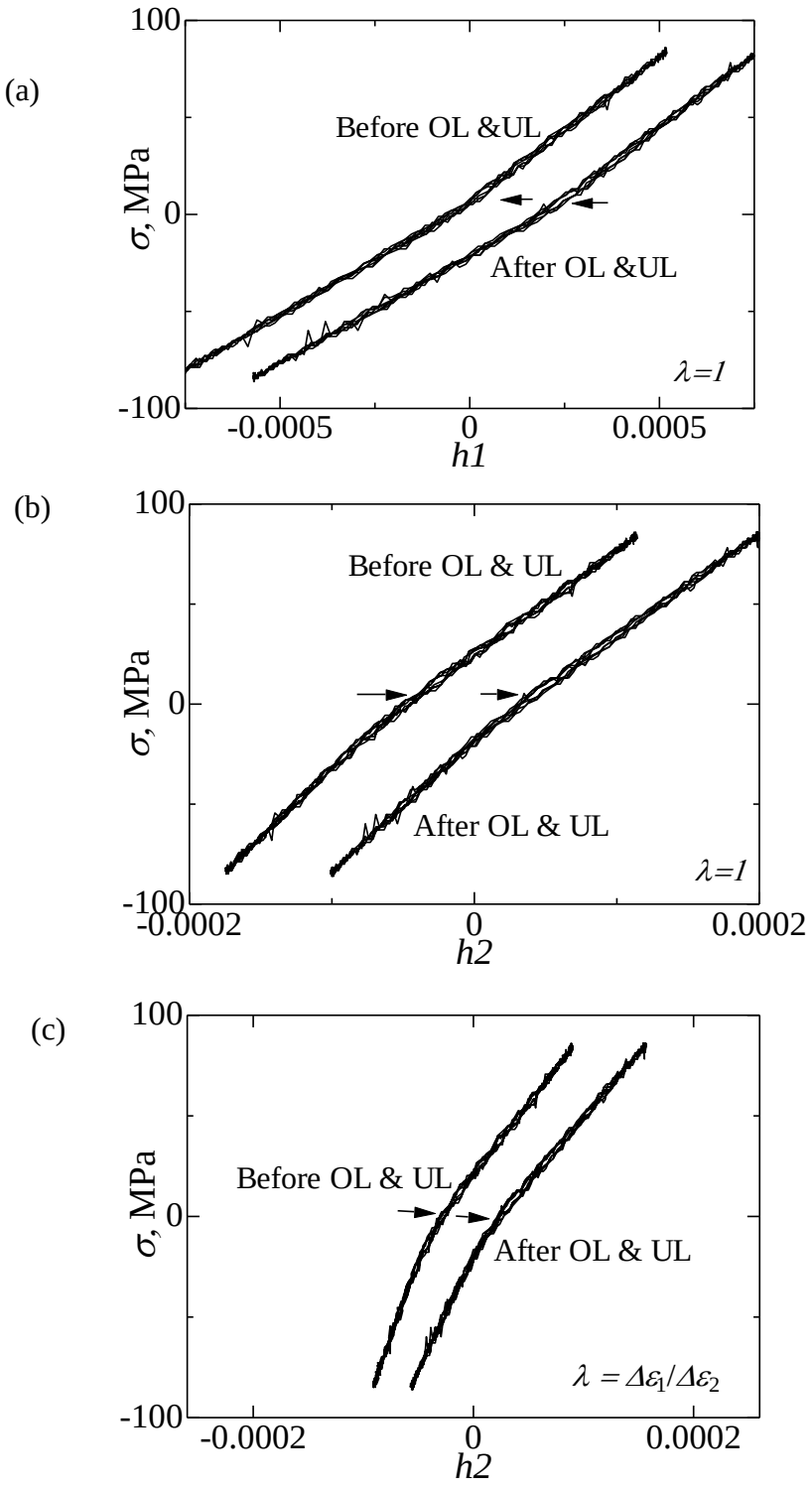

Figure 3. 7 Example of the relationship between stress and strain functions in the case of σ_{ul} = -113MPa. [Before OL & UL N = 313,760, a = 3.10 mm and after OL & UL N = 332,000, a = 3.15 mm, OL = Overload, UL = Underload]: (a) $\sigma - h1$ (λ =1), (b) $\sigma - h2$ (λ =1), (c) $\sigma - h2$ ($\lambda = \Delta\varepsilon_1 / \Delta\varepsilon_2$).

A hazardous load, which leads to crack growth acceleration, can be detected by measurement of crack closure points [2]. It is shown in the present study that the detection can be carried out without the information of stress data. Instead of stress data, we can use the data of strain function *h1*. By comparing the waveforms of strain functions of *h1* and *h2*, the detection of crack growth acceleration was performed. In the latter section of this paper, the results by which the strain functions are calculated by $\lambda = \Delta\varepsilon_1 / \Delta\varepsilon_2$ are shown.

In Figure 3.8 - 3.10, the waveforms of strain functions of *h1* and *h2* are shown. In these figures, the shape of the waveforms of h_1 are hardly changed before and after the application of overloading and underloading. Waveform *h1* showed the same tendency as the stress waveform which was not changed before or after overload and underload. Therefore, we confirmed whether the crack growth accelerated or not by analyzing waveform *h1* and *h2*. Thus, the waveform *h1* was used to check whether the loading conditions had changed or not. Waveform *h2* was for detecting the application of hazardous load.

When the variation of the crack growth rate against the crack length of stress intensity kept the same tendency as the baseline even after applying overload and/or underload, the shape of waveform *h2* hardly varied after those load applications, too, as shown in Figure 3.8. When the crack growth decelerated, the waveform *h2* changed its shape just after applying overload and underload.

However, after the crack grew from those application points. The waveform of *h2* returned to the shape of the waveform observed before those points as shown in Figure 3.9. In those cases, because the crack growth life will not be shortened, there is no need to change the maintenance plan of the machine or structure. However, in the case of Figure 3.10, the waveform of *h2* was changed after applying overload and underload. In this case the crack growth rate became higher after applying those loads. Therefore, after seeing this change of waveform, we should change the maintenance plan.

Figure 3.11 shows the examples of σ – *h2* loop after applying overload and underload. When crack growth did not accelerate after applying those loads, the crack opening stress and closing stress stayed at almost the same level after the application of those loads. However, when the crack growth accelerated, the crack opening stress and closing stress moved toward the minimum cyclic

stress because of plastic strain behavior in the vicinity of crack tips [3]. In that case, the effective stress range increases and the crack growth rate becomes higher.

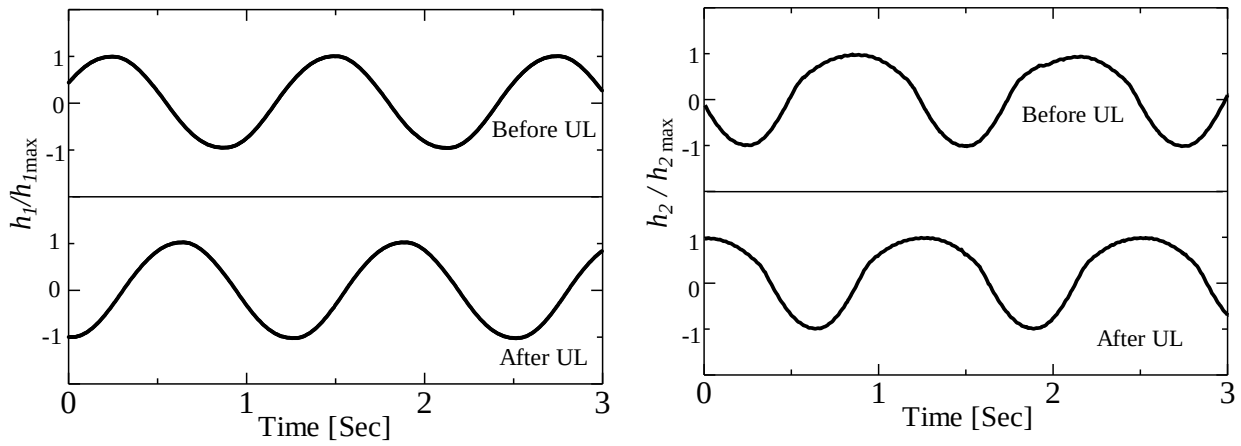

(a) (b)

Figure 3. 8 In the case of applying σ_{ul} = -113 MPa, when $\lambda = \Delta\varepsilon_1 / \Delta\varepsilon_2$: (a) Before underloading N = 20,000, a = 2.9mm, (b) After underloading N = 28,506, a = 3.13mm.

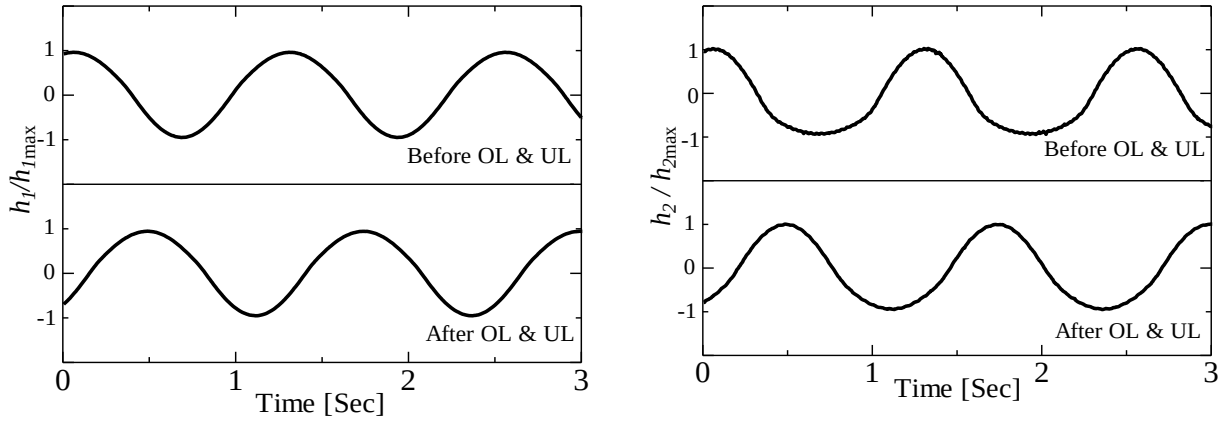

(a (b

Figure 3. 9 In the case of applying σ_{ul} = -113 MPa, σ_{ol} = 113 MPa when $\lambda = \Delta\varepsilon_1 / \Delta\varepsilon_2$, (α) Before application of UL & OL N=313,760, a = 3.10mm, (b) After application of UL & OL N = 322,000, a = 3.15mm

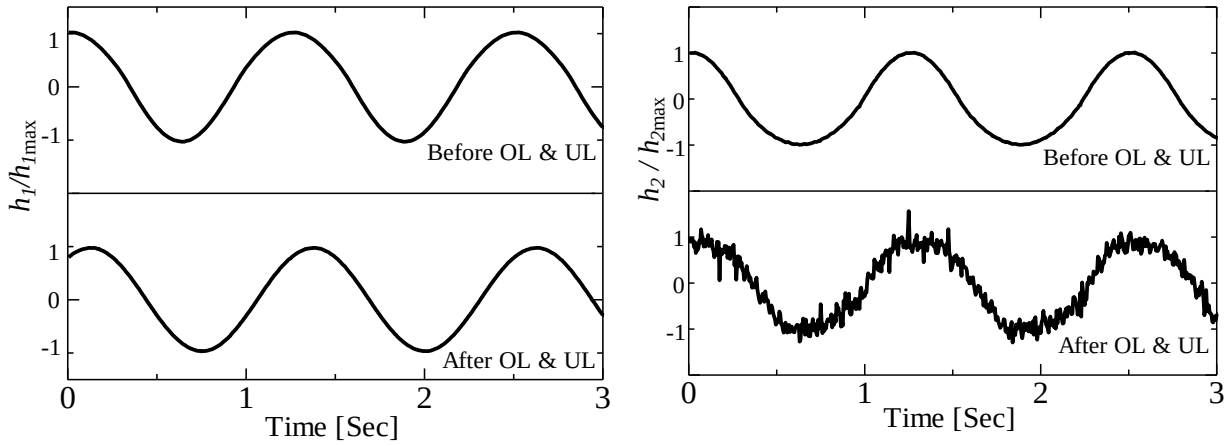

(a) (b)

Figure 3. 10 In the case of σ_{ul} = -185 MPa, σ_{ol} = 185 MPa when $\lambda = \Delta\varepsilon_1 / \Delta\varepsilon_2$, (a) Before application of UL & OL *N*= 240,110, a = 3.10mm; (b) After application of UL & OL *N* = 241,108, a = 3.13mm

The present study demonstrated a method of detecting whether or not a hazardous load was applied which can lead to crack growth acceleration, by using strain waveforms. This is a simple method, so it can be applied in some case whether cracked materials need to be maintained.

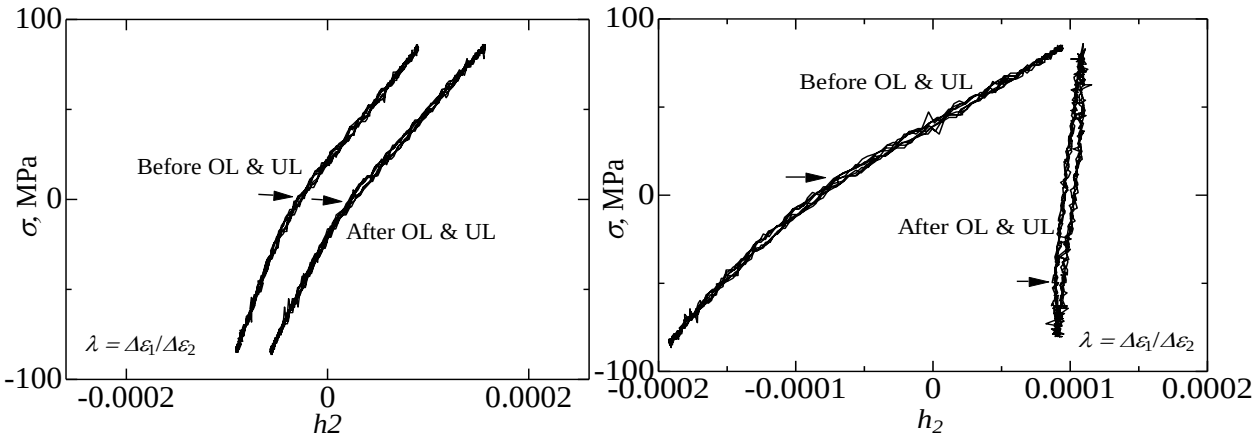

(a) (b)

Figure 3. 11 Comparison of $\sigma - h_2$ when $\lambda = \Delta\varepsilon_1 / \Delta\varepsilon_2$ [UL = Underload & OL = Overload]: (a) σ_{ul} = -113 MPa and σol = 113 MPa, (b) σ_{ul} = -185 MPa and σ_{ol} = 185 MPa.

3.4 Conclusion

The method of detecting whether an unexpected load which leads to the acceleration of fatigue crack growth was applied or not is done by using strain data. The variation tendency of the local strains in the vicinity of the crack was affected by whether acceleration or deceleration occurred due to the crack opening and closing behavior. By considering that behavior, two types of strain functions were proposed for detection of unexpected load. Even if the load data was not measured, the unexpected load which leads to the acceleration of fatigue crack growth can be detected by the strain functions proposed in this study. The following outcomes have been found from this study:

(1) Crack growth acceleration or deceleration were observed depending on the condition of overlaod and underload compared to the baseload i.e. without applying any overload or underload.

(2) By analyzing the shape of the waveform of strain information, whether an unexpected overlaod or underlaod was applied or not can be detected/predicted.

(3) The value of 'λ', which is the ratio of cyclic strain range, is an important parameter which can be used as a qualitative measurement tool of the variation of the strain function.

3.5 References

[1] S. M. Moshiar Rahman, Md. Shafiul Ferdous, Konosuke Tada, Chobin Makabe, A Method for Detecting an Unexpected Application of a Hazardous Load During Operation, Advances in Materials Science and Applications, 2017, PP 9-16

[2] M. Kikukawa, M. Jono, K. Takaka, M. Takatani, Measurement of Fatigue Crack Propagation and Crack Closure at Low Stress Intensity Level by Unloading Elastic Compliance Method, Journal of the Society of Materials Science Japan, 1976, pp.899-903.

[3] C. Makabe, A. Purnowidodo, T. Sueyoshi, T. Utsunomiya, "Detecting Overload from Strain Information during Fatigue Crack Propagation under Negative Stress Ratio," Testing and Evaluation, 2004, pp. 56-61.

[4] Nishida, S. Failure Analysis in Engineering Application, Butterworth-Heinemann Ltd., Oxford, 1986.

[5] Makabe, C., Kaneshiro, H., Nishida, S., and Urashima, C., "Detection of 1 mm Fatigue Crack Initiation Using Strain Waveform," Journal of Engineering Materials and Technology, Trans. ASME, Vol. 116, 1994, pp. 483–487.

[6] Makabe, C., Kaneshiro, H., Itokazu, M., and Ohba, K., "An Inspection of Fatigue Crack Extension Based on Strain Information," Engineering Fracture Mechanics, Vol. 45, 1993, pp. 655–662.

[7] Makabe, C., Nishida, S., and Kaneshiro, H., "A Detection Method of Fatigue Crack Initiation by Analyzing Strain Waveform," Journal of Testing and Evaluation, Vol. 21, 1993, pp. 339–345.

[8] Chobin Makabe, Hideo Kaneshiro, "Measurement of Crack Closure Points During Cyclic Loading by The Strain Interference Method", Engineering Fracture Mechanics, Vol.43, No.6, pp.993-1002,1992.

[9] C. Makabe, Hideo Kaneshiro, "A Method of Detecting the Fatigue Crack Titration and Growth in a Holed Specimen Based on Crack Tip Opening and Closing", Engineering Fracture Mechanics, Vol.41, No.3, pp.93-403, 1992.

Chapter Four

Effect of Fiber Direction and Stress Ratio on Fatigue Property in Carbon Fiber Reinforced Epoxy Composites

4.1 Introduction

A basic study was conducted on the strength characteristics of composite materials having long carbon fibers. It was shown that the stress concentration was not only the control parameter for evaluating fatigue limit of composite materials with a notch [1, 2]. It was found that the static tensile strength of carbon composites was strongly affected by fiber-matrix interfacial bonding strength. In previous study, the fatigue limit of the smooth specimen was predicted from the result of the slit specimen, and the effect of the long fiber direction on the fatigue behavior was analyzed [1, 2]. The characteristics of the strength of the carbon fiber composite material were examined in the present study. A composite material board was prepared by superimposing a commercially available carbon fiber sheet aligned in one direction and impregnating the cloth with the epoxy resin. Especially, the influence of anisotropy due to the different method of superimposing unidirectional carbon fiber sheets was examined, and the influence of local fracture behavior of fiber on fatigue strength was investigated. These experiments or investigations were performed due to develop the repair method of damaged carbon composite in the future.

4.2 Materials and Experimental Method

Thicker and thinner sheets of unidirectional carbon fiber were superimposed, and epoxy resin was allowed to penetrate between the sheets by the method of Vacuum Assisted Resin Transfer Molding (VARTM) [3, 4]. The thickness of one carbon fiber sheet is 0.23 mm and fiber diameter is 7 μm. According to the fiber directions and alignment of the carbon fiber sheets, three types of carbon reinforced composites were fabricated. Thicker specimens were tested in the case of stress ratio R (minimum cyclic stress / maximum cyclic stress) = -1 and thinner specimens were tested in the case of R = 0. The main tests were performed with R = - 1. To prevent the buckling of the specimen in the case of thin specimen, testing was performed with R = 0. For thicker specimens, 11 sheets were used to fabricate the carbon composites plate, and for thinner specimen 5 sheets were used.

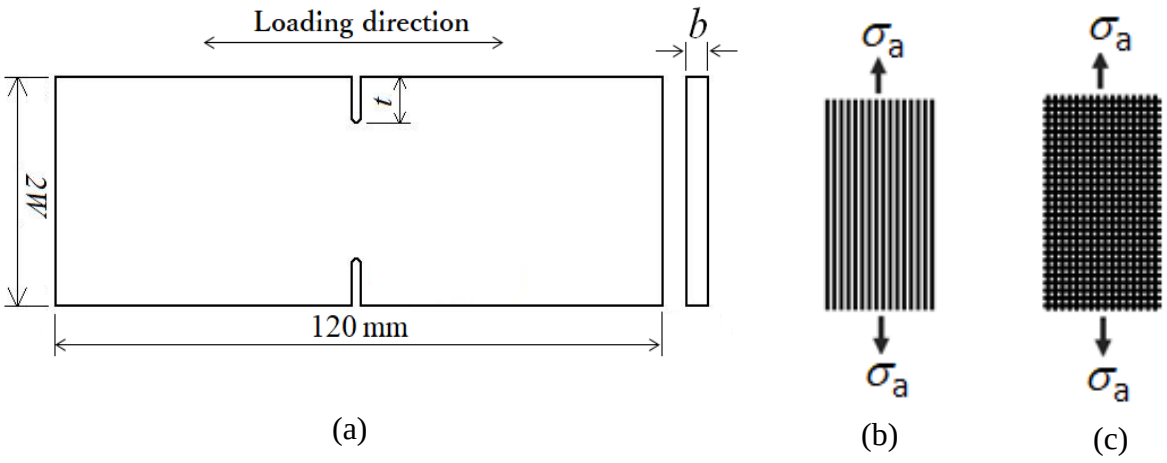

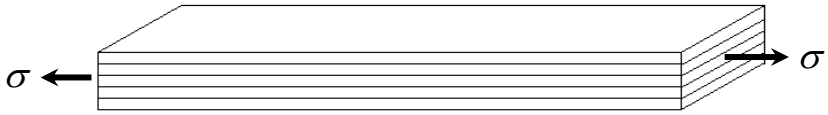

Type A: All carbon fiber sheets are in axial

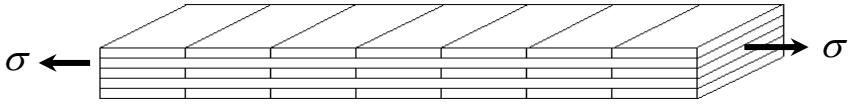

Type B: Alternately oriented carbon fiber sheets

Type C: Two sheets are in loading direction and then one is in normal to the loading direction

(d)

Figure 4. 1 Epoxy based carbon composites: (a) Geometry of the specimen, (b) Unidirectional carbon sheets, (c) Combination of different orientations, (d) Side view of the Specimen.

Type *A* is based on all the sheets stacked with carbon fibers aligned in the loading direction. Type *B* is obtained by alternately superimposing sheets whose fiber direction is in the loading

direction and in the vertical direction. Type *C* is a stack of sheets in such an orientation that two pieces in the loading direction, and then one piece in the vertical direction were superimposed.

Figure 4.1 shows the geometry of the specimen, fiber direction and fabricated epoxy carbon composites plate. Slit was processed from both ends of the specimen to lower the fatigue limit, and the experiment was carried out by changing the slit length. From the experimental results, the fatigue limit of the specimen was evaluated with net stress. The stress amplitude σ_a is calculated by the following equation,

$$\sigma_a = P/\{2b(W-t)\} \tag{4.1}$$

Where, *P* is the applied load, *W* is the half width of the specimen, *b* is the thickness of the specimen, and *t* is slit length.

The fatigue test was performed by using an electro-hydraulic servo testing machine with a loading capacity of 9.8*kN*. The stress ratio was $R = -1$ for thicker specimens, and $R = 0$ for thinner specimens. The frequency was 5Hz to 10Hz. Crack initiation and growth were observed directly from the surface of the specimen using a microscope. The microscope was connected to an image display monitor. In this study, the fatigue limit σ_w was defined as the maximum applied stress amplitude σ_a that could withstand 10^6 repeated cycles [1, 2, 5].

Generally, the fatigue limit σ_w is determined by the ordinary technique with *S-N* curve. However, depending on the conditions, σ_w can be approximated using single specimen by the load increment test, *LIT* [1, 2, 5]. In this study, the fatigue limit was obtained for both the cases of $R = -1$ and $R = 0$ by *LIT*. The example of this method is shown in Figure 4.2. In this experiment, the stress was increased 2MPa for every 2×10^4 cycles of stress application, and it is repeated until the specimen is broken. Therefore, the fatigue limit is determined by the stress amplitude of the step prior to the fracture load.

4.3 Experimental Results and Discussion

4.3.1 Evaluation of fatigue limit

Figure 4.3 shows the *S-N* curve for $R = -1$ and $t = 6.8$ mm. Figure 4.4 shows the experimental results of *LIT* in the cases of $R = -1$ and 0. From the *S-N* curves it was found that if the stress level did not break the specimen until 10^4 repetitions, there is a possibility that the material can withstand

10^6 stress repetitions. From this result, it is expected that the fatigue limit can be approximated by *LIT* in the present study. Figure 4.3 shows that the fatigue limit of *A* type specimen is about 340MPa, and that

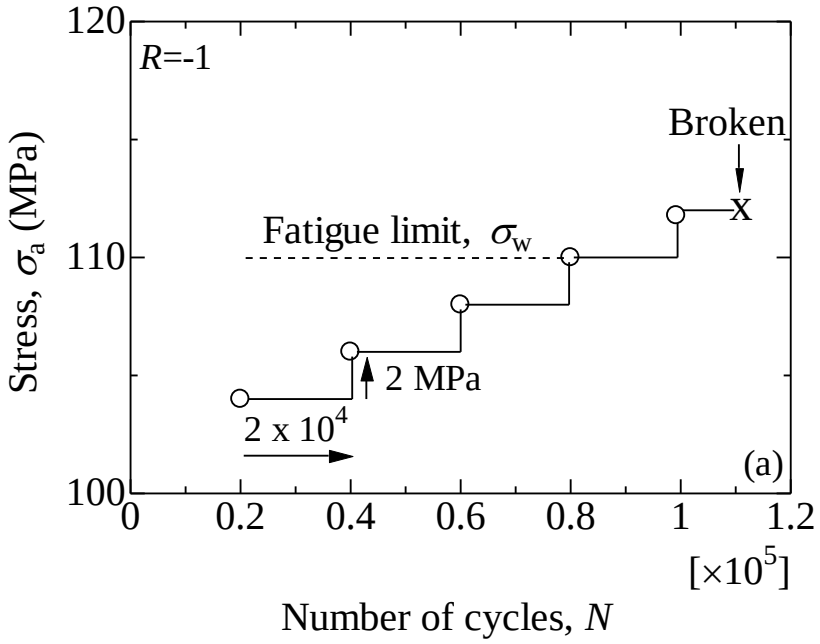

Figure 4. 2 Example of Load Increase Test (*LIT)*

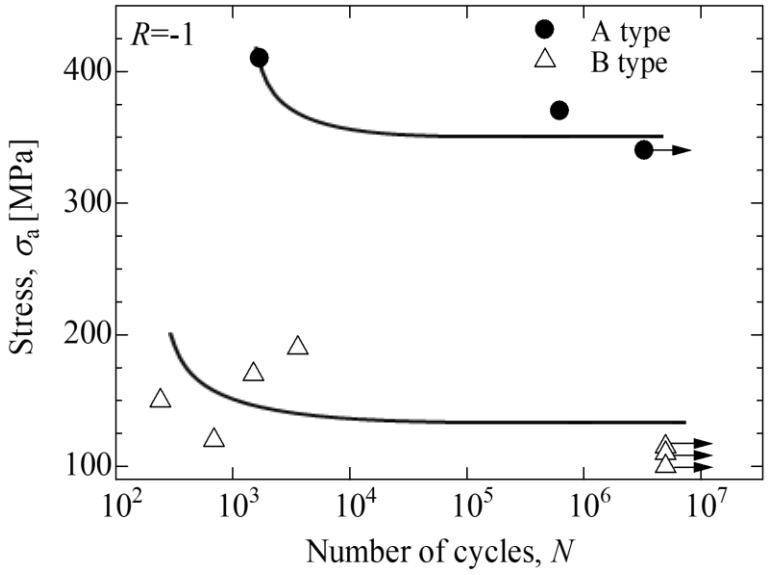

Figure 4. 3 *S-N* curve at *R*=-1

of *B* type is about 110MPa when *R* = -1. Our main objective was to determine the influence of anisotropy, local fracture behavior of fiber on fatigue strength, and the main experiments were performed with *R*= -1. Now, *S-N* curves were obtained in the case of *R* = -1, only. It is expected that almost the same tendency of *S-N* curves will be obtained in the cases of *R* =-1 and 0. Figure 4.4 shows the relation between the fatigue limit σ_w and the slit length, obtained by *LIT*. From the experimental results of present study, it is expected that the fatigue limit of the smooth specimen can be predicted from the fatigue limit of slit type specimen by using the net stress. It means that the fatigue limit has almost the same value in the case of slit specimen and smooth specimen when the net stress is used for the evaluation parameter.

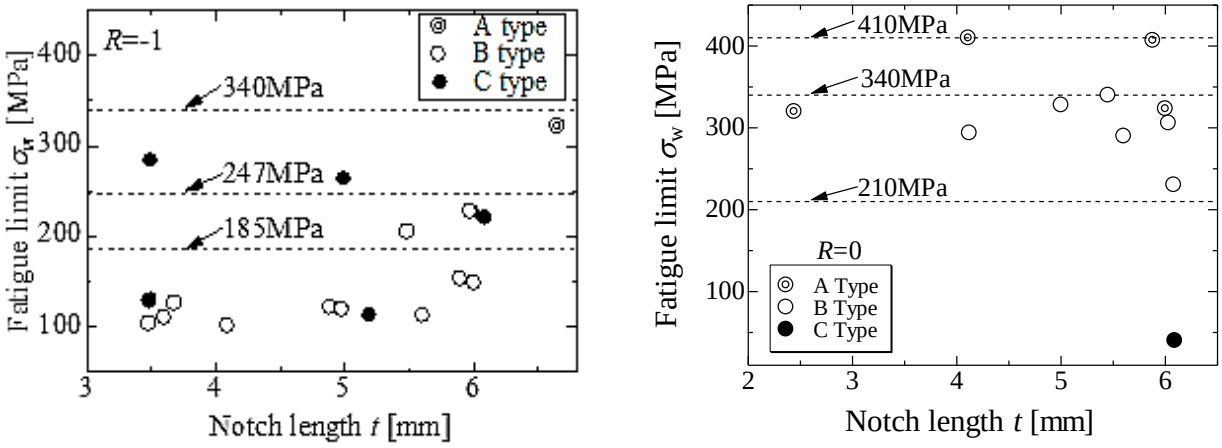

Figure 4. 4 Results of fatigue limit by *LIT*s: (a) *R*=-1, (b) *R*=0

In the present experiment, the fatigue limit varies according to the type of slit specimen. Scattering of the data was observed. It is due to the fabrication conditions of the specimen. When a shear fracture occurred due to decohesion of fiber and resin, the strength of the specimen became low. However, we expected that the fatigue limit of a smooth specimen can be estimated by taking the maximum value of the data as the expectation. The fabrication conditions of material should be better in a company than in this laboratory.

In the case of *A* type specimen, the crack grew along the fiber direction when the slit was short. Furthermore, the specimen did not break in the direction perpendicular to the loading axis except when the slit and ligament lengths were 7 mm and 1 mm, respectively. In that case, the breaking period of specimen was determined when the load could not to be applied with determined

frequency (10Hz). The fatigue limit of *A* type specimen was about 320MPa by *LIT*, which was closer to 340MPa which is the result obtained by the *S-N* curve at R = -1. The dotted line in the case of *A* type specimen in Figure 4.4 (a) shows the fatigue limit obtained from the *S-N* curve. That line, in the case of *A* type specimen in Figure 4.4 (b), shows the maximum value obtained by *LIT*. In the present study the fatigue limits of *B* type and *C* type specimens were predicted by that of *A* type specimen with dotted lines. For *A* type specimen, the base fatigue limit is 340MPa when R = -1, and 410MPa when R = 0.

It was assumed that the ratio of the number of fiber sheets alignment in the loading direction determines the fatigue limit of each type of specimen and is shown by dotted lines. Thus, the fatigue strength is determined by the strength of the fiber in the loading direction without substantial influence from the area (or volume) of the epoxy during fabrication, and the fatigue limits were assumed to be 185MPa, 210MPa for *B* type and 247MPa, 340MPa for *C* type specimen when R = -1 and R = 0, respectively.

The results obtained by Figure 4.4 also can be predicted the fatigue limit of the smooth specimen, if the fatigue limit is almost the same for the smooth and the slit specimens [1]. In the case of Figure 4.4 (a) of R = -1, some measurement data are located under the dotted line. Because unexpected defects were created during the manufacturing process, the data of *LIT* are scattered. In the case of *A* type specimen, we cannot obtain one data with t = 6.8 mm dependent on the loading capacity of the testing machine. Therefore, the fatigue limit of *A* type specimen can be somewhat higher than 340MPa. Therefore, the data of dotted line of Figure 4.4 (a) can be used to approximate value of fatigue limit of the smooth specimen.

In the case of Figure 4.4 (b) of R = 0, except for *C* type specimen, it is expected that the fatigue limits of the smooth specimen of *A* and *B* types are predicted by dotted lines. In the case of *C* type specimen, the specimen thickness was so thin that the specimen was expected to be damaged during the process of attaching it to the testing machine. From those results, the fatigue limit of the smooth specimen can be predicted from that of slit specimens.

4.3.2 Fatigue crack growth and fracture pattern

Figure 4.5 shows the broken specimen of *B* type specimen. In the case of R = -1 (Figure 4.5 (a)), the specimen was broken in the shallow area of slatted part. The crack initiated from the epoxy

with shear mode and cut the fibers within the slit area and closer to the slit area. On the other hand, in the case of $R = 0$ (Figure 4.5 (b)), the crack initiation parts were not in the vicinity of the slit. So, the extension of long fiber was observed from the broken specimen. The initial crack was initiated at the slitted area, but the growth of this crack did not bring the fracture of the specimen. After breakage of the fibers in plural parts, the specimen was broken. In the case of $R = 0$ also, the crack initiation in the slitted area strongly affected the fatigue limit. However, fracture pattern of the specimen was different in the cases of $R = -1$ and 0.

The fracture pattern and crack growth behavior has been discussed in the previous paper [1]. The crack initiated from the epoxy region. Then the crack grew by shear mode and the crack cut fiber by shear mode. This mechanism can be applied in the present cases. The crack initiation and growth behavior are related to the fatigue limit of the present specimens. In the case of the thinner specimen, we performed the testing with $R = 0$ to prevent buckling. The peeling of fiber from the epoxy occurs easily in the case of thinner specimens. So, the broken fibers were observed outside of the slit area. However, the initiation and growth behavior of a crack in the first stage of fracture is expected to be the same in the cases of $R = 0$ and -1. In the cases of the present study, long fibers located in the direction vertical to the loading direction cannot work to strength the specimen. The ratio of fibers in the loading direction is strongly related to the fatigue limit.

4.3.3 Discussion for tendency of present experiment

In the present experiment, the method of *LIT* was referred from the work by Goto et al. [5] When the specimen was made by the fiber sheet in which fiber direction was perpendicular to the loading direction, the fatigue limit became very low. So, we assumed that such sheet was not contributed to strength of the present composite specimen. Therefore, it is expected in the present specimen that the fatigue limit depends upon the ratio of fiber in the loading direction. Consequently, in the present experimental cases, it was shown that the A type of epoxy composites had the higher fatigue limit than type B.

In previous work [1], it was discussed that the volume fraction of voids in thin specimen is higher than that in thicker specimen. This is related to the peeling of fiber from the matrix as shown in Figure 4.5. The effects of thickness and stress ratio on the fracture behavior will be studied in the future. Also, followings were discussed. In the cases of the slit specimen, the growth direction

of crack initiated from slit was parallel the loading direction. Therefore, there was small effect of stress concentration of slit specimen on the fatigue limit. From that reason, the fatigue limit of the smooth specimens was not so much different from that of the slit specimens.

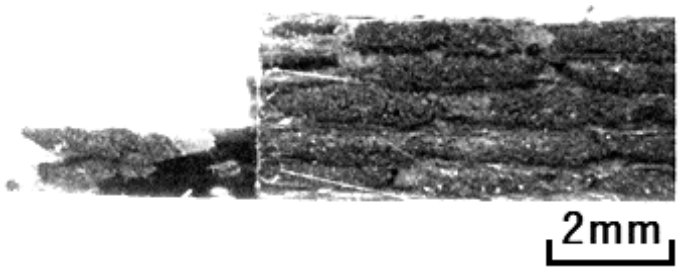

(a)

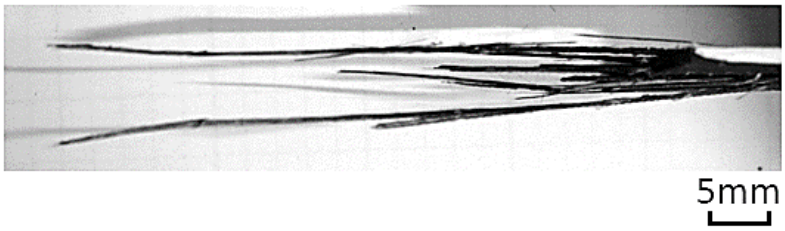

(b)

Figure 4. 5 Observations of fracture surface of *B* type specimen; (a) *b*=3mm, *t*=4mm, σ_w=102MPa in the case of *R* = -1, (b) *b*=1.4mm, *t*=5.5 mm, σ_w=410MPa in the case of *R* = 0.

The data of fatigue limit shown in Figure 4.4 was scattered. This is related to the specimens' conditions. It is expected that the volume fraction of voids is related to that scattering. The fatigue limits were determined by the crack growth behavior. The value of fatigue limit was determined from the data in which the crack growth stopped within short crack length in the loading direction.

4.4 Conclusions

The purpose of this study was to examine the influence of the anisotropy due to the characterization of the material by superimposing unidirectional long carbon fiber sheets and local fracture behavior of fiber on fatigue strength. The following results obtained are as follows:

(1) A higher fatigue limit was obtained when the alignment of all carbon fibers was in the loading direction.

(2) For composite materials with long fibers, it is expected that the fatigue limit of smooth specimens can be predicted from the results of slit specimens.

(3) The crack initiated from the epoxy region. Then the crack grew by shear mode and the crack cut fiber by shear mode. This mechanism can be applied in the present cases.

(4) The ratio of fibers in the loading direction is expected to be related to the fatigue limit.

(5) The results obtained in the present experiment will be applied to a repair method for damaged carbon composites which will be investigated in future.

4.5 References

[1] C. Makabe, M. Fujikawa, M.S. Ferdous, S. A. Setyabudi, Journal of High-Pressure Institute, Vol. 51, No. 6 (2013), p. 303.

[2] C. Makabe, T. Nakayama, M. Fujikawa, K. Arakawa, D. Chen, "Effect of Specimen Thickness on Fatigue Limit in Carbon Composites", Advanced Materials Research, Vol. 1110 (2015), p.13-18.

[3] M. Yamashita, T. Sakagawa, F. Takeda, F. Kimata, "Development of Advance Vacuum-Assisted Resin Transfer Molding Technology for Use in an MRJ Empennage Box-Structure", Mitsubishi Heavy Industries, Ltd. Technical Review, No. 45-4 (2008), p.1-4.

[4] D. Chen, K. Arakawa, S. Jiang, "Novel Joints Development from Partially Un-Moulded Carbon Fiber Reinforced Lamination", Journal of Composite Materials, Vol. 49, No. 14 (2015), p.1777-1786.

[5] K. Goto, H. Hatta, D. Katsu, T. Machida, "Tensile Fatigue of a Laminated Carbon-Carbon Composite at Room Temperature", Carbon, Vol. 41 (2003), p. 1249-1255.

[6] T. Tohkubo, M. Fujikawa, C. Makabe, S.A. Setyabudi, A. Murdani, "Effect of Fiber Direction on Strength of Notched Specimen of C/C Composite", Journal of the Society of Materials Science, Japan, Vol.61, No.12, pp.973-979, 2012.

[7] S.A. Setyabudi, C. Makabe, M. Fujikawa, T. Tohkubo, "Fatigue and Static Fracture of Machineable C/C Composites", Journal of Solid Mechanics and Materials Engineering, Vol.5, No.11, pp.640-654, 2011.

[8] H. Hatta, K. Goto, T. Aoki, "Strengths of C/C Composites Under Tensile, Shear, and Compressive Loading: Role of Interfacial Shear Strength," Composite Science and Technology, Vol.65, pp.2550-2562, 2005.

[9] L. Denk, H. Hatta, A. Misawa, S. Somiya, "Shear Fracture of C / C Composites with Variable Stacking Sequence", Carbon, Vol.39, pp.1505-1513, 2001.

Chapter Five

Fatigue and Fracture Mechanism of Aluminum-Carbon Fiber Reinforced Hybrid Composites

5.1 Introduction

Fatigue tests on a carbon fiber reinforced epoxy composite combined with aluminum foil or on aluminum plate were conducted. Carbon fiber reinforced epoxy composites are used in the structural application of integral parts for automobiles, aircraft and so on because of their light weight, high strength, and low-density characteristics. Lower weight and a higher modulus of elasticity makes it mostly applicable to the structural sectors. In the previous study, a basic study was conducted on the strength characteristics of notched specimens or slit specimens of composite materials with woven carbon fibers [1, 6-10]. It was discussed that the fatigue limit of the smooth specimen was predicted from the result of the notched specimen, and the effect of the long fiber direction on the fatigue behavior was analyzed [1-4]. The hybrid composites were prepared for the present study by assembling them one after another from commercially available woven carbon fiber cloth along with the aluminum foil or thin aluminum plate aligned in a uniaxial direction, and then impregnating the cloth/sheet with epoxy resin. Vacuum Assisted Resin Transfer Molding (*VaRTM*) system was applied to fabricate the hybrid composites. In the present study, the discussion was limited to the notched specimen for comparison to the previous study [1].

5.2 Materials and Experimental Method

Three types of specimen were prepared to conduct the experiment. Fig. 5.1 shows the specimen geometry and type of specimen. For the manufacture of the *A* type specimen only woven carbon fiber sheets were piled up in the loading direction. In this specimen, eleven carbon fiber sheets were used. Epoxy resin was allowed to spread/transfer through the carbon fiber sheets by the *VaRTM* method [4, 5]. The thickness of one woven carbon fiber sheet was about 0.35 mm. The *B* type specimen was fabricated by incorporating layers of aluminum foil as a filler material between the same carbon fiber sheets as used for the *A* type specimen. In this case, six woven carbon fiber sheets were used with five aluminum foil sheets in the longitudinal direction. The thickness of the aluminum foil was 0.01mm. The *C* type hybrid composites were fabricated with 0.5mm thick

aluminum plate which was placed in the middle with three woven carbon fiber sheets layered on each side of the aluminum plate. The aluminum plate was polished by abrasive paper and rinsed with ethanol to make it clean and dry prior to fabricating the hybrid composites.

The *A* and *B* types of specimens were tested at the stress ratio of *R*=-1, and the *C* type specimen was tested at the stress ratio *R*=0. The fiber orientation of the woven carbon fiber sheet/cloth is shown in Fig. 5.1. A Slit was introduced from both sides of the specimen to limit the discussion to the notched specimen case. The length of the slit and ligament differed for each type of specimen; the thickness was 2.4mm to 3.0mm, and the length of the specimens was 120.0mm. The experiment was carried out by changing the notch length for each type of specimen. The fatigue limit of a specimen was evaluated with net stress [1]. The stress amplitude, σ_a was calculated by the following Eq. (5.1):

$$\sigma_a = P/\{2b(W-t)\} \tag{5.1}$$

Where, *P* is the applied load to the specimen, 2*W* is the total width of the specimen, *b* is the thickness of the specimen, and *t* is the slit length on each side of the specimen.

The fatigue test was carried out by using an electro-hydraulic servo testing machine with a loading capacity of 9.8kN. The frequency was set as *f* =10Hz. Crack initiation and growth were monitored directly on the surface of the specimen by using an optical microscope which was connected to an image display monitor to investigate the fracture process of the material used. The *S-N* curve is being used as an essential tool to determine the fatigue limit, σ_w. In this study, the fatigue limit was obtained for both the cases of *R*=-1 and *R*=0. The fatigue limit σ_w was the maximum applied stress σ_a that the material could endure10^7 repeated cyclic stress. The objective of the present study was to investigate the feasibility of producing light-weight aluminum-based hybrid carbon fiber composites with high strength to use as structural materials.

5.3 Experimental Results and Discussion

5.3.1 Determination of Fatigue Limit

Fig. 5.2 (a) shows the *S-N* curve for *R*=-1 based on Type *A* and Type *B* specimens. It is found that the fatigue limit of the *A* type specimen was 300MPa and for the *B* type specimens it was 140MPa. Therefore, the fatigue limit of the specimen fabricated by only with carbon fiber sheets

was higher than that of the hybrid composite specimen made with the combination of aluminum foil and woven carbon fiber sheet. The ratio of the number of carbon fiber sheets aligned in the loading direction determines the fatigue limit [1]. Here, the maximum number of woven carbon fiber sheets was in the loading direction in the *A* type specimen. From those results, it is expected that the maximum number of unidirectional carbon fibers aligned in the loading direction contributed to the fatigue limit of the *A* type specimen.

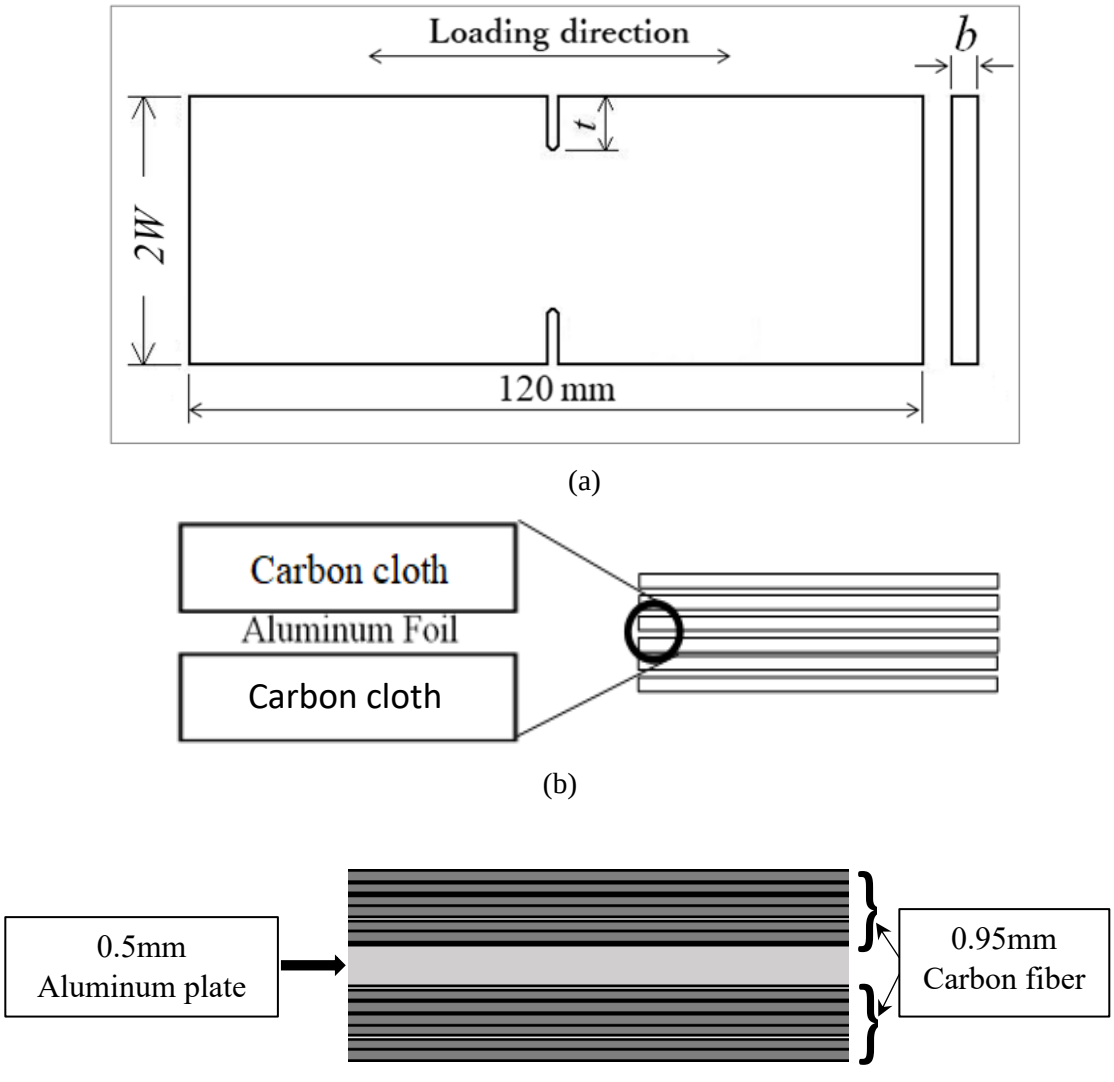

Figure 5.1 Epoxy based carbon composites: (a) Geometry of the specimens (A type, B type, and C type) (b) Combination of carbon fiber sheet and aluminum foil (*B* type specimen), (c) Combination of carbon fiber sheet and aluminum plate (*C* type specimen).

In future, we will make a sensor to detect internal crack growth in the specimen made with carbon composite material. We made the present composite material, and the experiment was performed with the addition of aluminum foil or the aluminum plate to make it cost effective. For the *C* type specimen, a fatigue test was conducted for both *R*=-1 and *R*=0. For negative stress ratio at *R*=-1, the fatigue limit was not satisfactory for the *C* type specimen. Specimens were broken in an indistinct manner because of machine accidents. Therefore, those tests should be performed again in the future. When the stress ratio is *R*=0, the specimen can survive 10^7 repetition cycles or more at 410MPa as is shown in Fig. 5.2 (b). The experimental results for the *C* type specimen are shown in Table 5.1. From this behavior of the specimen, it may be expected that the *C* type specimen has higher tension-tension load bearing capacity.

From previous experimental results, it is found that the fatigue limit of the *A* type specimen at *R*=0 was 410MPa [1]. It is discussed that the fatigue limit of the *C* type specimen was almost the same as for the *A* type specimen even with the incorporation of the aluminum plate. These results show that the combination of carbon fiber and thin aluminum plate composite has a good fatigue limit. It indicates that the fiber orientation in the loading direction has an effective influence on the critical limit during the fatigue test. The fatigue limit become higher when tension-tension loading was applied than when tension-compression loading was applied. Also, the *A* type [1] and *C* type specimens show the same fatigue behavior in the case of tension-tension loading condition.

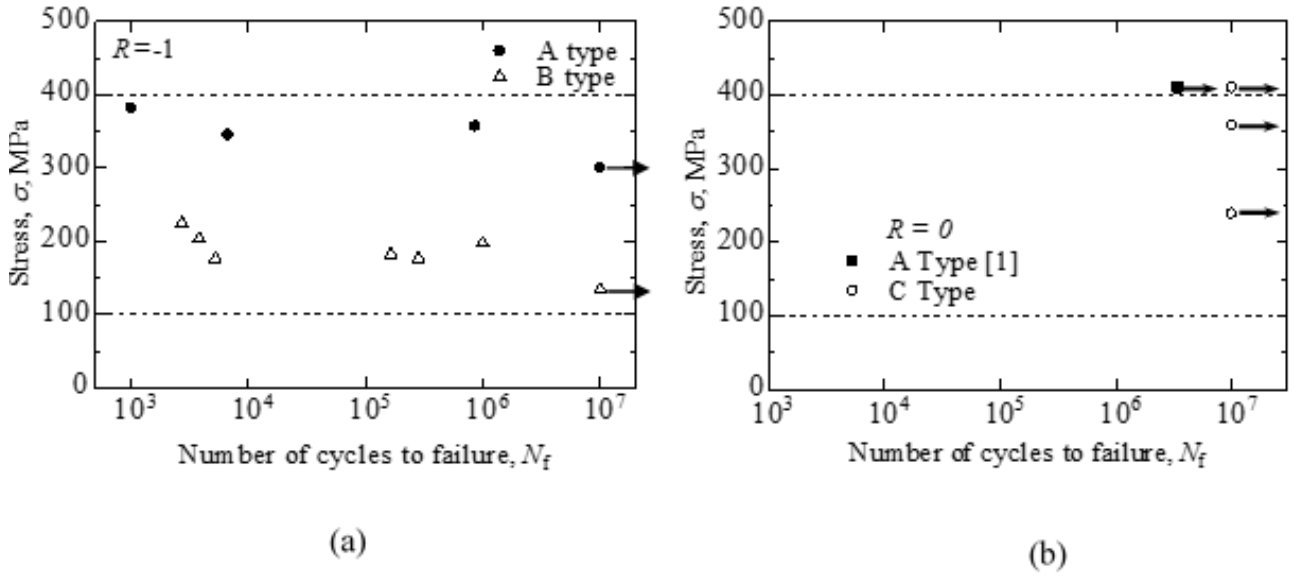

Figure 5.2 *S-N* curve: (a) *R*=-1, (b) *R*=0

Table-5.1: Experimental results for the *C* type specimen at stress ratio, $R = 0$

Ligament length (mm)	Ligament thickness (mm)	Load, σ (MPa)	Cycle to failure, N, 10^7	$2w$, (mm)	Slit, $t1$ (mm)	Slit, $t2$ (mm)
8.00	2.40	240.0	Not broken	24.00	8.00	8.00
8.00	2.40	360.0	Not broken	25.00	9.00	8.00
8.00	2.40	410.0	Not broken	24.00	8.00	8.00

From the experimental results of the present study, the fatigue limit of a notched specimen can be used to determine the fatigue limit of a specimen without a notch or a smooth specimen by analyzing the stress. When a shear fracture occurs due to decohesion of fiber and resin, the strength of the specimen became lower. It may be estimated that the fatigue limit also depends on the fabrication process. By applying the sensors to the composite plate, we can investigate the internal crack initiation and growth behavior of the specimen.

5.3.2 Obervation of Crack Growth Behavior

For the *A* type specimen, the crack initiated from both sides of the notch tip which is shown in Fig. 5.3 (a) and propagated parallel to the loading direction, that is along the fiber direction. The specimen did not break in the direction perpendicular to the loading direction, and after a few millimeters of crack propagation in the parallel direction of loading, final fracture suddenly occurred in shear mode. Carbon fiber composite is a brittle material. Aluminum foil is a brittle material too and most brittle fractures occur in shear mode.

The fracture surface is inclined to the maximum and the minimum principle axis is at an angle of $25^0 < x < 45^0$ and parallel to the intermediate axis. This angle is influenced by the cohesion property of the carbon fiber reinforced epoxy resin composite. From Fig. 5.3 (a & b), it is found that pure tensile and compressive load was applied along the *y*-axis to conduct the fatigue test. The Crack initiated from the tip of the manually generated notch along the *y*-axis and then the final fracture took place parallel to the intermediate *xy*-axis (Fig. 5.3 (a & b)). In this experiment, the shear fracture happened suddenly [11]. It may be said that when one fiber breaks with the application of tensile and compressive load, the applied load was redistributed uniformly over all

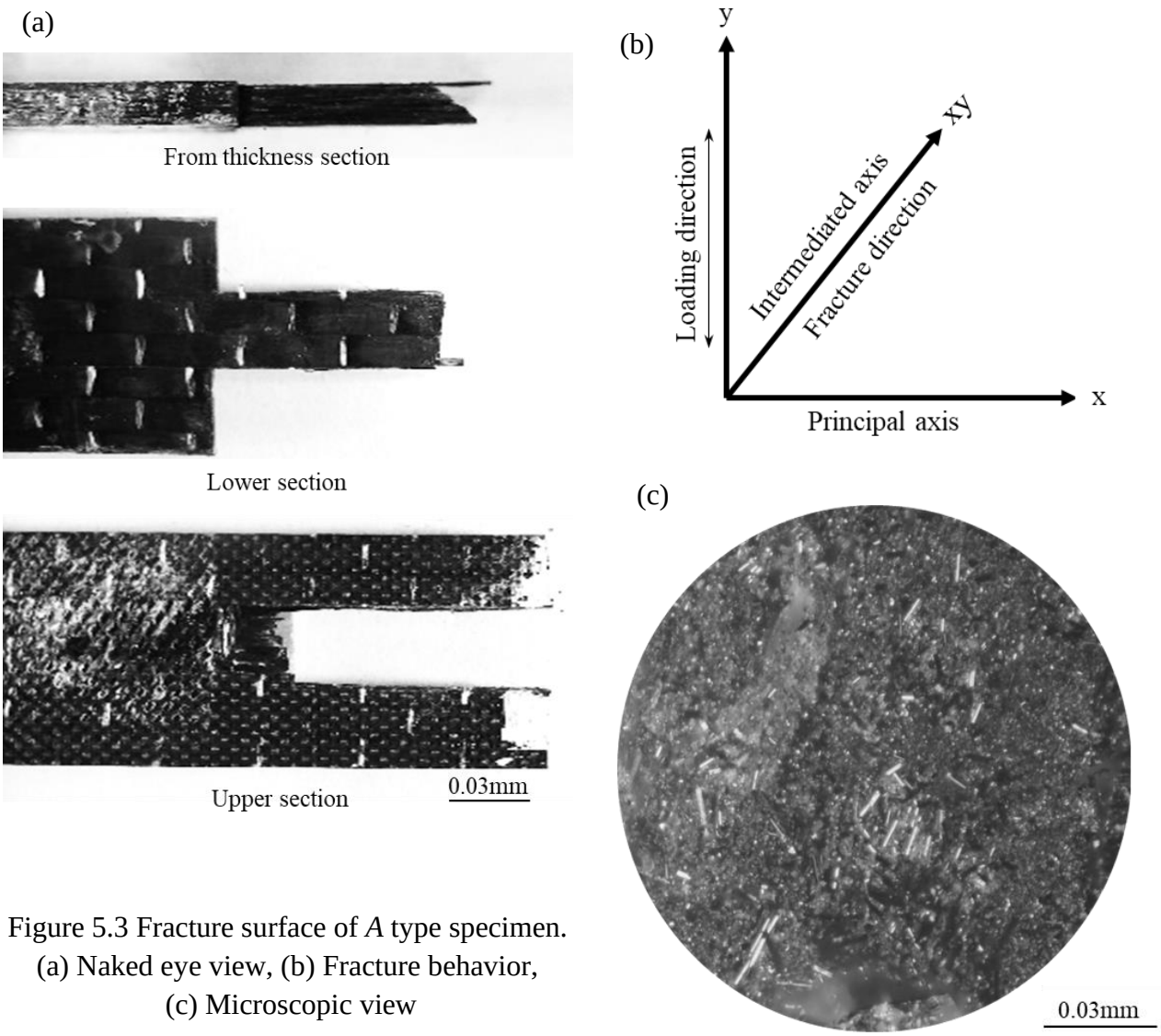

Figure 5.3 Fracture surface of *A* type specimen.
(a) Naked eye view, (b) Fracture behavior,
(c) Microscopic view

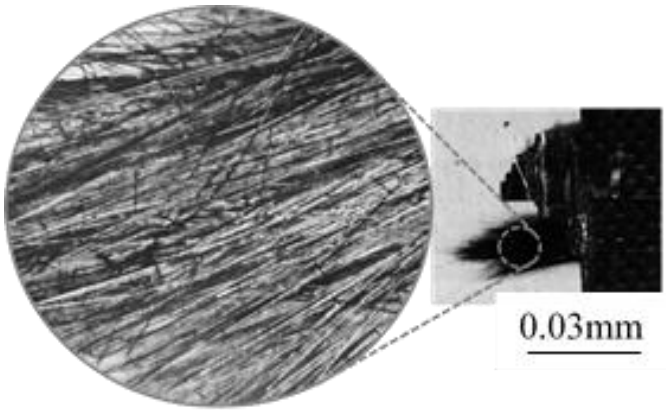

Figure 5.4 Fracture surface of *B* type specimen (Microscopic view).

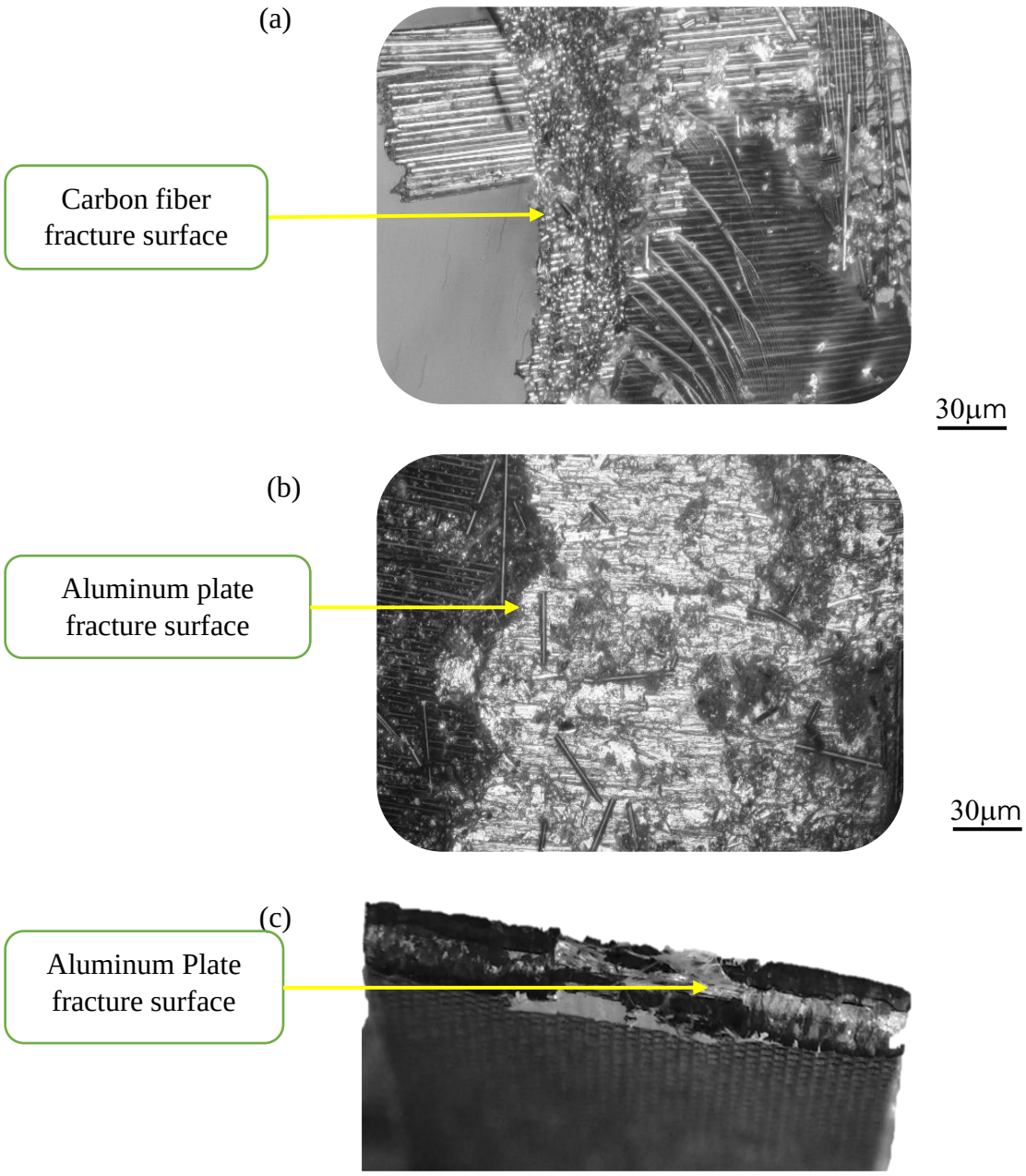

Figure 5.5 Fracture surface of *C* type specimen at *R* = -1 (shear fracture): (a) & (b) Microscopic view (c) Naked eye view

the reamining fibers by the influence of stress concentration on its nearest unbroken fiber and demonstrated that failure of even a very limited number of fibers may lead to the failure of the whole specimen. It is because the loading area become shorter gradually that the final fracture took place momentarily.

In the *B* type specimen, a similar shaped of *S-N* curve was found but the fatigue strength of the specimen was much lower than that of the *A* type specimen. It may be due to the reduced number of carbon fiber sheets incorporated in the fabrication of this type of specimen. The thickness of the aluminum foil is 0.01mm versus the 0.35mm thickness of a single carbon fiber sheet and had a negligible contribution to the strength of the specimen.

Interlaminar shear strength is one of the important material parameters which affets the load bearing capacity of the material in as a structural applications. For the *A* type specimen, from Fig. 5.3 (a & c), no noticeable delamination characteristics were found, i.e., interlaminar bonding with adjacent fibers was good. But for the *B* type specimen, a tiny proportion of delamination tendency was found which was completely absent in the *A* type specimen. We can say that interlaminar bonding between the woven carbon fiber material and the aluminum foil or plate was not effective.

The fracture pattern and crack growth behavior have been discussed in the previous article [2]. For the *B* and *C* type specimens, the crack initiated from the notch tip and cut the fibers in shear mode within the notch tip area and then the crack propagated in shear mode. Also, delamination/separation of the fiber from the aluminum foil was observed. On some parts of the fracture surface, shown in Fig. 5.4 the carbon fiber layers delaminated from each other before the final fracture of the specimen. However, the fracture pattern of the *B* and *C* type specimens was different in the cases of R=-1.

5.4 Conclusion

In this study, the effect of incorporating aluminum foil or an aluminum plate with the woven carbon fiber cloth in hybrid composites by using slits on both sides of a specimen were investigated. The main results obtained are as follows:

(1) A higher fatigue limit was obtained in the case of the *A* type specimen when all the carbon fibers were in the loading direction. Also, the mechanical strength of the carbon fiber in the loading direction is higher than that of the aluminum foil or the aluminum plate at $R = -1$. The strength also differs due to variations in the thickness of the woven carbon fiber, aluminum foil and aluminum plate.

(2) The fracture behavior is different for different types of specimens, as the composition and the number of layers of woven carbon fiber material are different. The fracture behavior depends on the interfacial bonding between the woven carbon fiber material and aluminum foil in the *B* type specimen or between the woven carbon fiber material and aluminum plate in the *C* type specimen. The strength properties of the specimen could be improved by improving the interlaminar bonding between the woven fiber cloth and aluminum foil or plate.

(3) For the application of tension-tension loading conditions, the *A* type and *C* type specimens showed almost the same fatigue limit even though a reduced number of carbon fiber sheets were used.

5.5 References

[1] Md. Shafiul Ferdous, S.M. Moshiar Rahman, Chobin Makabe, "Effect of Fiber Direction and Stress Ratio on Fatigue Property in Epoxy Carbon Composites, Material Science Forum, ISSN: 1662-9752, Vol. 940, p. 79.

[2] C. Makabe, M. Fujikawa, M.S. Ferdous, S. A. Setyabudi, Journal of High-Pressure Institute, Vol. 51, No. 6 (2013), pp. 303.

[3] C. Makabe, T. Nakayama, M. Fujikawa, K. Arakawa, D. Chen, "Effect of Specimen Thickness on Fatigue Limit in Carbon Composites", Advanced Materials Research, Vol. 1110 (2015), p.13-18.

[4] M. Yamashita, T. Sakagawa, F. Takeda, F. Kimata, "Development of Advance Vacuum-Assisted Resin Transfer Molding Technology for Use in an MRJ Empennage Box-Structure", Mitsubishi Heavy Industries, Ltd. Technical Review, No. 45-4 (2008), p.1-4.

[5] D. Chen, K. Arakawa, S. Jiang, "Novel Joints Development from Partially Un-Moulded Carbon Fiber Reinforced Lamination", Journal of Composite Materials, Vol. 49, No. 14, (2015), pp.1777-1786.

[6] K. Goto, H. Hatta, D. Katsu, T. Machida, "Tensile Fatigue of a Laminated Carbon-Carbon Composite at Room Temperature", Carbon, Vol. 41 (2003), p. 1249-1255.

[7] Ozturk A., Moore RA. "Tensile Fatigue Behavior of Tightly Woven Carbon/Carbon Composites", Composites, Vol. 23, (1992), pp.39-46.

[8] Erich Fitzer, "The Future of Carbon-Carbon Composite", Carbon, Vol. 25 (2), (1987), pp.163-190.

[9] H. Hatta, K. Suzuki, T. Shigei, S. Somiya, Y. Sawada, "Strength Improvement by Densification of Carbon-Carbon Composite", Carbon, Vol.39, (2001), pp.83-90.

[10] Y. Kogo, H. Hatta, A. Okura, Y. Obayashi, Y. Sadawa, M. Fujikawa, "Strength and Toughness of Carbon-Carbon Composite at Elevated Temperature", Trans. Tokyo Inst. Polytech, Vol.17, Issue.1, (1994), pp.50-58.

[11] L. Denk, H. Hatta, A. Misawa, S. Somiya, "Shear Fracture of C / C Composites with Variable Stacking Sequence", Carbon, Vol.39, (2001), pp.1505-1513.

Chapter Six

Effects of Existence of Unexpected Defects on Fatigue Strength

6.1 Introduction

Material quality has been improved with the development of industrial technology. The fatigue limit of structural material has been improved, too. However, fracture incidents have happened for unexpected reasons[1)]. Also, some commercially sold material shows unexpected strength. In this study, the fatigue limit σ_w of such material was investigated. The fatigue limit of a plain specimen has been evaluated by Vickers hardness *HV* in many kinds of steel[2)]. On the other hand, the fatigue limit of a metal containing a defect has been evaluated by the functions of the size of the defect (*area* of defect) and Vickers hardness[3)]. Those evaluation methods were represented by the following equations, respectively,

$$\sigma_w = 1.6HV \tag{6.1}$$

$$\sigma_w = \frac{1.43(HV + 120)}{(\sqrt{area})^{1/6}} \tag{6.2}$$

Where, unit of σ_w, *HV* and 'area' are MPa, kgf/mm^2 and μm^2, respectively. Now, *HV* is the average value of Vickers hardness.

In the previous study[4)], the relationship between Eqs. (6.1) and (6.2) were discussed from the viewpoint of evaluation of fatigue limit σ_w of a plain specimen or smooth specimen. In that case, the initiation of a fatigue crack was related to the grain size of perlite. Figure 1 shows an example of relationship between the fatigue limit σ_w, ultimate tensile strength σ_B and carbon % in the cases of annealed steel[5)]. There is a variation in the strength of materials. Therefore, the strength of materials is related to the distribution of microstructures, defects, production methods and so on. Also, the strength of materials could be evaluated from the previous data and physical conditions.

The carbon steel used in the present study showed a lower fatigue limit than the expected value from Eq. (6.1). Also, it is expected that this fatigue limit was not related to the grain sizes. There is some inconvenient situation in the material used. So, the decrease of fatigue strength of a carbon steel from its expected value from Eq. (6.1) was discussed in consideration of the apparent size of defects which lead crack growth faster.

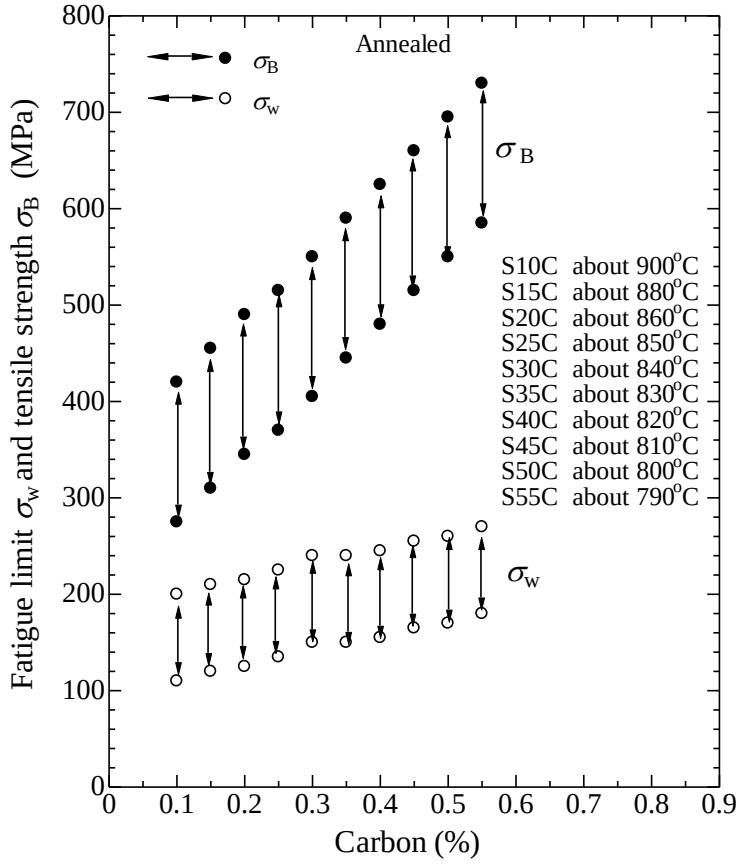

Figure 6.1 Relationship between σ_w, σ_B and carbon% in annealed carbon steels.

6.2 Material and Experimental Procedure

The material used for the test was low carbon steel for which the chemical composition (wt, %) is 0.25%C, 0.30%Si, 0.50%Mn, 0.013%P, 0.013%S, 0.19%Cr, 0.05%Ni, 0.14%Cu and bal. of Fe. The mechanical properties of material are 283 MPa of lower yield strength, 439 MPa of ultimate tensile strength and 60 % of reduction of area.

The examples of microstructures after a heat treatment are shown in Fig.6.2. There is a large size defect (or inclusion) and a section in which distances of defects are very short. The size of some defect was larger than grain size: average perlite size was 21 μm and average ferrite size was 28 μm. It is not expected that that material was produced for use in a machine equipment. However, if it is used for a machine equipment, inconvenient problems will happen. The material was annealed for 1 hour under 860°C. After annealing, the specimen was machined by lathe. Figure

6.3 shows the specimen geometry. To ease the observation of fatigue cracks, a partial notch was cut in the test section of some specimens. That notch shape is shown in Fig. 6.3 (b). Also, the specimens having a hole whose diameter and depth were 0.2mm (Fig. 6.3 (c)) were used.

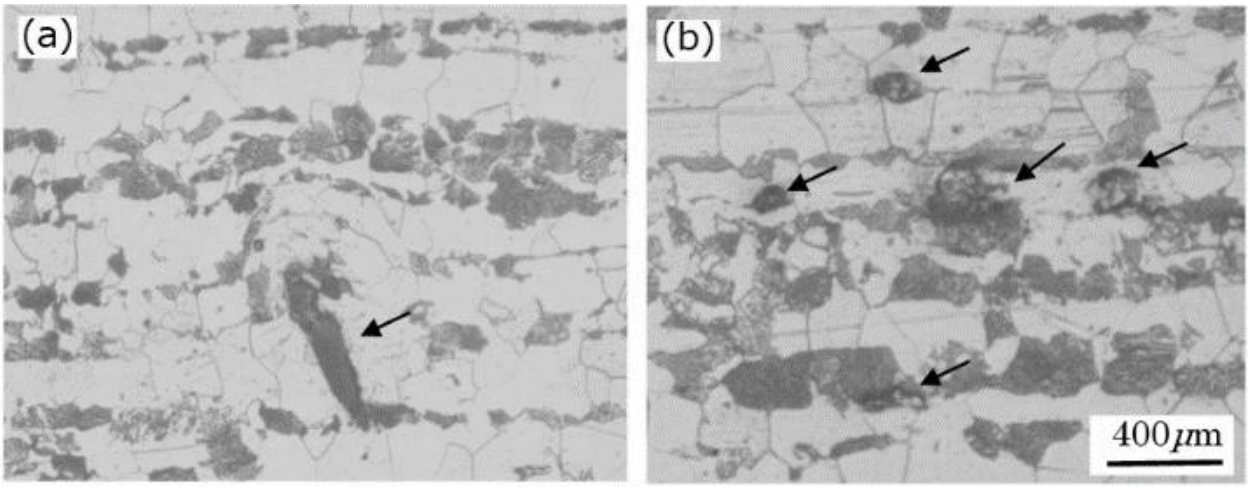

Figure 6.2 Microstructure (Longitudinal section) and inclusions; (a) Large inclusion, (b) Plural small inclusions.

Hereinafter, a specimen with a partial notch or a hole is called a partial notch specimen or holed specimen, respectively. A specimen which does not have notch or hole is called a smooth specimen. Smooth specimens and the holed specimens were annealed for 1 hour at 600^{o}C by an electric vacuum furnace. The electric vacuum furnace did not work because of an air leaking when the heat treatment of the partial notch specimen was going to start, and it took time to restore the electric furnace to normal conditions. Therefore, in the case of the partial notch specimen, annealing by the electric furnace was not performed. As a result, that heat treatment conditions did not affect the results of the present study. Also, the purpose of using the partial notch specimen was observation of fatigue crack initiation and growth. Because the stress concentration factor of the partial notch bottom is about 1.4, the partial notch specimen can be regarded as a smooth specimen [6)]. Now, the partial notch specimen was used for observation of crack behavior instead of the smooth specimen. The surface of all specimens was finished by emery papers and metal polish powder. The push-pull fatigue test was performed by an electrohydraulic servo type testing machine. The main tests were performed with a stress ratio R of -1 that is the ratio of minimum

cyclic stress σ_{min} to maximum cyclic stress σ_{max}, and a frequency of 10Hz. The observation of crack initiation and growth was performed with a replication technique.

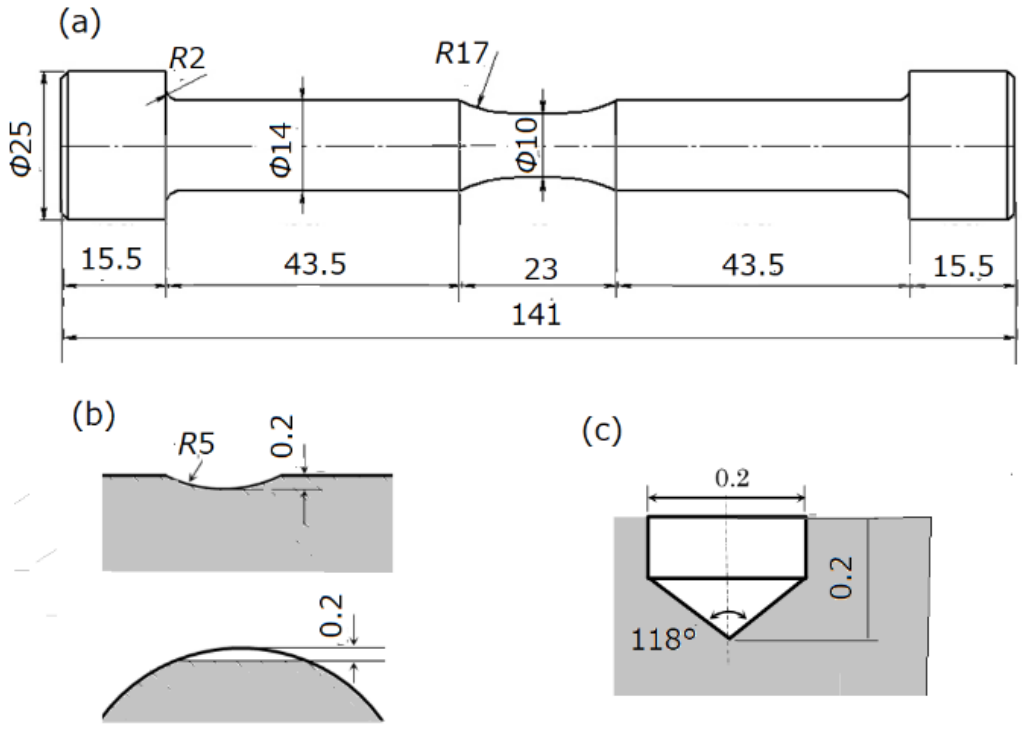

Figure 6.3 Geometry of the specimen, partial notch, and hole; (a) Specimen, (b) Partial notch, (c) hole.

6.3 Results and Discussions

6.3.1 Fatigue limit and crack growth

Figure 6.4 shows the *S-N* curves, that is the relationship between the stress amplitude σ_a and number of cycles to failure N_f. It can be approximated that the fatigue limit of the smooth specimen was almost the same as that of the holed specimen and the partial notch specimen. Since the average of Vickers hardness was 125, the fatigue limit σ_w of the smooth specimen was evaluated as being 200 MPa from Eq. (6.1). However, the experimental result of σ_w was165 MPa. Thus, that is clearly different from the evaluation value from Eq. (6.1).

Because of the dimensions of the hole, that is, 0.2 mm for both hole depth and diameter and 118 deg of angle of drill point, *area* that obtained by projection of hole geometry in the axial direction of the specimen was 6800 μm^2. The calculated value of σ_w of the holed specimen from Eq. (6.2) was 160 MPa. This value is almost the same as the experimental result (σ_w for the holed specimen = 164 MPa). It is well known that the fatigue limit of a specimen including a defect can be evaluated from Eq. (6.2) with high accuracy. In the present experimental case, the fatigue limit of a holed specimen can be represented by the function of Vickers hardness and defect size, also.

In this study, the reason that the fatigue limit of the smooth specimen had a lower value than the evaluation value from Eq. (6.1) was discussed from the viewpoint of the fatigue crack initiation and growth. Now, in the case of a holed specimen, the leading crack initiated from another part of the hole and this crack led to specimen failure when the number of stress cycles N reached 1.04×10^6. This data is shown with the symbol * in Fig. 6.4. That means that there was a large defect which may have led to the specimen failure in addition to the drilled hole.

The crack growth behaviour is related to the fatigue life. Figure 6.5 shows the crack growth curves or relationship between the number of stress cycles N and crack length l. In the case of a holed specimen, crack length includes hole diameter (0.2 mm). It is expected that the crack initiation and growth behavior of the smooth specimen and the partial notch specimen are not so much different. The applied stress level affect to the crack initiation life and growth life[7]. Therefore, some stress amplitudes close to the expected fatigue limit, which was evaluated from Eq. (6.1), were selected for the conditions of crack growth tests. Thus, 204 MPa and 190 MPa were the stress amplitudes for the testing and it was in reference to the 200 MPa of σ_w.

In the case of the partial notch specimen, crack initiation was confirmed when the relative number of cycles N/N_f was 0.5. Because a linear relationship is obtained between the number of stress cycles and crack length where N/N_f is larger than 0.6, it is approximated that the crack growth rate dl/dN is proportional to the logarithm of crack length l [8]. In the case of the holed specimen, stable crack growth was observed where N/N_f was larger than 0.2. The stress concentration at the hole bottom somewhat affected the crack growth behaviour[9]. However, it is expected that the crack growth rate dl/dN is proportional to the crack length when the crack grows stably. There is some difference between the tendencies of crack growth rate in the holed specimen and partial notch specimen because of the difference of the crack initiation life. However, the size of crack initiation

of the smooth specimen is close to 0.1mm. This size is not so much different from the hole diameter of the holed specimen. It is important that the size of the defect observed in Fig.6.2 is related to the crack behavior, and the crack initiation size is not related to the grain sizes. Thus, the crack initiation and growth behavior are related to the fatigue limit of the smooth specimen, partial notch specimen and holed specimen.

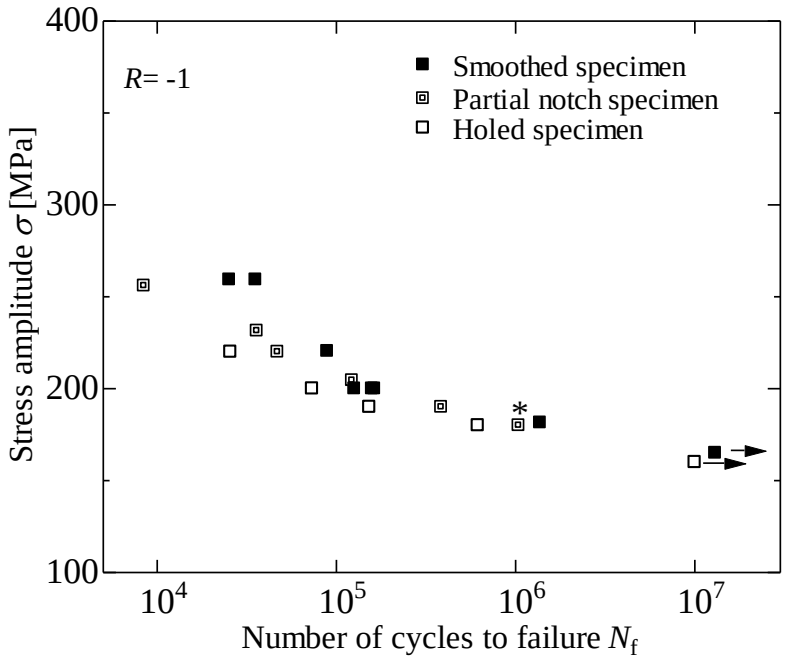

Figure 6.4 *S-N* curves of smooth specimen, partial notch specimen and holed specimen.

6.3.2 Observation of crack growth and fracture surface

Examples of observation of crack growth are shown in Figs. 6.6 and 6.7 in the case of the partial notch specimen. Crack initiation was observed when N/N_f reached about 0.5. The coalescence of cracks was observed in almost all cases of the partial notch specimen. The crack growth was observed by plastic replication techniques without etching the specimen surface. So, the crack initiation site is hard to detect in the pictures in Figs. 6.6 and 6.7. However, the pictures in those figures show almost the same sites of specimen surface, respectively. From those figures, immediately after crack initiation, the crack grew larger than 0.2 mm by cyclic stress. Now, arrows in Figs. 6.6 and 6.7 show the crack tips. The observation of fracture surface was performed by using a surface view microscope, an optical microscope and usual camera. Figure 6.8 shows

examples of a part of the fracture surface including crack initiation site in the case of partial notch specimen (The stress amplitudes are 180 MPa).

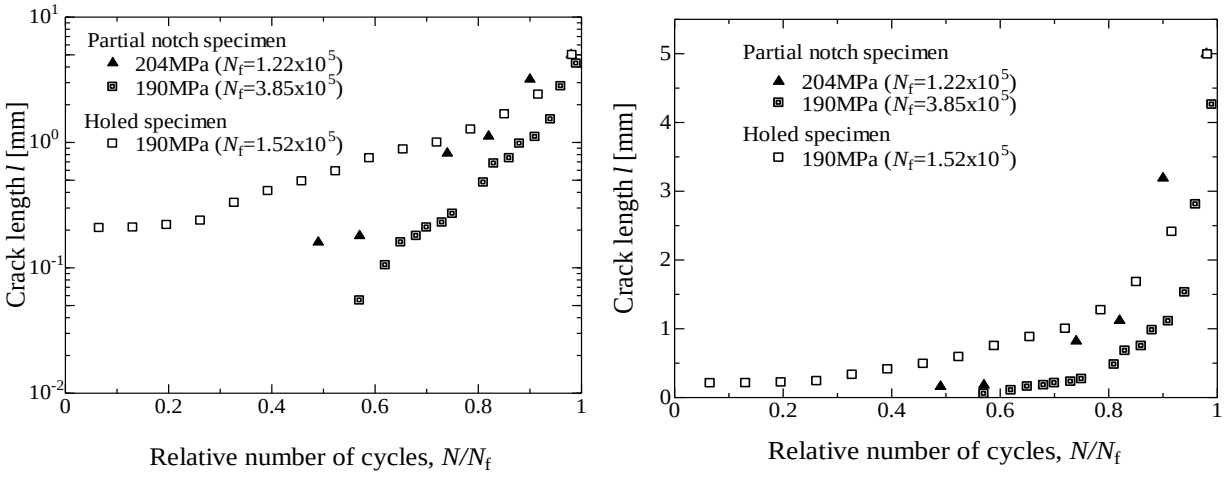

Figure 6.5 Crack growth curves: (a) l vs. N/N_f, (b) ln l vs. N/N_f

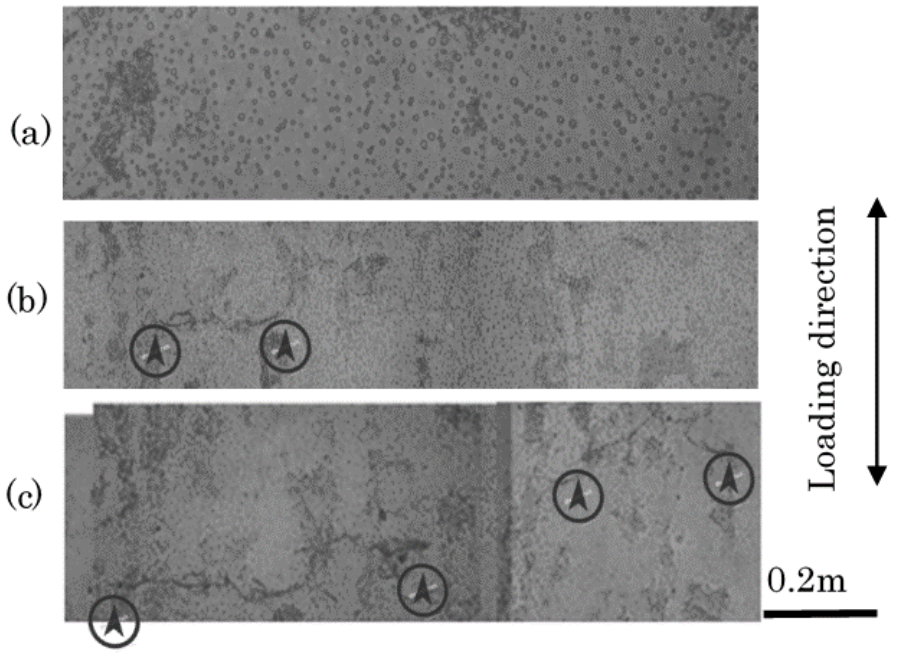

Figure 6.6 Observation of crack (σ_α= 205MPa); (a) N=5.0x10^4, N/N_f=0.41, l=0mm, (b)N=6.0x10^4, N/N_f=0.49, l=0.16mm, (c) N=9.0x10^4 , N/N_f=0.70, l=0.82mm

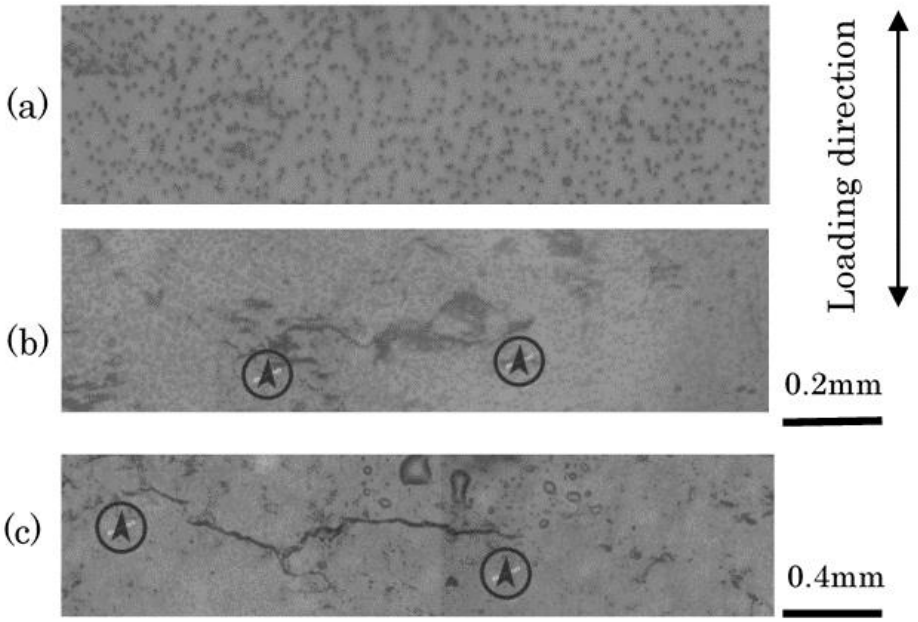

Figure 6.7 Observation of crack (σ = 190MPa); (a) N=1.8x10^5 N/N_f=0.47, l=0mm, (b)N=2.4x10^5 N/N_f=0.62 l=0.105mm, (c) N=2.7x10^5 N/N_f=0.70, l=0.21mm

The crack initiation site is expected to be detected by the surface roughness patterns and marks of existence of defects. The arrows show the crack initiation site from defects. There are areas which can be approximated by semi-circle with diameter of 100 μm to 300 μm. Those areas can be the crack initiation sites. The crack was initiated from a large size defect. Also, crack coalescence can happen in the crack growth stage as represented by Fig. 6.9. If there is a section in which distances of defects are very short and plural cracks initiate from them, the crack coalescence can happen in the very early stage of crack growth. Also, the coalescence of cracks initiates from defects at surface and internal sections.

Figure 6.10 shows the observation of the fracture surface of the holed specimen. The leading crack that led to about specimen failure did not initiate from the hole. On the specimen surface, a relatively large size of crack was observed at the hole. If the crack growth did not proceed from a site other than the hole, the origin of leading crack must be the hole. From the observation results of crack growth and fracture surface, the cause of the lower fatigue limit than the expected value was the existence of abundant, large size defects in the carbon steel used in the present study. That material is not expected to be produced for use the machine equipment.

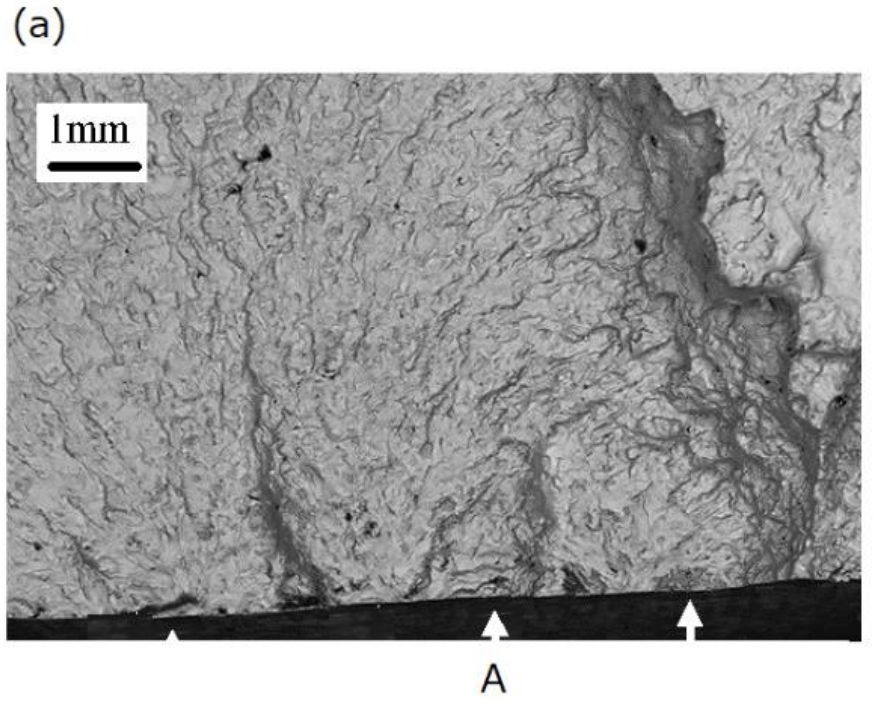

Figure 6.8 Observation of fracture surface by a surface view microscope (σ_a=180 MPa); (a) Plural initiation sits, (b) Detail of part A.

However, it is not good if such materials are used without any warning about the existence of such defects. That material was obtained through the usual commercial system. When a material is used for machine equipment, the size of defects had better be checked. Also, when a material is used for machine equipment without inspection of defects, it had better to be designed applying stress under the conditions that material has a relatively large size defect. For example, the expectation diameter of defect can be set to 0.2 mm or more. The material used in the present study was purchased as S25C from a local business company, but it is not thought that it has a standard quality of S25C.

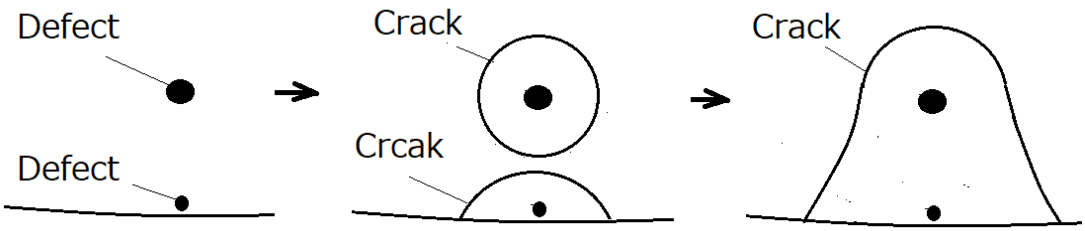

Figure 6.9 Schematic representation of crack growth from defects.

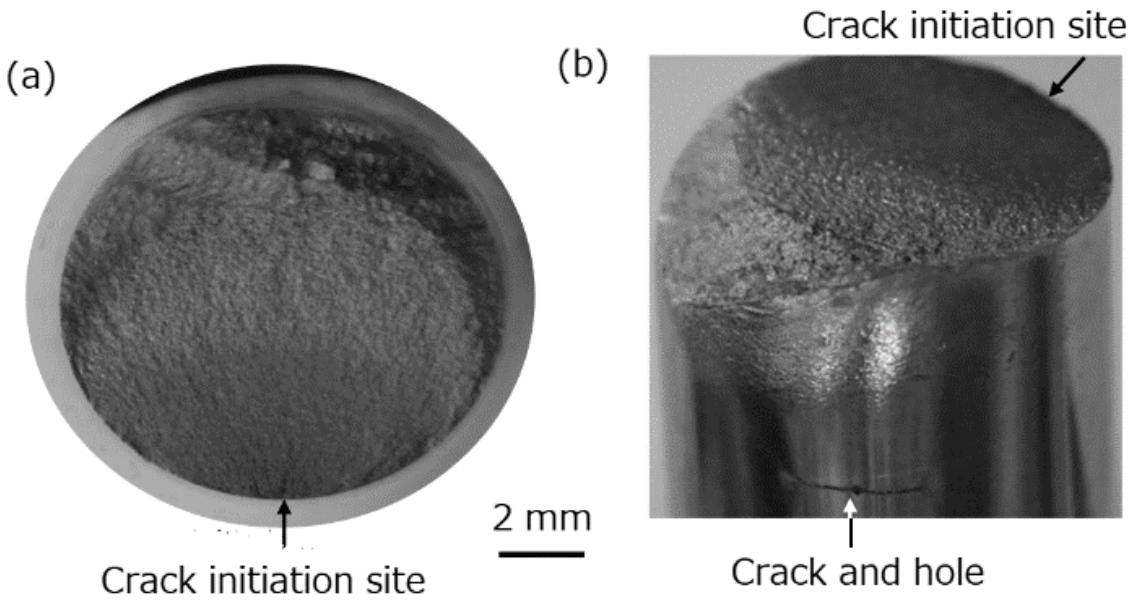

Figure 6.10 Observation of fracture surface of holed specimen when specimen broken from another part of hole (σ_a= 180 MPa); (a) Top view, (b) View from inclined direction.

6.4 Conclusion

Fatigue limit and crack behavior were investigated in a commercially sold carbon steel. After annealing, three types of specimen were machined. That is, the smooth specimen, partial notch specimen and holed specimen. The results obtained are as follows,

1) The fatigue limit of the smooth specimen shows clearly a lower value than the evaluated value from Vickers hardness.
2) The fatigue limit of the holed specimen had almost the same value as the evaluated value from Vickers hardness and projected area of the hole in the axial direction of specimen.
3) Fatigue limits for the smooth specimen and the holed specimen had almost the same value. That is related to the crack initiation behavior. Because, the material used has large size defects and a section in which distances of defects are very short, the crack initiation size was larger than 0.1 mm in the case of the smooth specimen and partial notch specimen. The existence of such defects and the crack growth behavior is related to the fatigue limit.
4) The material used is not expected to be produced for use in machine equipment. It is good such kind of material is sold with a warning about the existence of defects.

6.5 References

[1] S. Nishida; “Failure Analysis in Engineering Applications”, Butterworth-Heinemann Ltd, pp. 1-5 (1991).

[2] M. F. Garwood, H. H. Zurburg and M. A. Erickson; “Correlation of Laboratory Tests and Service Performance”, Interpretation of Tests and Correlation with Service, ASM, Publication, PA, pp. 1-77 (1951).

[3] Y. Murakami and M. Endo; “Effects of Hardness and Crack Geometry on ΔK_{th} on Small Cracks”, J. Soc., Mater. Sci., Japan, Vol. 35, No. 395, pp. 911-917 (1986).

[4] C. Makabe, S. A. Jafari, K. Ishikawa and T. Miyazaki; “A Study on Relationship among Crack Initiation Size, Fatigue Limit and Hall Petch Relation”, J. Soc., Mater. Sci., Japan, Vol .66, No. 5, pp. 365-371 (2017).

[5] Mechanical system design handbook, “Fatigue Strength of Steels”, URL of Japanese Standard Association Group,http://ebw.engbook.com/pdfs/ecb7c8688913e12a4494939494498e79.pdf#search='%E7%82%AD%E7%B4%A0%E9%8B%BC%E3%81%AE%E7%96%B2%E5%8A%B4%E5%BC%B7%E5%BA%A6' 2012).

[6] H. Nisitani and K. Takao; “Significant if Initiation, Propagation and Closure of Microcracks in High cycle Fatigue of Ductile Metals”, Eng. Frac. Mech., Vol. 15. No. 3-4, pp. 445-456 (1981).

[7] H. Nisitani and M. Goto; “Effect of Stress Ratio on the Propagation of Small Crack pf Plain Specimen under High and Low Stress Amplitudes (Fatigue under Axial Loading of Annealed 0.45% Carbon Steel)”, Tras. Japan Soc. Mech. Eng., Ser. A., Vol. 50, No. 453, pp. 1090-1096 (1984).

[8] Y. Murakami, Md S. Ferdous and C. Makabe; “Low Cycle Fatigue Damage and Critical Length Affecting Loss of Fracture Ductility”, Int. J. Fatigue, Vol. 82, No. 1, pp. 89-97 (2016).

[9] Y. Nakai, K. Tanaka and Y. Kawashima; “Propagation and Non-Propagation of Fatigue Cracks in Notched Plates of Low-Carbon Steel”, J. Soc., Mater. Sci., Japan, Vol. 32, No. 356, pp. 535-541 (1983).

Chapter Seven

A Method for Prediction of Fatigue Limit and Life in Carbon Steel

7.1 Introduction

For the reliability and safety designing of engineering structural components metal fatigue should be taken in account. Hence, the study on metal fatigue property of materials is very important. The evaluation of fatigue life and investigation of crack initiation and propagation have been performed by many researchers [1-10]. In the case of carbon steel, there is a clear fatigue limit σ_w under constant stress amplitude, which is measured from the knee point of the *S-N* curve [11]. The fatigue limit is affected by the size of internal defects and inclusions (which size is defined by projected area in the load axis direction). Some method of evaluating the fatigue limit using hardness have been proposed as in the following equations [12, 13]

$$\sigma_w = 1.6HV \tag{7.1}$$

$$\sigma_w = \frac{1.43(HV + 120)}{(\sqrt{area})^{1/6}} \tag{7.2}$$

Where, the units of σ_w, *HV* and area are defined as MPa, kgf/mm^2 and μm^2 respectively. *HV* is the average value of Vickers hardness. Eq. (7.1) is used for evaluating fatigue limit of so-called smooth specimen without having any defects, and Eq. (7.2) for evaluating the fatigue limit σ_w of the material presence of defects. Murakami and Endo [12] proposed Eq. (7.2) using the fracture mechanics parameter, and many researchers have used it to evaluate the fatigue limit of defective materials for its high accuracy.

It is considered that examination is required to use the Eq. (7.1) and (7.2) so as to be useful in application. The authors previous study [14] conducted an experiment using carbon steel S25C and experienced that the fatigue limit of smooth specimen may be lower than the fatigue limit evaluated by the Eq. (7.1) with Vickers Hardness *HV*. The reason of that was the material used for the experiment of S25C had inclusions with an equivalent diameter of about 0.2 mm. In that study suggested that if there is data on the crack initiation and growth of fatigue test, it will be possible to make an effective prediction of the fatigue limit and fatigue life of materials, when the presence of inclusions and defects is unknown. In this study, the correlation between crack growth, fatigue

life, and fatigue limit was investigated using carbon steel S45C. Since the fatigue limit and fatigue life depend on the initial size of defects and cracks, we examined how fatigue strength can be evaluated by predicting the size of crack initiation.

7.2 Materials and Experimental Methods

The material used in this experiment is commercially sold S45C. A longitudinal microstructure is shown in Fig. 7.1, and the spacing between the pearlite and ferrite layers in the microstructure may be related to the crack initiation and non-propagating phenomena. The chemical composition and mechanical properties of the material are shown in Table 7.1 and Table 7.2, respectively. The average grain sizes of ferrite and pearlite are 19 μm and 15 μm, respectively. The grain size is measured in the direction parallel to the tensile loading direction was about 50 μm. The diameter of the purchased material was 25 mm, and after cutting it in to the specified size, it was annealed at 845^0C for 1 hour. After heat treatment, the specimen was machined. The shape of the specimen is shown in Fig. 7.2. The specimen was polished on the surface (in the testing section) with emery paper and metal polisher before conducting the experiment.

Table 7.1: Chemical composition of the material tested

C	Si	Mn	P	S	Cu	Ni	Cr	Fe
0.45	0.27	0.74	0.015	0.02	0.02	0.01	0.10	Bal.

Table 7.2: Mechanical properties

Lower yield stress σ_{SL} (MPa)	Ultimate Tensile Stress σ_B (MPa)	Reduction of Area ψ (%)
325	607	60

Since the stress concentration factor of the partial notch shown in Fig. 7.2(b) is negligible, the fatigue phenomenon does not affect greatly between with and without having a partial notch of small size [7]. Therefore, in this study, in order to facilitate the observation of crack initiation and propagation, the partial notch shown in Fig. 7.2(b) was machined at the center of the testing section of the specimen, and the specimen, partially notched whose stress concentration factor is

insignificant to the fatigue life and limit, was regarded as a smooth specimen. In the case of previous study for S25C, the specimen used had inclusions with a size equivalent to a diameter of 0.2 mm from the stating of the test.

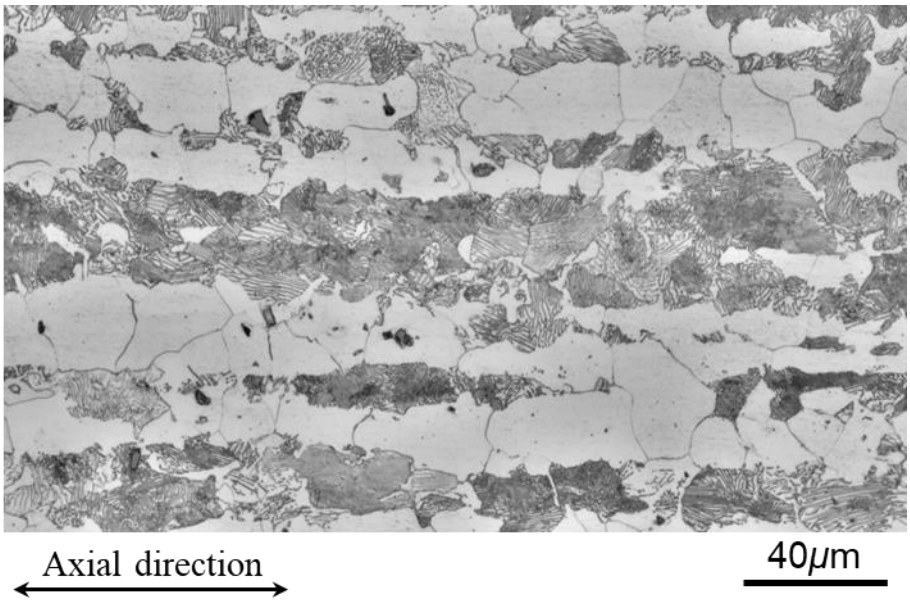

Figure 7.1 Microstructure (Longitudinal section)

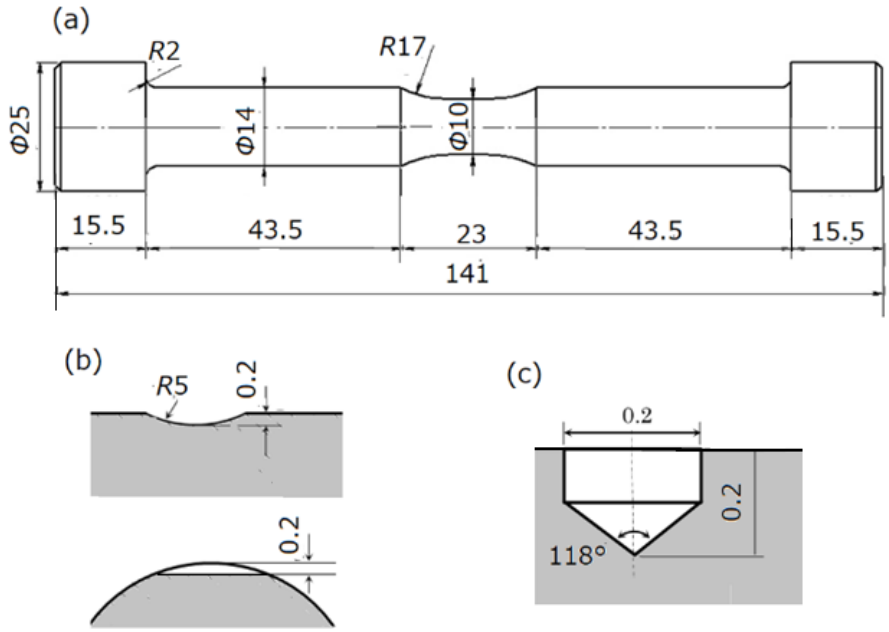

Figure7.2 Specimen geometry; (a) Dimensions of the specimen (mm), (b) Partial notch, (c) Hole.

In the S45C material used in this study, such large inclusions did not exist, but some discussion was also made in terms of the existence of inclusions. It is studied how each fatigue life can be evaluated from the crack growth curves of smooth and pre-cracked specimen. Therefore, in the present experiment, a specimen with a hole shown in Fig. 7.2(c) was also used. In usual use of structural material, heat treatment may not be conducted after manufacturing of the material. Therefore, in this experiment as well, a fatigue test was performed without heat treatment after machining the specimen.

Using an electro-hydraulic servo-type fatigue testing machine, a fatigue test was conducted with a stress ratio (= minimum cyclic stress/maximum cyclic stress) of R = -1 and a frequency of 10 Hz. A replication technique using an acetyl cellulose film was used to observe crack initiation and growth behavior. Also, the intermediate fracture surface observation was conducted by a surface view microscope to examine the existence of defect and inclusion and hardness test using a micro Vickers hardness tester were performed to determine the Vickers hardness *HV*.

7.3 Experimental Results and Discussion

7.3.1 Fatigue limit obtained from S-N curves

Figure 7.3 shows the *S-N* curves obtained from the experimental results. Regarding the specimen using S25C in the previous study [6], the *S-N* curve of the smoothed and holed specimen processed with the holes of the dimensions shown in Fig. 7.2(c) have almost the same shape, and the fatigue limit was also almost same. On the other hand, in S45C used in this experiment, there is a clear difference in the *S-N* curve and fatigue limit between the smooth specimen and the holed specimen. The size of inclusions those are present in the specimen may differ depending on the material used, which affects fatigue strength. In S45C used in this experiment, there is no large inclusions that affect the fatigue limit, but discussion is also given to the case where such inclusions exist. Murakami and Endo [15] made a proposal of fatigue limit of the materials having defect which reduces the fatigue limit of the materials, and conducted a study based on that.

The experimental value of the fatigue limit σ_w obtained from the *S-N* curve shown in Fig. 7.3 is approximately 230MPa, and the fatigue limit σ_w evaluated from Eq. (7.1) using the average Vickers hardness *HV* (170 or 170 kgf/mm^2) was almost 270 MPa. Comparing these values, the fatigue limit calculated from *HV* in Eq. (7.1) is about 17% higher than the experimental value. In

light of this results, it may consider that Vickers hardness *HV* is not the only parameter to evaluate the fatigue of material having defect or inclusion which is investigated by Murakami and Endo [12, 13]

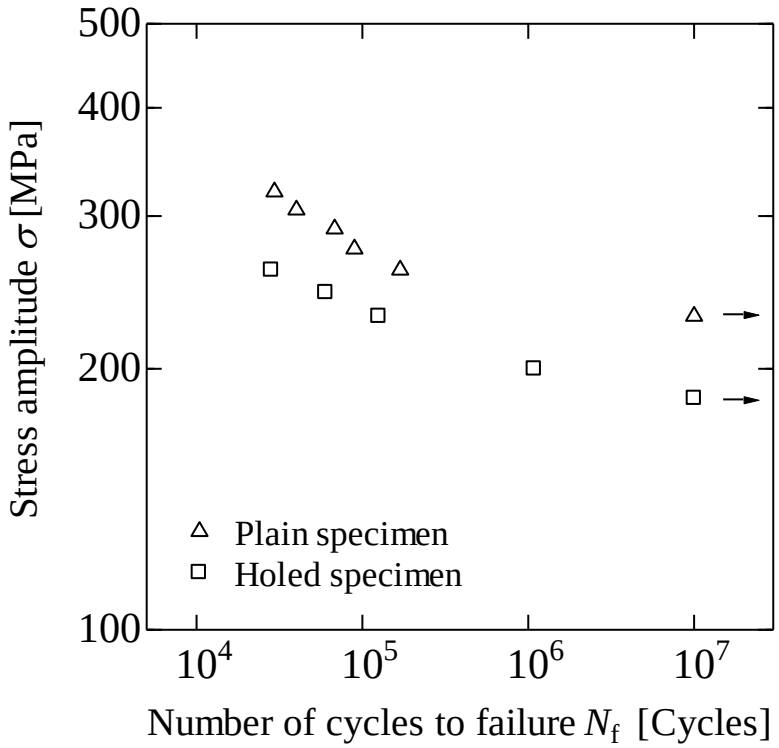

Figure 7.3 *S-N* curves

7.3.2 Crack growth behavior of smooth specimen

Figure 7.4 shows the crack growth curve. Figure 7.4(a) shows the crack growth curve on linear scale, and Figure 7.4(b) shows the crack growth curve on a semi-logarithmic scale. In the case of linear scale, it is difficult to distinguish the initial crack growth behavior, so in this study semi-logarithmic scale was used to evaluate the crack growth behavior.

The horizontal axis of the figure uses the relative number of cycles N/N_f made dimensionless by the number of times of fracture from the viewpoint of evaluating the relationship between stress amplitude and fatigue life in a unified manner. It can be seen from Figure 7.4 that the semi-logarithmic scale can be used in a small crack length range and the crack growth curve can be evaluated in detail. There are variations in the crack initiation size, and the crack length l_0 at $N \approx 0$

differs depending on the individual specimen (The crack growth curve is different at each stress level). Figure 7.5 shows an example of a fish-eye type pattern starting from an inclusion observed on the fracture surface. This pattern is not formed on the surface of the specimen, rather slightly inside from the surface.

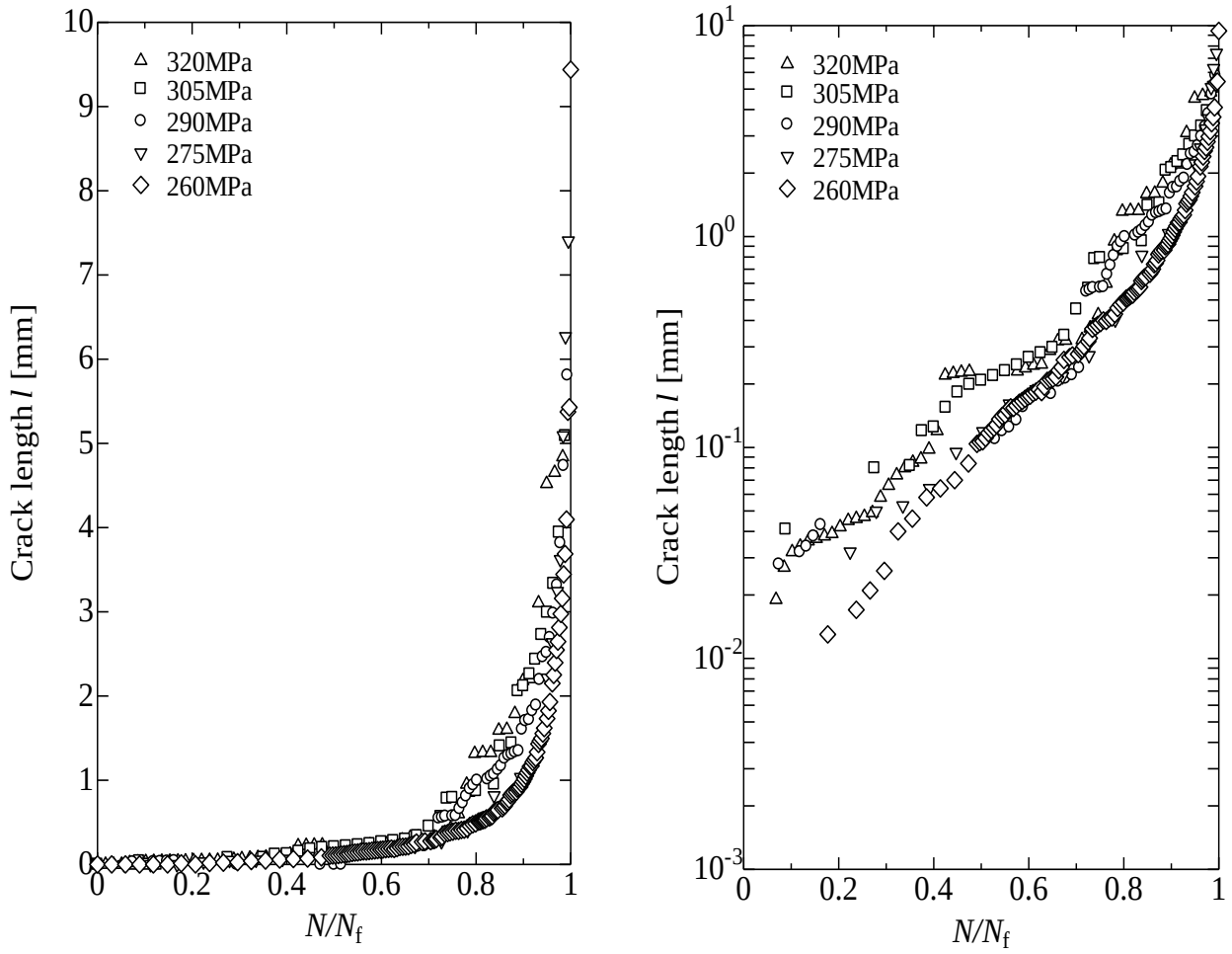

Figure 7.4 Crack propagation curve; (a) Crack length l_0 vs. relative number of cycles N/N_f, (b) $\ln l_0$ vs. N/N_f

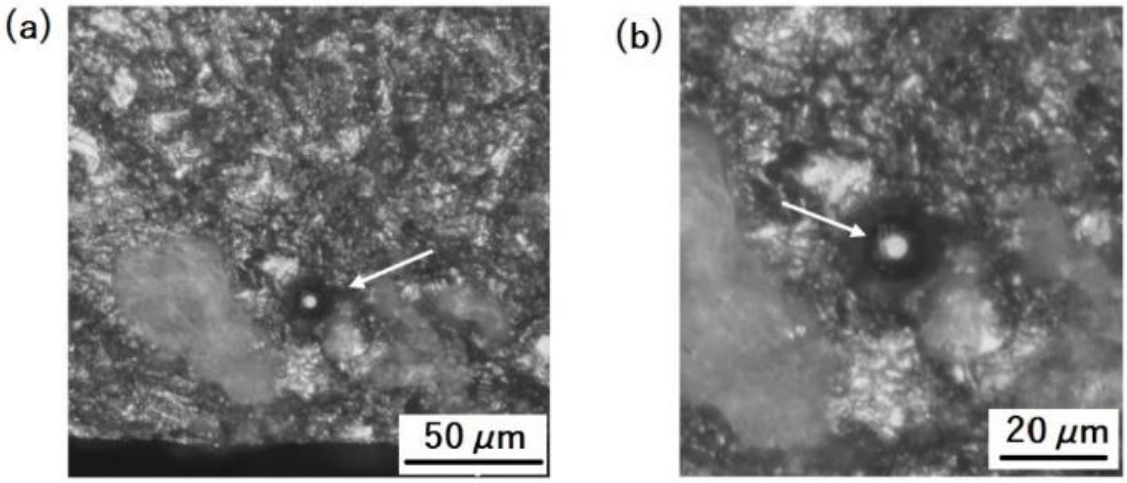

Figure 7.5 Example of observation of fracture surface (σ＝260MPa, Arrow shows inclusion)

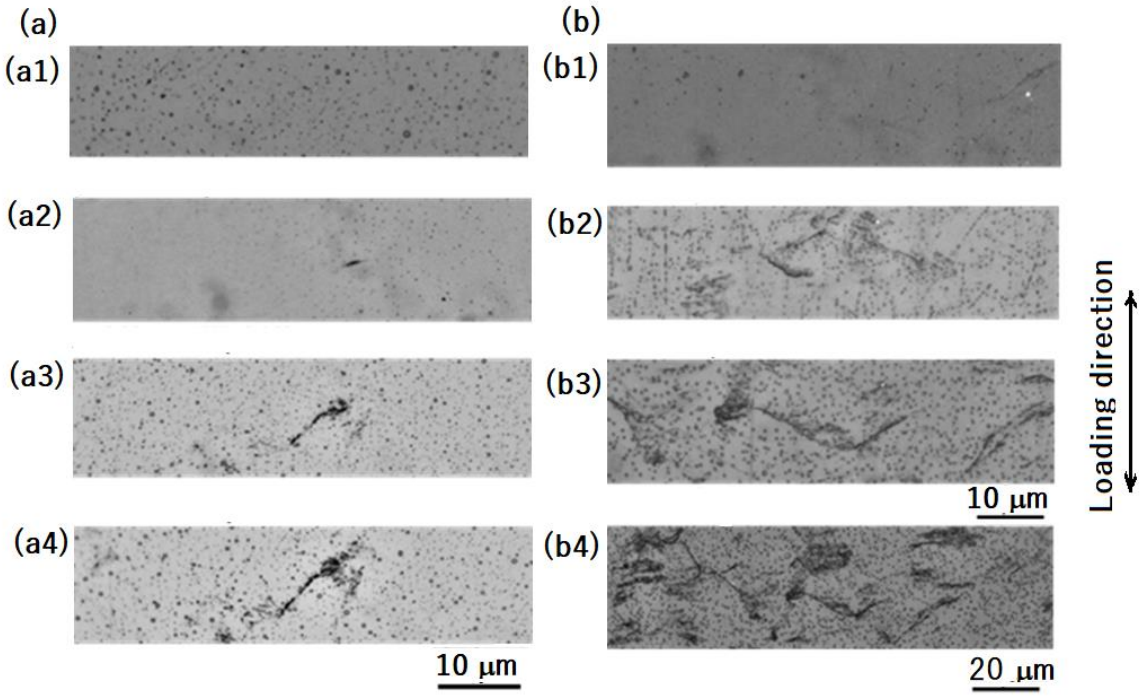

Figure7.6 Observation of crack initiation and growth; (a) σ_a = 260MPa, (a_1) l_0 = 0.0mm and N/N_f=0.03, (a_2) l_0 = 0.004mm, N/N_f=0.059, (a_3) l_0 = 0.008mm, N/N_f=0.089, (a_4) l_0 = 0.013 mm, N/N_f=0.177; (b) σ_a = 320MPa, (b_1) l_0 = 0.0mm, N/N_f=0.003, (b_2) l_0 = 0.019mm, N/N_f=0.068, (b_3) l_0 = 0.032mm, N/N_f=0.102, (b_4) l_0 = 0.038mm, N/N_f=0.170.

In the specimen (stress amplitude 260MPa) where this fracture surface was observed, the crack initiation length l_0 was smaller than the average pearlite grain size (15μm) and ferrite grain size (19μm), and the cracks initiated from the inside of the specimen. The length at which is reached is measured as l_0. Figure 7.6 is an example of observation of crack growth behavior. Fig. 7.6(a) shows the case of the same specimen as in Fig. 7.5, where l_0 is below the average grain size on the surface due to the expansion of cracks from the inside. In Fig. 7.6(b), cracks were observed with a length of about 50μm, which is similar to the largest grain size shown in Fig.7.1 of the specimen. It can be confirmed that such variations in the crack initiation length cause variations in the crack growth curve in Fig. 7.4. According to the experiment by Nishitani et al. [8], the crack growth rate dl/dN of a small crack in a smooth specimen of carbon steel is

$$dl/dN = C_1 \sigma^n l \tag{7.3}$$

It is known that C_1 and 'n' in Eq. (7.3) are material-dependent constants. Since the form of the equation is simple when the stress ratio is -1, we also study the crack growth behavior in Eq. (7.3) without using the stress intensity factor in this experiment. By transforming Eq. (7.3) and integrating, the following equation is obtained.

$$\ln l = C_1 \sigma^n N + C_2 \tag{7.4}$$

C_2 is a constant, and it can be seen from this equation that if σ = constant, a semi-logarithmic scale can be made and the crack length l and the number of repetition cycles N have a simple linear relationship. When the initial crack length at the number of repetitions N=0 is l_0 and the crack length at immediately before fracture $N \approx N_f$ is l_f, the constants C_1 and C_2 in Eq. (7.4) can be determined.

$$C_2 = \ln l_0,$$
$$C_1 = \{\ln (l_f / l_0)\}/\sigma^n \cdot (1/N_f) \tag{7.5}$$

Next substitute the values of C_1 and C_2 from Eq. (7.5) in Eq. (7.4), we obtained

$$\ln l = \{\ln (l_f / l_0)\} (N/N_f) + \ln l_0 \tag{7.6}$$

It can be seen that the crack growth curve in Fig. 7.4(b) is approximated by Eq. (7.6). Also, Eq. (7.3), can be transformed as

$$(dl/dN)/l = C_1 \sigma^n \tag{7.7}$$

Substituting C_1 from Eq. (7.5) into this yields the dimensionless crack growth rate.

$$(dl/dN)/l = \{\ln (l_f / l_0)\}. (1/N_f) \quad (7.8)$$

It follows that if l_f and l_0 are fixed to a certain value, the dimensionless crack growth rate is inversely proportional to N_f and becomes a function of stress amplitude σ.

Therefore, reviewing Fig.7.4(b) of this experimental result, and suppose that for the application of all stress amplitudes, different size of crack initiation length (due to the presence of defect or inclusion) become same size at a single point 'D' in Fig. 7.7(a), l_0 = 12 μm (average grain size) after the application correction method [11]. The crack length was approximated from the crack growth curve as l_f = 2.0 mm to create a temporary crack growth curve with little variation.

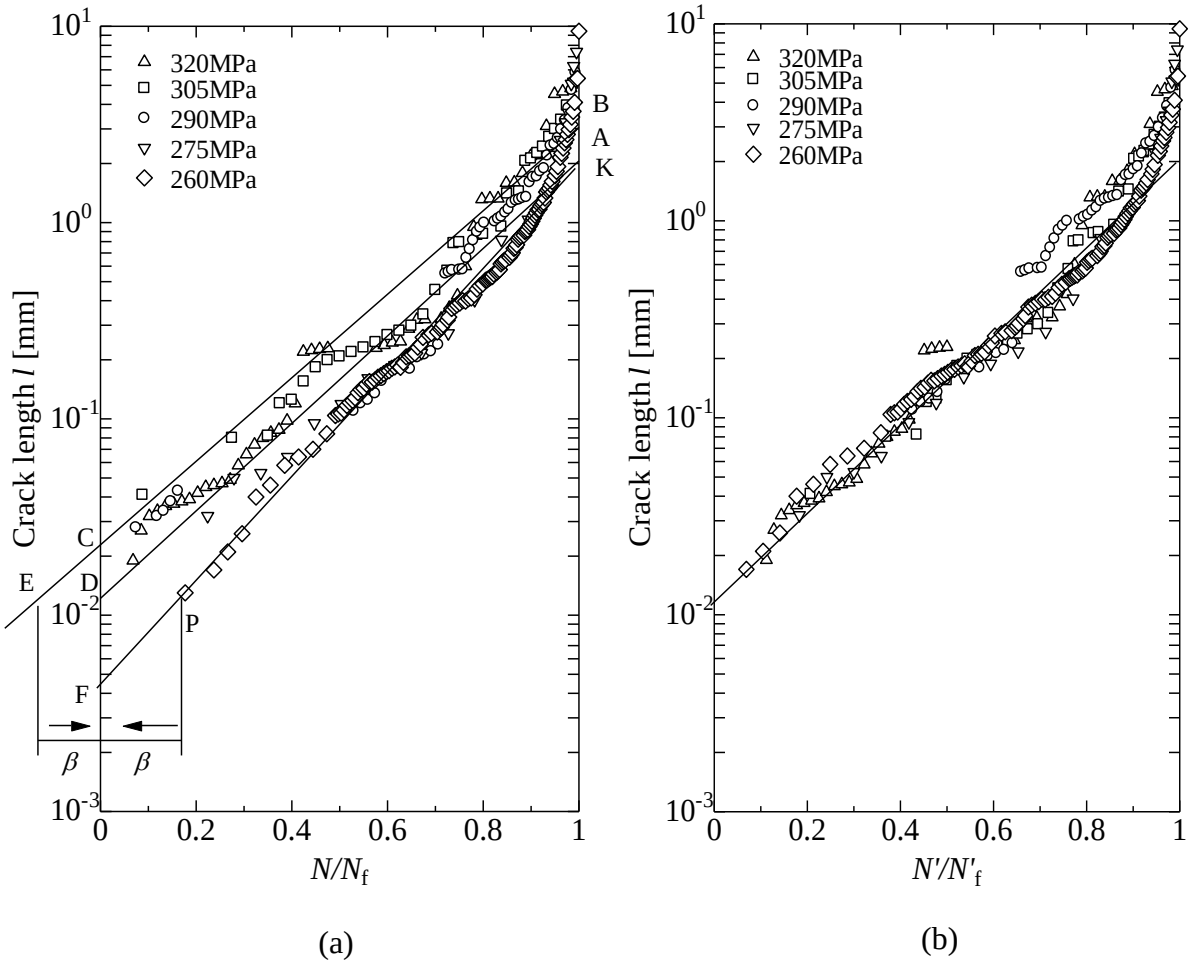

Figure 7.7 Correction of crack initiation length; (a) Method of correction of the crack growth curve, (b) Corrected crack growth curves

Figure 7.7(a) is the correction method, and Figure 7.7(b) is the corrected result. The symbols A, B, C, D, etc. in Fig. 7.7(a) are the end points of the crack growth curve that were taken into consideration when the correction was performed, and detailed description is omitted. Note that equation (7.4) can be transformed into the following equation.

$\ln l_0 = C_1'N/N_f + C_2$

Here, $C_1' = C_1\sigma^n N_f$ = constant. This equation shows an approximate equation for the crack growth curve in Fig.7.4(b), and Eq. (7.4) itself is related to the *S-N* curve ($\sigma^n N_f$ = constant can be approximated).

Table 7.3: Coefficients for prediction of *S-N* curve from crack growth curves (l_0=12μm, l_f =2.0mm).

σ, MPa	β	N_f	$N'_f = (1+\beta) N_f$
320	0.050	2.9×10^4	3.1×10^4
305	0.150	4.0×10^4	4.6×10^4
290	- 0.180	6.8×10^4	5.6×10^4
275	- 0.050	8.9×10^4	8.5×10^4
260	- 0.180	1.7×10^5	1.4×10^5

As a method of correcting the crack growth curve [11], if the crack initiation length l_0 for each stress amplitude is longer than 12μm, the fatigue life is extended and N_f is corrected to $N'_f = (1+\beta) N_f$. In that case, the arbitrary number of repetition cycles is $N'=N+\beta N_f$. If l_0, which is assumed from the crack growth curve, is shorter than 12 μm, the fatigue life is shortened and corrected, so β becomes a negative value. Table 7.3 shows some of the above correction factors for each specimen.

Fig. 7.8 shows the relationship between the dimensionless crack growth rate (dl/dN)/l and the stress amplitude σ using the corrected number of cycles to failure N'_f. The value of (dl/dN)/l was calculated from the value of N_f corresponding to σ from Eq. (7.8). It can be seen from Fig. 7.8 that the crack growth law can be expressed by Eq. (7.7).

Here, Eq. (7.7) is transformed into the following equation.

$$dl/l = C_1 \sigma^n dN$$

From the crack growth curve corrected from Fig. 7.8, the coefficient in the above equation is n = 7.0, C_1 = 6.0 x 10^{-22}. The crack length when N=0 is l_0 and the number of failure cycles is N_f. Integrating the above equation with the crack length as l_f.

$$\ln (l_f / l_0) = C_1 \sigma^n N_f \quad (7.9)$$

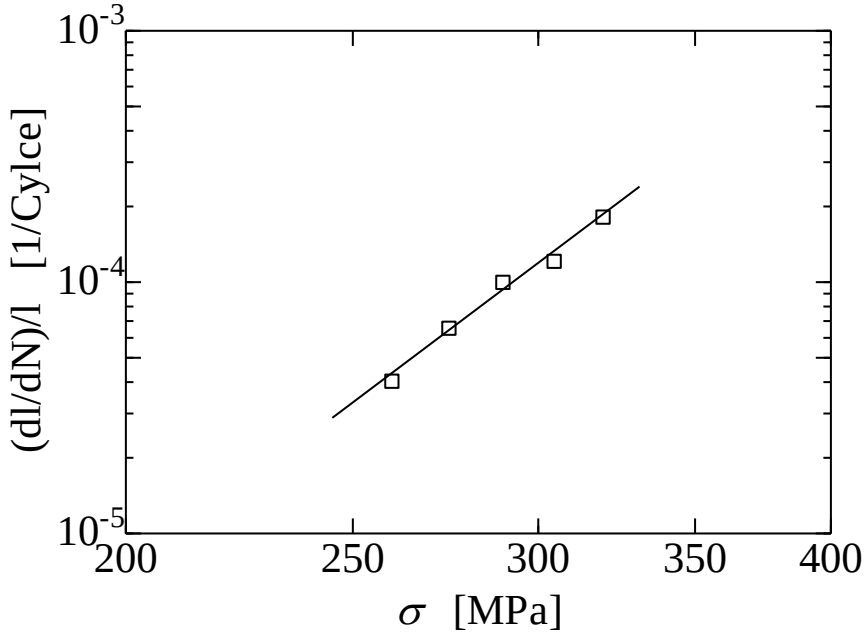

Figure 7.8 Relationship between corrected (dl/dN)/l vs. stress amplitude σ

Based on the corrected crack growth curves in Fig.7.7 and 7.8, if l_0 = 12 μm, l_f = 2 mm, n =7.0, and C_1 = 6.0 x 10^{-22}, the S-N curve in the finite life range given by the following equation; (In this case, N'_f in Table 7.3 is changed to N_f).

$$\sigma^{7.0} N_f = 8.5 \times 10^{21} \quad (7.10)$$

These results are shown in Fig. 7.9. The plotted points in Fig. 7.9 are the experimental values for smooth specimen, and the solid line is the predicted value from the corrected crack growth curve in the finite life region. In the case of this experiment, there is little variation in the experimental data, and the experimental values and the predicted values agreed relatively well. It is considered that the reason is that, although the crack initiation length at each stress amplitude

varies, there is no significant variation between the crack length l until the fracture and the relative number of cycles N/N_f.

In the case of this experiment, the S-N curve in the finite life region could be predicted with relatively good accuracy from the corrected average crack growth curve. However, due to the presence of inclusions and microdefects, it is assumed that the crack growth curve may not be conveniently predicted by an average relationship as in Eq. (7.3). In such a case, we considered how to evaluate (predict) the fatigue life and fatigue limit by the *S-N* curve as shown in the next section.

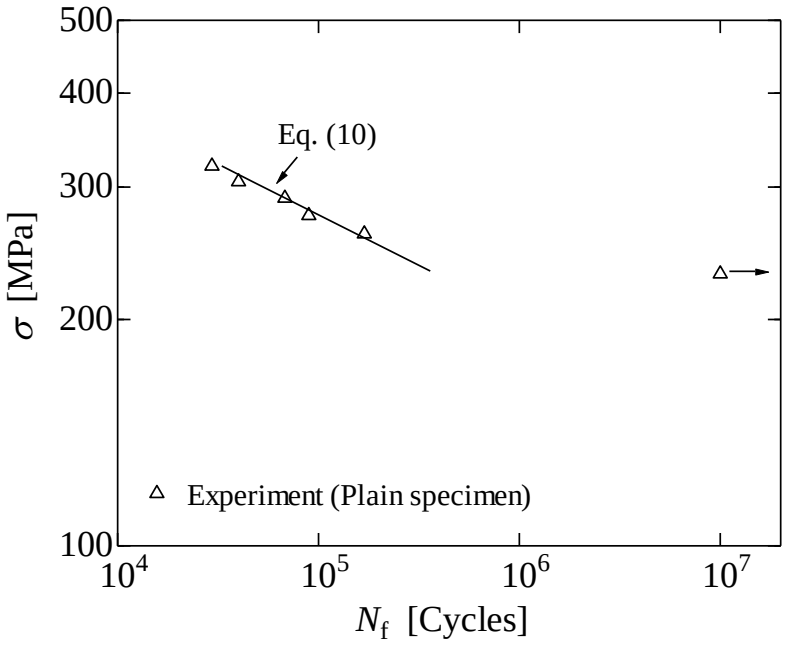

Figure 7.9 S-N curve which predicted from crack growth curves

7.3.3 Evaluation of S-N curve and fatigue limit due to difference in crack initiation length

From the viewpoint of investigating the relationship between the crack initiation length and the fatigue life and fatigue limit, the relationship between fatigue crack growth behavior and fatigue life was investigated compared to the holed specimen. Figure 7.10 shows the crack growth curve of the holed specimen. Since the crack growth curve in Fig. 7.10 can be approximated by almost the same straight line regardless of the stress level, n = 13.9 and $C_1 = 2.0 \times 10^{-38}$ when the coefficient value of Eq. (7.9) is calculated.

Based on these values and Fig. 7.10, assuming that l_0 = 0.15 mm and l_f = 3 mm, equation (7.9) can be expressed as the following equation.

$$\sigma^{13.9} N_f = 1.5 \times 10^{38} \tag{7.11}$$

The *S-N* curve obtained from the crack growth curve and the experimental results shown in the plot are coincided well. The crack initiation length was set to l_0 = 0.15 mm from Fig. 7.10, but as shown in Fig.7.2, the hole diameter d and the depth h were 0.2 mm. The crack initiation size and the critical defect size of the material do not necessarily relate to the fatigue life. From the shape shown in Fig.7.2, the projected area of the hole is 'Area' = 33991 μm^2, and when the average Vickers hardness *HV* = 170 is substituted into Eq. (7.2), the fatigue limit is σ_w = 174 MPa. This value is a little bit lower than the experimental value of fatigue limit σ_w = 185 MPa, and this predicted value of fatigue limit seems to be effective from the viewpoint of safety.

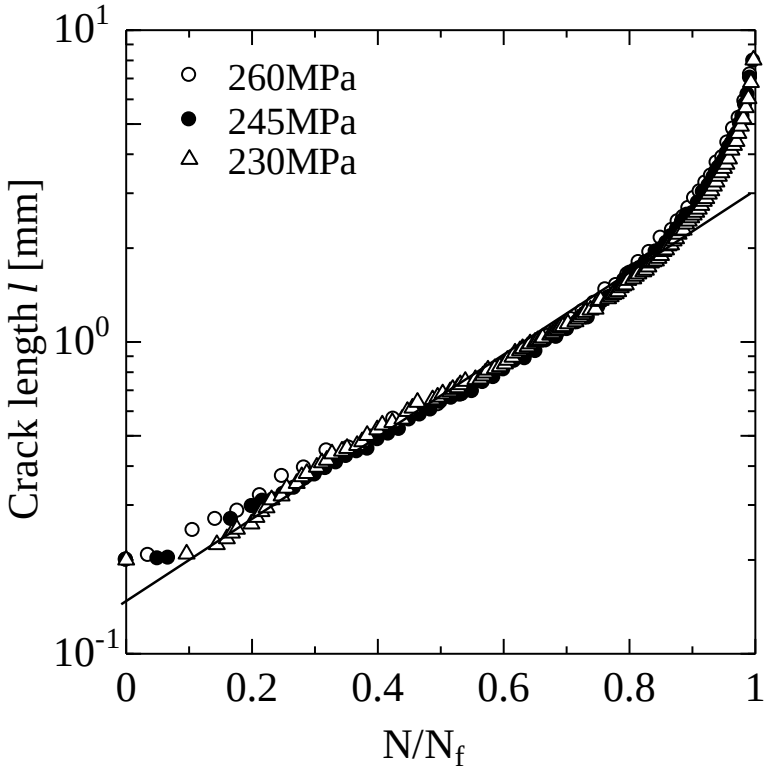

Figure 7.10 Crack growth curves of holed specimen, l_0=0.15mm, l_f = 3.0 mm.

Based on the fact that the crack initiation size and the size of defects or inclusions that affect the fatigue limit and fatigue life do not necessarily matched, the fatigue strength of the smooth specimen in the previous section and the *S-N* curve assumed on the safe side were examined. The fatigue limit of smooth specimen may be evaluated by Eq. (7.1), but since it is empirical, it is not necessary to consider according to the predicted value. Also, in the case of Eq. (7.2), it is an empirical value that *HV* is used as the resistance value of the material, but it takes into account the fracture mechanics parameter [5].

Therefore, in this study, we examined whether it is possible to evaluate the fatigue limit on the safe side using Eq. (7.2) or not. Murakami and Endo [8] investigated the fatigue limit reduction of specimens with artificial holes (which is considered as defects) in various fatigue tests. From the results, tensile and compression fatigue test of S45C at R = -1, it is considered that the fatigue

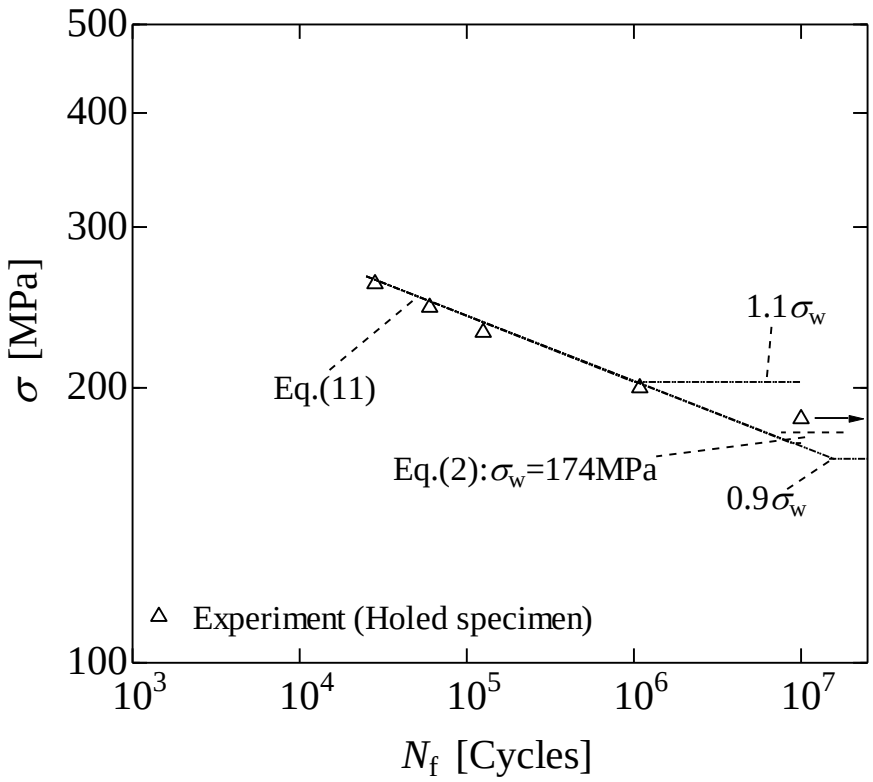

Figure 7.11 *S-N* curve and evaluated fatigue limit from Eq. (2) for holed specimen

limit of the specimen with artificial hole does not decrease compared to the smooth specimen if the diameter and depth of the hole is 35μm or less. Murakami [10] also considers the relationship

between the critical size of such artificial holes and cracks that affect the fatigue limit and the microstructure.

The area of the artificial hole (defect) is 1041 μm^2. Therefore, in this study, the hole is regarded as a semi-circular initial crack with a surface length of l_0 = 50 μm (area = 982 μm^2), and the fatigue limit and the crack growth from the crack based on that crack are considered. The fatigue life was examined. Note that l_0 = 50 μm is almost on the order of the length of the pearlite and ferrite microstructure shown in Fig.7.1. If the crack initiation length l_0 is 50 μm and the crack growth curve at each stress amplitude is corrected by the method shown in the previous section, each coefficient can be obtained as shown in Table 7.4. In other words, if l_0=50 μm, l_f=2.0 mm, n=7.4, C_1=6.0 x 10^{-23}, the following *S-N* curve is obtained from the corrected crack growth curve.

$$\sigma^{7.4} N_f = 6.1 \times 10^{22} \tag{7.12}$$

Table 7.4: Coefficients for prediction of *S-N* curve from crack growth curves (l_0=0.05mm, l_f =2.0mm).

σ, MPa	β	N_f	$N'_f = (1+\beta) N_f$
320	- 0.26	2.9 x 10^4	2.2 x 10^4
305	- 0.18	4.0 x 10^4	3.3 x 10^4
290	- 0.37	6.8 x 10^4	4.3 x 10^4
275	- 0.32	8.9 x 10^4	6.1 x 10^4
260	- 0.36	1.7 x 10^5	1.1 x 10^5

Also, substituting area = 982 μm^2 and average hardness *HV* = 170 into Eq. (7.2) gives σ_w = 234 MPa. Figure 7.12 compares σ_w using Eq. (7.2) and (7.12) with the experimental values shown in the plot. The correction value for finite fatigue life is given on the safe side compared to the experimental value. It is also considered that the fatigue limit can be evaluated on the safety side by adopting a value 10% lower than the predicted value by Eq. (7.2) with l_0 = 50 μm.

The crack growth law based on Eq. (7.3) and (7.9) is equivalent to the fatigue life law in the finite fatigue life region, and the effect of stress amplitude that contributes to fatigue life is evaluated by the value of their exponent n, and the *S-N* curve. The gradient of the curve is approximated (note that, the crack initiation size and the crack growth curve of the experiment at

each stress level are different but summarization by Eqs. (7.3) and (7.9) become effective by utilizing the average value of crack initiation size. It is necessary to be careful about that.)

In this study, since the effect of inclusions on crack growth is negligible, there is no significant difference on the logarithmic scale between the experimental data shown in Fig. 7.9 and the predicted value of fatigue life. However, when there are relatively large inclusions, the crack initiation size increases, and this effect appears in the fatigue life. In the case of smooth specimen, it is better to set the crack initiation length larger than the average value when predicting fatigue life and fatigue strength, or when evaluating the safe design using by obtained data. In that case, it may be better to consider the prediction on the safety side, taking into consideration the factors that affect the value of 'n' and the initial crack length l_0. In addition, it is also effective to check the fatigue life and fatigue strength tendency of defective materials for strength evaluation of smooth materials. There is a limit to the size of a defect that reduces the fatigue limit. In this study, if the fatigue life and fatigue limit are predicted by focusing on that limit, the life of the smooth specimen may be evaluated on the safe side. The possibility that there is considered.

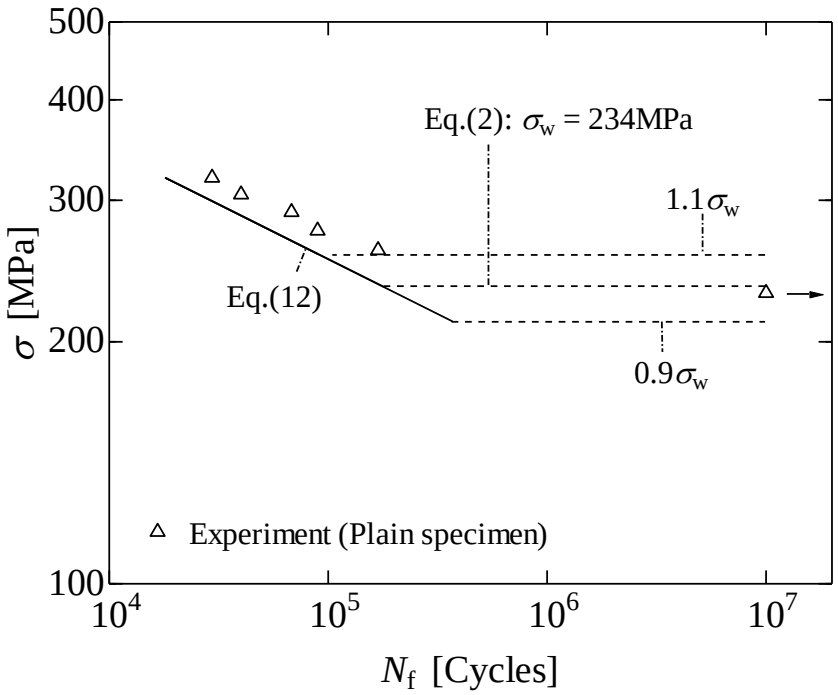

Figure 7.12 Evaluation of fatigue life and fatigue limit of a plain specimen with initial crack (l_0=50μm).

In the case of rolled carbon steel, it may be possible to measure on the safe side by the size of the layer of microstructure and the size of maximum inclusions. In the future, we would like to investigate a method to evaluate the fatigue life from the value of the gradient ‘n’ of the standard *S-N* curve when the initial size of the crack generated by inclusions and defects differs.

7.4 Conclusion

In this study, we examined one method to evaluate the fatigue life and fatigue limit on the safe side at the basic experiment level in the fatigue test of materials with variations in crack initiation length. The main results obtained are as follows.

(1) In the material of this experiment with relatively small inclusion size, it is possible to predict the *S*-*N* curve from the crack growth curve by predicting the crack growth curve using the crack initiation size of the average grain size.

(2) It was possible to estimate the safe fatigue limit by using the critical initial crack size and Vickers hardness *HV* that do not affect the fatigue limit of the smooth or plain specimen.

(3) Since the critical initial crack size and the initial crack size generated at an arbitrary stress amplitude are different, assuming that the initial crack size is the same as the critical crack size, it is possible to set the *S*-*N* curve on the safe side.

(4) The method of this study may be applied to the evaluation of the fatigue life of smooth materials in the presence of relatively large defects or inclusion.

7.5 Reference

[1] J. McEvily, “Metal Failure”, John Wiley & Sons, Inc., (2002) .

[2] H. Nakazawa, H. Honma, “Fatigue Strength of Metals”, Yokendo Co. Ltd, Tokyo, 1982.

[3] S. Nishida; “Failure Analysis in Engineering Applications”, Butterworth-Heinemann Ltd, (1991).

[4] Y. Murakami, Metal Fatigue, Elsevier Science Ltd., Oxford pp.1-128, 2002.

[5] J. A. Ewing and J.W.C. Humfrey, The Fracture of Metals under Repeated Alternations of Stress, Philosophical Transaction of Royal Society of London, Vol.200 (1903), pp.241-253.

[6] Herbert John Gough, Fatigue of Metals, Scott Greenwood, London, 1924.

[7] Kenichi Takao, Hironobu Nishitani; “Study on the mechanism of labor crack initiation by continuous surface observation”, Transactions of the Japan Society of Mechanical Engineers, Volume A, Vol46, N0.402, pp.123-133 (1980).

[8] Hironobu Nishitani, Masahiro Goto, Norio Hashigoishi; “Study on Crack Propagation Law under Large and Small Stresses”, Proceedings of the Japan Society of Mechanical Engineers, Vol. 50, No. 449, pp.23-32 (1984).

[9] Takanori Murakami, Masahiro Endo; “Influence of artificial micro-defects on torsional fatigue of S45C annealed material (compared with bending)”, Transactions of the Japan Society of Mechanical Engineers, Vol. 47, No. 415, pp.249. -256 (1981).

[10] Takanori Murakami; “Metal fatigue: Effects of micro defects and inclusions”, pp.1-12, Yokendo (1993).

[11] Chobin Makabe, Hideo Kaneshiro, Masaya Itokazu, “Fatigue Crack Propagation and Life of Specimen with inclusion in a Low Cycle Fatigue Resime”, Proceedings of the Third International Conference on Very High Cycle Fatigue (VHCF-3) pp.232-293, 2004.

[12] Murakami, Y., and Endo, M., Effects of Hardness and Crack Geometry on Δ*K*th of Small Cracks, Journal of the Society of Materials Science, Japan, Vol. 35, No. 395, pp. 911-917 (1986)

[13] M. F. Garwood, H. H. Zurburg and M. A. Erickson; “Correlation of Laboratory Tests and Service Performance”, Interpretation of Tests and Correlation with Service, ASM, Publication, PA, pp. 1-77 (1951).

[14] S. M. Moshiar Rahman, Chobin Makabe, Kaito Naka, Akihiro Yamauchi, “Effect of Existence of Inclusions on Fatigue Strength”, Journal of High-Pressure Institute of Japan, Vol.58, No.4, pp.11-17, 2020, ISSN 0387-0154 Atsuryoku gijitsu.

[15] Murakami, Y. and Endo, T., “Effect of Small Defects on the Fatigue Strength of Metals,” International Journal of Fatigue, Vol. 2, ISSN: 0142-1123, pp.23–30, 1980.

Chapter Eight

Conclusion

The fatigue mechanism has been investigated in this dissertation. Many fracture accidents are related to the fatigue fracture of engineering materials. Fracture accident should be arrested to save human life. This dissertation has been concluded considering the literature reviewed in the preceding chapters are concluded in the following manner. The conclusion reviews on the respective topics are included in each of the respective topics.

(1) The investigation of detection of fatigue crack initiation, crack growth behavior, and subsequent fatigue life of materials due to application of unexpected overload and underload while the machine is in running condition or the structures are in loading condition has been concluded.

(2) Fatigue phenomena of carbon fiber reinforced epoxy composite and aluminum-carbon fiber composite have been studied. This study has shown promising result with some conditional aspect.

(3) Prediction of fatigue life and fatigue limit of material having pre-defect and inclusion beyond the permissible crack initiation length and outcomes have been well agreed to researches conducted by many researchers earlier.

The conclusion of subsequent chapter was summarized as follows:

Chapter Two

A Method for Detecting an Unexpected Application of a Hazardous Load During Operation

The method of detecting application of an unexpected load which leads to the acceleration of fatigue crack growth. The main results obtained are as follows:

(1) The acceleration of fatigue crack growth occurred when the tensile residual stress created in front of the crack tips and the crack opening and closing stresses reached a lower level.

(2) The shapes of stress – strain loops were changed when the crack growth rate was changed due to applying an unexpected load.

(3) The crack opening and closing stresses could be easily measured by using the relationship between the stress and the strain function which was proposed by Kikukawa et al.

(4) Monitoring for the detection of an application of a dangerous load can continuously be performed by using the waveform of the stress and the strain function.

Chapter Three

Method of Detecting Unexpected Load Leading by Using Strain Information

The method of detecting whether an unexpected load which leads to the acceleration of fatigue crack growth was applied or not is done by using strain data. The variation tendency of the local strains in the vicinity of the crack was affected by whether acceleration or deceleration occurred due to the crack opening and closing behavior. By considering that behavior, two types of strain functions were proposed for detection of unexpected load. Even if the load data was not measured, the unexpected load which leads to the acceleration of fatigue crack growth can be detected by the strain functions proposed in this study. The following outcomes have been found from this study:

(1) Crack growth acceleration or deceleration were observed depending on the condition of overlaod and underload compared to the baseload i.e. without applying any overload or underload.

(2) By analyzing the shape of the waveform of strain information, whether an unexpected overlaod or underlaod was applied or not can be detected/predicted.

(3) The value of 'λ', which is the ratio of effective cyclic strain range, is an important parameter which can be used as a qualitative measurement tool of the variation of the strain function.

Chapter Four

Effect of Fiber Direction and Stress Ratio on Fatigue Property in Carbon Fiber Reinforced Epoxy Composites

The purpose of this study was to examine the influence of the anisotropy due to the characterization of the material by superimposing unidirectional long carbon fiber sheets and local fracture behavior of fiber on fatigue strength. The following results obtained are as follows:

(1) A higher fatigue limit was obtained when the alignment of all carbon fibers was in the loading direction.

(2) For composite materials with long fibers, it is expected that the fatigue limit of smooth specimens can be predicted from the results of slit specimens.

(3) The crack initiated from the epoxy region. Then the crack grew by shear mode and the crack cut fiber by shear mode. This mechanism can be applied in the present cases.

(4) The ratio of fibers in the loading direction is expected to be related to the fatigue limit.

(5) The results obtained in the present experiment will be applied to a repair method for damaged carbon composites which will be investigated in future.

Chapter Five

Fatigue and Fracture Mechanism of Aluminum-Carbon Fiber Reinforced Hybrid Composites

In this study, the effect of incorporating of aluminum foil and aluminum plate with the woven carbon fiber cloth in hybrid composites by using both sides slit specimen was investigated. The main results obtained are as follows:

(1) The higher fatigue limit were obtained in the case of *A* type specimen when all the carbon fibers were in the loading direction. Also, mechanical strength of the carbon fiber in the loading direction is higher than that of aluminum foil and aluminum plate at $R = -1$. The strength also differ due to the variation of thickness of the woven carbon fiber, aluminum foil and aluminum plate.

(2) The fracture behavior are different for different types of specimen as the composition and the number of woven carbon fiber cloths are different. The fracture behavior depends on the interfacial bonding between the woven carbon fiber cloth and aluminum foil in *B* type specimen or between woven carbon fiber cloth and aluminum plate in *C* type specimen. The property of the specimen could be improved by improving the inter laminar bonding between the woven fiber cloth and aluminum foil or plate.

(3) For the application of tension-tension loading condition, *A* type and *C* type specimen have shown almost the same fatigue limit even though reduced number of carbon fiber sheet

have been used.

Chapter Six

Effects of Existence of Unexpected Defects on Fatigue Strength

Fatigue limit and crack behavior were investigated in a commercially sold carbon steel. After annealing, three types of specimen were machined. That is, the smooth specimen, partial notch specimen and holed specimen. The results obtained are as follows,

(1) The fatigue limit of the smooth specimen shows clearly a lower value than the evaluated value from Vickers hardness.

(2) The fatigue limit of the holed specimen had almost the same value as the evaluated value from Vickers hardness and projected area of the hole in the axial direction of specimen.

(3) Fatigue limits for the smooth specimen and the holed specimen had almost the same value. That is related to the crack initiation behavior. Because, the material used has large size defects and a section in which distances of defects are very short, the crack initiation size was larger than 0.1 mm in the case of the smooth specimen and partial notch specimen. The existence of such defects and the crack growth behavior is related to the fatigue limit.

(4) The material used is not expected to be produced for use in machine equipment. It is good such kind of material is sold with a warning about the existence of defects.

Chapter Seven

A Method for Prediction of Fatigue Limit and Life in Carbon Steel

In this study, we examined one method to evaluate the fatigue life and fatigue limit on the safe side at the basic experiment level in the fatigue test of materials with variations in crack initiation length. The main results obtained are as follows.

(1) In the material of this experiment with relatively small inclusion size, it is possible to approximate the *S-N* curve from the crack growth curve by approximating the crack growth curve using the crack initiation size of the average grain size.

(2) It was possible to estimate the safe fatigue limit by using the critical initial crack size and Vickers hardness *HV* that do not affect the fatigue limit of the smooth or plain specimen.

(3) Since the critical initial crack size and the initial crack size generated at an arbitrary stress amplitude are different, assuming that the initial crack size is the same as the critical crack size, it is possible to set the *S*-*N* curve on the safe side.

(4) The method of this report may be applied to the evaluation of the fatigue life of smooth materials in the presence of relatively large defects or inclusion.